UNIVERSIDADE FEDERAL DO RIO GRANDE DO SUL

INSTITUTO DE PESQUISAS HIDRÁULICAS

PROGRAMA DE PÓS-GRADUAÇÃO EM RECURSOS HÍDRICOS E SANEAMENTO AMBIENTAL

GUILHERME KRUGER BARTELS

DINÂMICA DA UMIDADE DO SOLO NA GERAÇÃO DE ESCOAMENTO SUPERFICIAL EM UMA PEQUENA BACIA HIDROGRÁFICA

PORTO ALEGRE

2022

GUILHERME KRUGER BARTELS

DINÂMICA DA UMIDADE DO SOLO NA GERAÇÃO DE ESCOAMENTO SUPERFICIAL EM UMA PEQUENA BACIA HIDROGRÁFICA

Tese apresentada ao Programa de Pós-graduação em Recursos Hídricos e Saneamento Ambiental da Universidade Federal do Rio Grande do Sul, como requisito parcial à obtenção do grau de doutor.

Orientadora: Nilza Maria Dos Reis Castro

Coorientador: Gilberto Loguercio Collares

PORTO ALEGRE

2022

CIP - Catalogação na Publicação

Bartels, Guilherme Kruger
Dinâmica da umidade do solo na geração de escoamento superficial em uma pequena bacia hidrográfica / Guilherme Kruger Bartels. -- 2022.
132 f.
Orientadora: Nilza Maria dos Reis Castro.

Coorientador: Gilberto Loguercio Collares.

Tese (Doutorado) -- Universidade Federal do Rio Grande do Sul, Instituto de Pesquisas Hidráulicas, Programa de Pós-Graduação em Recursos Hídricos e Saneamento Ambiental, Porto Alegre, BR-RS, 2022.

1. Escoamento superficial. 2. Umidade do Solo. 3. Redes neurais artificiais. 4. OpenLISEM. 5. Pequena bacia hidrográfica. I. Castro, Nilza Maria dos Reis, orient. II. Collares, Gilberto Loguercio, coorient. III. Título.

Elaborada pelo Sistema de Geração Automática de Ficha Catalográfica da UFRGS com os dados fornecidos pelo(a) autor(a).

GUILHERME KRUGER BARTELS

DINÂMICA DA UMIDADE DO SOLO NA GERAÇÃO DE ESCOAMENTO SUPERFICIAL EM UMA PEQUENA BACIA HIDROGRÁFICA

Tese apresentada ao Programa de Pós-graduação em Recursos Hídricos e Saneamento Ambiental da Universidade Federal do Rio Grande do Sul, como requisito parcial à obtenção do grau de doutor.

Aprovada em: Porto Alegre, 31 de março de 2022.

_____

Profª. Drª Nilza Maria Dos Reis Castro – UFRGS
Orientadora

_____

Prof. Dr. Gilberto Loguercio Collares – UFPel
Coorientador

_____

Prof. Dr. Olavo Correa Pedrollo - UFRGS
Examinador

_____

Profª. Drª Claudia Alessandra Peixoto de Barros - UFRGS
Examinador

_____

Profª. Drª Tirzah Moreira Siqueira - UFPel
Examinador

AGRADECIMENTOS

Agradeço à minha família pelo acompanhamento na minha trajetória. Em especial aos meus pais, Rute e Jorge, que sempre me incentivaram e mesmo com todas as dificuldades, lutaram e garantiram educação aos seus filhos. À minha irmã Janaina, um exemplo de pessoa, e minha sobrinha Cecília, que trouxe mais alegria para toda a família. À minha querida companheira Luciana, por todo o apoio durante esta etapa da vida, e que venham muitas outras conquistas juntos.

Aos meus orientadores, professora Nilza e professor Collares, pela oportunidade concedida, orientação, amizade, confiança e incentivo. Às duas universidades públicas e de qualidade (UFRGS e UFPel), que garantiram a execução desta pesquisa. Aos professores do IPH, em especial Olavo, Fernando Fan, Masato e Louzada, por todos os conhecimentos transmitidos e amizade. Aos colegas do PPGRHSA, em especial Fernando, Karla e Maurício, por toda a amizade nestes anos.

Ao grupo HidroSedi da UFPel, principalmente pela ajuda indispensável nas atividades desempenhadas em campo e laboratório. Em especial: Alessandra, Gabriel, Larissa, Lukas, Leandra, Pedro, Rafael, Renan e Victória. Aos servidores George, Lucas e Reginaldo pela amizade e apoio nas inúmeras saídas de campo para os trabalhos na bacia. Às professoras Angélica e Viviane e ao professor Alexandre, por toda ajuda, troca de ideias e experiências, muito obrigado. Essa é a nossa turma!

Aos moradores da bacia hidrográfica do Arroio do Ouro, que gentilmente cederam as áreas para instalação das estações de monitoramento.

Ao CNPq pela bolsa de estudo.

RESUMO

Diversos processos hidrológicos estão associados à condição de umidade do solo e às características dos eventos de precipitação. O conteúdo de água no solo pode impactar na geração de escoamento tanto superficial, quanto subsuperficial, bem como na conexão dos caminhos do fluxo preferencial. Dependendo da escala de observação, todos os processos podem ocorrer de forma conjunta, com maior ou menor relevância, conforme as características do ambiente. Em pequenas bacias hidrográficas, a geração do escoamento está associada à interação existente entre as características do solo e da paisagem, à aspectos dinâmicos, como a umidade antecedente do solo e à precipitação, além do possível efeito das ações antrópicas. No entanto, a maioria das pequenas bacias hidrográficas monitoradas, não possuem a disponibilidade de medidas de umidade do solo, ou então detêm informações limitadas a poucas observações. Assim, o objetivo desta pesquisa é avaliar os principais fatores que contribuem para a dinâmica da umidade do solo na camada superficial e subsuperficial e a influência da condição da umidade antecedente do solo na geração de escoamento, em uma pequena bacia hidrográfica no sul do Brasil. Para isso, foi primeiramente desenvolvido um modelo de redes neurais artificiais para a estimativa consistente da umidade do solo, em seguida realizada a análise dos principais fatores que afetam os resultados dos modelos. Posteriormente, foi verificado os possíveis impactos da umidade antecedente do solo na geração de escoamento. Isto foi feito de duas formas: i) analisando 104 eventos de chuva – vazão que ocorreram durante 4 anos de monitoramento; ii) utilizando a umidade antecedente do solo como parâmetro de entrada nas simulações de 15 eventos de chuva-vazão com um modelo físico distribuído baseado em eventos, o OpenLISEM (open source Limburg Soil Erosion Model). Os resultados indicam que os modelos de umidade do solo obtiveram um bom desempenho e conseguiram estimar a umidade do solo para ambas as camadas. Enquanto as variáveis relacionadas ao clima são as mais importantes para o desempenho do modelo de superfície, para a camada subsuperficial as variáveis relacionadas ao solo são as mais importantes. Em relação à geração de escoamento na bacia hidrográfica do Arroio do Ouro, não foi observado um limiar claro entre a umidade antecedente do solo e o coeficiente de escoamento. Porém, os maiores coeficientes de escoamento foram registrados nos eventos cuja umidade antecedente do solo era muito próxima ou superior à capacidade de campo. A utilização da umidade antecedente como parâmetro de entrada nas simulações com o OpenLISEM mostrou-se promissora, visto os resultados sólidos encontrados durante a etapa de validação do modelo. Mesmo considerando as incertezas associadas às estimativas da umidade antecedente do solo, foi possível representar a forma de hidrogramas complexos.

Palavras-chave: Umidade do solo. Redes neurais artificiais. Escoamento. OpenLISEM. Pequena bacia hidrográfica

ABSTRACT

Several hydrological processes are associated with the soil moisture condition and the characteristics of rainfall events. Soil water content can impact the generation of overland flow and subsurface flow and the connection of preferential flow paths. Depending on the observation scale, all processes may be occurring together, with greater or lesser relevance, depending on the characteristics of the environment. In small watersheds, the generation of runoff is associated with the interaction between soil and landscape characteristics, dynamic aspects, such as antecedent soil moisture and precipitation, and the possible effect of human actions. However, most of the small watersheds monitored do not have the availability of soil moisture measurements, or they have limited information to a few observations. Thus, this research aims to evaluate the main factors that contribute to soil moisture dynamics in the surface and subsurface layer and the influence of the antecedent soil moisture condition on the generation of runoff in a small watershed in southern Brazil. For this, firstly, an artificial neural network model was developed for the consistent estimation of soil moisture and analysis of the main factors that affect the results of the models. Subsequently, verified the possible impacts of previous soil moisture on runoff generation. Did this done in two ways: i) analyzing 104 rainfall-runoff events that occurred during four years of monitoring; ii) using the antecedent soil moisture as an input parameter in the simulations of 15 rainfall-runoff events with an event-based distributed physical model, the OpenLISEM (open source Limburg Soil Erosion Model). The results indicate that the soil moisture models performed well and could satisfactorily estimate the soil moisture for both layers. While the climate-related variables are the most important for the performance of the surface model, for the subsurface layer, the soil-related variables are the most important. A clear threshold between the antecedent soil moisture and the runoff coefficient was not observed in the Arroio do Ouro catchment. However, the highest runoff coefficients were recorded in events whose antecedent soil moisture was close to or greater than field capacity. The use of antecedent moisture as an input parameter in the simulations with OpenLISEM proved to be promising, given the solid results found during the model validation stage. Even considering the uncertainties associated with the antecedent soil moisture estimates, it was possible to represent the form of complex hydrographs.

Keywords: Soil moisture. Artificial neural networks. Runoff. OpenLISEM. Small watershed

LISTA DE FIGURAS

LISTA DE TABELAS

SUMÁRIO

CAPÍTULO 1

1.1 Introdução

A umidade do solo tem um papel crucial nos componentes do ciclo hidrológico. Sobretudo, esta variável governa a troca de água e energia entre a superfície terrestre e a atmosfera (Bogena et al., 2015). Ela contribui com o fornecimento de vapor d'água para a atmosfera a partir da evaporação em solos descobertos ou evapotranspiração da vegetação, tendo um efeito positivo na geração das chuvas (Corradini, 2014). Além disso, as características hidráulicas do solo, em conjunto com o teor de água presente no solo, influenciam na capacidade de armazenamento da água no solo e, consequentemente, a geração de escoamento (Uber et al., 2018). Desta forma, uma série de aplicações se beneficiam das informações de umidade do solo, como as previsões de inundações, deslizamentos de terra e manejo de irrigação (Brocca et al., 2017).

Diversos processos hidrológicos estão associados à condição de umidade do solo e às características dos eventos de precipitação. Além disso, estes processos são dependentes da escala de observação. À medida que a escala passa de local para regional, os processos tornam-se mais complexos. Na escala pontual até a escala de parcela, são representados principalmente os fenômenos superficiais (e.g. escoamento superficial), e os processos de infiltração relacionados às características de solo (Sidle et al., 2017).

Os processos hidrológicos em escala de vertente (*hillslope*) são integrados pelos efeitos da precipitação, propriedades físico-hídricas do do solo, condições da superfície do solo, vegetação, fluxo subsuperficial e dinâmica de fluxos preferenciais, que redistribuem a água do escoamento superficial e subsuperficial (Sidle et al., 2017, 2000). Dentre outros fatores que influenciam o comportamento do fluxo subsuperficial, a condição de umidade antecedente do solo, e do volume e intensidade da precipitação, foram constatados em vários estudos (Guo et al., 2014; Liao et al., 2016; Newman et al., 1998; Penna et al., 2011). Uma maior umidade do solo promove a conexão entre os caminhos de fluxo preferenciais (Sidle et al., 2001). Com o incremento da área saturada, aumenta o número de caminhos de fluxo preferenciais ativos,

gerando um fluxo subsuperficial maior na vertente (Sidle et al., 2000). Assim, com o solo mais úmido, os caminhos preferenciais ficam mais conectados, sendo necessário um volume menor de precipitação para ativar o fluxo preferencial subsuperficial (Guo et al., 2014).

Já na escala de bacia hidrográfica (escala de observação utilizada neste estudo) os processos hidrológicos são controlados pelo solo, geomorfologia, regime climático e vegetação (Sidle et al., 2017). A interação existente entre a vertente e a rede de drenagem é crucial na resposta hidrológica em ambientes mais complexos como bacias hidrográficas (Cammeraat, 2004; Sidle et al., 2017). Desta forma, a condição de umidade do solo pode afetar a conectividade da encosta com a rede de drenagem em uma bacia hidrográfica. Algumas encostas podem permanecer conectadas à rede de drenagem durante todo o tempo, enquanto outras, apenas durante períodos mais úmidos ou em grandes eventos de precipitação (Jencso et al., 2009).

Além da umidade do solo, a influência da intensidade da precipitação no escoamento é notadoa como um fator importante em trabalhos conduzidos em bacias hidrográficas de regiões semiáridas (Cammeraat, 2004; Cantón et al., 2001; Mayor et al., 2011), e temperadas (Ares et al., 2016; Gomi et al., 2008; Penna et al., 2015). Além da geração de escoamento subsuperficial, destacam-se outros dois processos de geração de escoamento superficial em uma bacia hidrográfica: i) quando a intensidade das chuvas excede a capacidade de infiltração de água no solo, o escoamento é dependente da intensidade da chuva e das características da camada superficial do solo; ii) quando a capacidade de armazenamento de água no solo é excedida ocorre o escoamento superficial de saturação, sendo o escoamento dependente da lâmina de precipitação (Scherrer et al., 2007).

Em bacias hidrográficas, também é observado o efeito das ações antrópicas sobre a geração de escoamento, principalmente aquelas relacionadas a modificações no terreno (construção de terraços, canais de drenagem, estradas, etc.) (Bracken et al., 2013). A construção de terraços em áreas agrícolas pode trazer benefícios como o aumento da infiltração de água no solo e a redução do escoamento e vazão de pico (Londero et al., 2018). Já as estradas modificam os padrões de drenagem e de geração de escoamento,

devido à concentração do escoamento gerado sobre a superfície, e à interceptação do fluxo subsuperficial (Montgomery, 1994).

Dependendo das características de uma bacia hidrográfica, todos os processos acima descritos podem ocorrer de forma conjunta, com maior ou menor importância. No entanto, informações de longo prazo sobre a umidade do solo são escassas e distribuídas de maneira não uniforme (Sungmin and Orth, 2021). Por exemplo, a *International Soil Moisture Network* (ISMN), uma rede global que reúne medições *in situ* de umidade do solo, coletadas e compartilhadas gratuitamente, apresenta 73% dos dados que estão em seu repositório, oriundos da América do Norte, Europa e Ásia (Dorigo et al., 2021). No Brasil, a rede de monitoramento de umidade do solo do Centro Nacional de Monitoramento e Alertas de Desastres Naturais (CEMADEN) é restrita à região do semiárido (Zeri et al., 2020). Além disso, mesmo em bacias hidrográficas experimentais, o monitoramento da umidade do solo é muito limitado (Melo et al., 2020).

Esta pesquisa foi desenvolvida em uma pequena bacia hidrográfica experimental no sul do Brasil. A bacia hidrográfica do Arroio do Ouro é monitorada desde 2013 permanentemente. Possui a coleta de dados de precipitação em três locais distintos, além de duas seções de monitoramento de nível, velocidade e vazão. Para contornar a indisponibilidade de medidas de umidade do solo para este estudo, foram realizadas campanhas de amostragem. Em seguida, foi desenvolvido um modelo de redes neurais artificiais para a estimativa consistente da umidade do solo, além de analisados os possíveis impactos da umidade antecedente do solo na geração de escoamento.

1.2 Objetivos

O objetivo deste estudo é avaliar os principais fatores que contribuem para a dinâmica da umidade do solo na camada superficial e subsuperficial e a sua influência na geração de escoamento superficial em uma pequena bacia hidrográfica no sul do Brasil. Para atingir o objetivo geral, os seguintes objetivos específicos foram propostos:

- Avaliar a capacidade de modelos de redes neurais em estimar a umidade do solo para a camada superficial e subsuperficial;
- Analisar quais foram as variáveis mais importantes para prever a dinâmica da umidade do solo na camada superficial e subsuperficial;
- Investigar os efeitos da precipitação e da umidade antecedente do solo na geração de escoamento;
- Verificar a existência de um limiar claro entre a umidade antecedente do solo e o coeficiente de escoamento;
- Investigar a utilização dos dados de umidade do solo provenientes dos modelos de redes neurais para a calibração e validação dos hidrogramas simulados com o modelo OpenLISEM.
- Avaliar os efeitos das incertezas das estimativas da umidade antecedente do solo nos hidrogramas simulados com o modelo OpenLISEM.

1.3 Organização da Tese

Para alcançar os objetivos deste estudo, esta tese está organizada em seis capítulos, sendo três na forma de artigos (Capítulos 2 ao 4). Estes manuscritos estão publicados, submetidos ou aguardado submissão. Na Figura 1.1 é apresentada uma visão geral dos estudos abordados em cada capítulo e a relação entre eles. As referências estão apresentadas no final de cada capítulo. No capítulo 1 é apresentada uma introdução geral com os aspectos relacionados à dinâmica da umidade do solo em diferentes escalas de

observação até o nível de bacia hidrográfica. Também são relatados os objetivos desta pesquisa. No capítulo 5 são retomadas as conclusões obtidas durante esta pesquisa e são comentadas as limitações encontradas neste estudo. Já o capítulo seis possui o apêndice A, cujo conteúdo possui informações quanto as características do solo da região do estudo e o uso e cobertura do solo na bacia hidrográfica do Arroio do Ouro.

No capítulo 2 foi avaliado o desempenho das redes neurais artificiais (RNAs), na modelagem da umidade do solo a partir de informações climáticas, propriedades do solo, características topográficas e variáveis relacionadas à precipitação. Além de analisar a dinâmica espacial e temporal da umidade do solo e os principais fatores que controlam esse processo, tanto na camada superficial como na subsuperficial. Para isso, intensas campanhas de monitoramento da umidade do solo foram realizadas, na bacia hidrográfica do Arroio do Ouro. Referência para este capítulo:

- Bartels, G.K., Castro, N.M. dos R., Pedrollo, O., Collares, G.L., 2021. Soil moisture estimation in two layers for a small watershed with neural network models: Assessment of the main factors that affect the results. CATENA 207, 105631. https://doi.org/10.1016/j.catena.2021.105631

No capítulo 3 é apresenta uma investigação da relação entre a umidade do solo, a chuva e o escoamento na bacia hidrográfica do Arroio do Ouro. Nela, são avaliados os possíveis impactos da umidade antecedente do solo no coeficiente de escoamento. Para isso, foram analisados 104 eventos de chuva – vazão, que ocorreram durante 4 anos de monitoramento (8/2017 – 9/2021). Possível referência para este capítulo:

- Bartels, G.K., Castro, N.M.D.R., Collares, G.L., 2021. Influence of Initial Soil Moisture and Precipitation on Runoff Generation in a Small Catchment. Hydrological Sciences Journal. (Submetido)

No capítulo 4 foi investigada a utilização da abordagem de estimativa da umidade antecedente do solo a partir dos modelos desenvolvidos no capítulo 2, para a calibração e validação de hidrogramas simulados com o OpenLISEM (open source Limburg Soil Erosion Model). Também foram avaliados os efeitos das incertezas associadas à estimativa da umidade antecedente do solo. Para

melhor representação da bacia hidrográfica, foi utilizado um banco de dados de alta qualidade relacionado às propriedades físicas de solo, e um modelo digital de elevação (DEM) mais detalhado (resolução de 5 m). Possível referência para este capítulo:

- Bartels, G.K., Castro, N.M.D.R., Collares, G.L., 2021. Runoff generation and the relevance of initial soil moisture: consequences of hydrographs simulated with the OpenLISEM in a small catchment. CATENA. (Aguardando submissão)

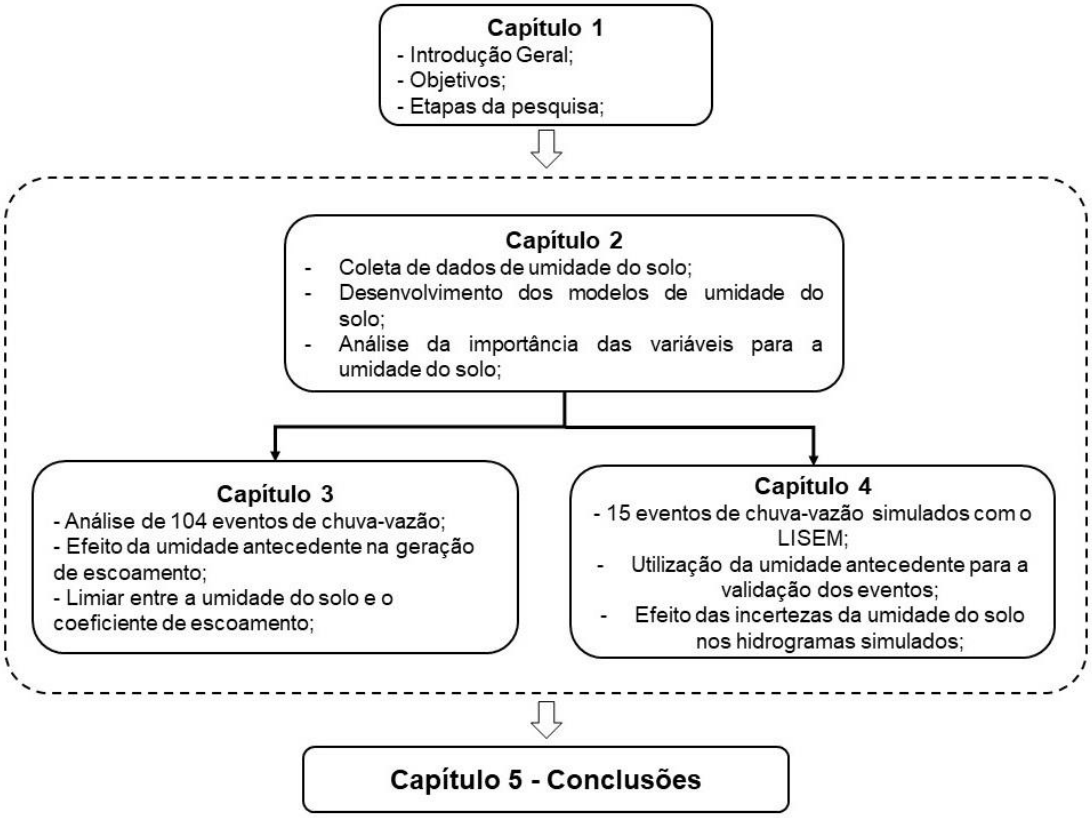

Figura 1.1 - Fluxograma da organização da pesquisa, com as principais etapas realizadas em cada capítulo.

Referências

Ares, M.G., Bongiorno, F., Holzman, M., Chagas, C., Varni, M., Entraigas, I., 2016. Water erosion and connectivity analysis during a year with high precipitations in a watershed of Argentina. Hydrol. Res. 47, 1239–1252. https://doi.org/10.2166/nh.2016.179

Bogena, H.R., Huisman, J.A., Güntner, A., Hübner, C., Kusche, J., Jonard, F., Vey, S., Vereecken, H., 2015. Emerging methods for noninvasive sensing

of soil moisture dynamics from field to catchment scale: a review. WIREs Water 2, 635–647. https://doi.org/10.1002/wat2.1097

Bracken, L.J., Wainwright, J., Ali, G.A., Tetzlaff, D., Smith, M.W., Reaney, S.M., Roy, A.G., 2013. Concepts of hydrological connectivity: Research approaches, pathways and future agendas. Earth-Science Rev. 119, 17–34. https://doi.org/10.1016/j.earscirev.2013.02.001

Brocca, L., Ciabatta, L., Massari, C., Camici, S., Tarpanelli, A., 2017. Soil Moisture for Hydrological Applications: Open Questions and New Opportunities. Water 9, 140. https://doi.org/10.3390/w9020140

Cammeraat, E.L.H., 2004. Scale dependent thresholds in hydrological and erosion response of a semi-arid catchment in southeast Spain. Agric. Ecosyst. Environ. 104, 317–332. https://doi.org/10.1016/j.agee.2004.01.032

Cantón, Y., Domingo, F., Solé-Benet, A., Puigdefábregas, J., 2001. Hydrological and erosion response of a badlands system in semiarid SE Spain. J. Hydrol. 252, 65–84. https://doi.org/10.1016/S0022-1694(01)00450-4

Corradini, C., 2014. Soil moisture in the development of hydrological processes and its determination at different spatial scales. J. Hydrol. 516, 1–5. https://doi.org/10.1016/j.jhydrol.2014.02.051

Dorigo, W., Himmelbauer, I., Aberer, D., Schremmer, L., Petrakovic, I., Zappa, L., Preimesberger, W., Xaver, A., Annor, F., Ardö, J., Baldocchi, D., Bitelli, M., Blöschl, G., Bogena, H., Brocca, L., Calvet, J., Camarero, J.J., Capello, G., Choi, M., Cosh, M.C., van de Giesen, N., Hajdu, I., Ikonen, J., Jensen, K.H., Kanniah, K.D., de Kat, I., Kirchengast, G., Kumar Rai, P., Kyrouac, J., Larson, K., Liu, S., Loew, A., Moghaddam, M., Martínez Fernández, J., Mattar Bader, C., Morbidelli, R., Musial, J.P., Osenga, E., Palecki, M.A., Pellarin, T., Petropoulos, G.P., Pfeil, I., Powers, J., Robock, A., Rüdiger, C., Rummel, U., Strobel, M., Su, Z., Sullivan, R., Tagesson, T., Varlagin, A., Vreugdenhil, M., Walker, J., Wen, J., Wenger, F., Wigneron, J.P., Woods, M., Yang, K., Zeng, Y., Zhang, X., Zreda, M., Dietrich, S., Gruber, A., van Oevelen, P., Wagner, W., Scipal, K., Drusch, M., Sabia, R., 2021. The International Soil Moisture Network: serving Earth system science for over a decade. Hydrol. Earth Syst. Sci. 25, 5749–5804. https://doi.org/10.5194/hess-25-5749-2021

Gomi, T., Sidle, R.C., Miyata, S., Kosugi, K., Onda, Y., 2008. Dynamic runoff connectivity of overland flow on steep forested hillslopes: Scale effects and runoff transfer. Water Resour. Res. 44, 1–16. https://doi.org/10.1029/2007WR005894

Guo, L., Chen, J., Lin, H., 2014. Subsurface lateral preferential flow network revealed by time-lapse ground-penetrating radar in a hillslope. Water Resour. Res. 50, 9127–9147. https://doi.org/10.1002/2013WR014603

Jencso, K.G., McGlynn, B.L., Gooseff, M.N., Wondzell, S.M., Bencala, K.E., Marshall, L.A., 2009. Hydrologic connectivity between landscapes and streams: Transferring reach- and plot-scale understanding to the catchment scale. Water Resour. Res. 45, 1–16.

https://doi.org/10.1029/2008WR007225

Liao, K.-H., Lv, L.-G., Yang, G.-S., Zhu, Q., 2016. Sensitivity of simulated hillslope subsurface flow to rainfall patterns, soil texture and land use. Soil Use Manag. 32, 422–432. https://doi.org/10.1111/sum.12282

Londero, A.L., Minella, J.P.G., Deuschle, D., Schneider, F.J.A., Boeni, M., Merten, G.H., 2018. Impact of broad-based terraces on water and sediment losses in no-till (paired zero-order) catchments in southern Brazil. J. Soils Sediments 18, 1159–1175. https://doi.org/10.1007/s11368-017-1894-y

Mayor, Á.G., Bautista, S., Bellot, J., 2011. Scale-dependent variation in runoff and sediment yield in a semiarid Mediterranean catchment. J. Hydrol. 397, 128–135. https://doi.org/10.1016/j.jhydrol.2010.11.039

Melo, D.C.D., Anache, J.A.A., Almeida, C. das N., Coutinho, J. V., Ramos Filho, G.M., Rosalem, L.M.P., Pelinson, N.S., Ferreira, G.L.R.A., Schwamback, D., Calixto, K.G., Siqueira, J.P.G., Duarte-Carvajalino, J.C., Jhunior, H.C.S., Nóbrega, J.D., Morita, A.K.M., Leite, C.M.C., Guedes, A.C.E., Coelho, V.H.R., Wendland, E., 2020. The big picture of field hydrology studies in Brazil. Hydrol. Sci. J. 65, 1262–1280. https://doi.org/10.1080/02626667.2020.1747618

Montgomery, D.R., 1994. Road surface drainage, channel initiation, and slope instability. Water Resour. Res. 30, 1925–1932. https://doi.org/10.1029/94WR00538

Newman, B.D., Campbell, A.R., Wilcox, B.P., 1998. Lateral subsurface flow pathways in a semiarid Ponderosa pine hillslope. Water Resour. Res. 34, 3485–3496. https://doi.org/10.1029/98WR02684

Penna, D., Tromp-van Meerveld, H.J., Gobbi, A., Borga, M., Dalla Fontana, G., 2011. The influence of soil moisture on threshold runoff generation processes in an alpine headwater catchment. Hydrol. Earth Syst. Sci. 15, 689–702. https://doi.org/10.5194/hess-15-689-2011

Penna, D., van Meerveld, H.J., Oliviero, O., Zuecco, G., Assendelft, R.S., Dalla Fontana, G., Borga, M., 2015. Seasonal changes in runoff generation in a small forested mountain catchment. Hydrol. Process. 29, 2027–2042. https://doi.org/10.1002/hyp.10347

Scherrer, S., Naef, F., Fach, A.O., Cordery, I., 2007. Formation of runoff at the hillslope scale during intense precipitation. Hydrol. Earth Syst. Sci. 11, 907–922. https://doi.org/10.5194/hess-11-907-2007

Sidle, R.C., Gomi, T., Loaiza Usuga, J.C., Jarihani, B., 2017. Hydrogeomorphic processes and scaling issues in the continuum from soil pedons to catchments. Earth-Science Rev. 175, 75–96. https://doi.org/10.1016/j.earscirev.2017.10.010

Sidle, R.C., Noguchi, S., Tsuboyama, Y., Laursen, K., 2001. A conceptual model of preferential flow systems in forested hillslopes: evidence of self-organization. Hydrol. Process. 15, 1675–1692. https://doi.org/10.1002/hyp.233

Sidle, R.C., Tsuboyama, Y., Noguchi, S., Hosoda, I., Fujieda, M., Shimizu, T., 2000. Stormflow generation in steep forested headwaters: a linked

hydrogeomorphic paradigm. Hydrol. Process. 14, 369–385. https://doi.org/10.1002/(SICI)1099-1085(20000228)14:3<369::AID-HYP943>3.0.CO;2-P

Sungmin, O., Orth, R., 2021. Global soil moisture data derived through machine learning trained with in-situ measurements. Sci. Data 8, 1–14. https://doi.org/10.1038/s41597-021-00964-1

Uber, M., Vandervaere, J.-P., Zin, I., Braud, I., Heistermann, M., Legoût, C., Molinié, G., Nord, G., 2018. How does initial soil moisture influence the hydrological response? A case study from southern France. Hydrol. Earth Syst. Sci. 22, 6127–6146. https://doi.org/10.5194/hess-22-6127-2018

Zeri, M., Costa, J.M., Urbano, D., Cuartas, L.A., Ivo, A., Marengo, J., dos Santos Alvalá, R.C., 2020. A soil moisture dataset over the Brazilian semiarid region. Mendeley Data, V2. https://doi.org/10.17632/xrk5rfcpvg.2

CAPÍTULO 2

Soil moisture estimation in two layers for a small watershed with neural network models: Assessment of the main factors that affect the results

Guilherme Kruger Bartels[a], Nilza Maria dos Reis Castro[a], Olavo Correa Pedrollo[a], Gilberto Loguercio Collares[b]

[a] Instituto de Pesquisas Hidráulicas, Universidade Federal do Rio Grande do Sul (Institute of Hydraulic Research, Federal University of Rio Grande do Sul - IPH/UFRGS), Av. Bento Gonçalves, 9500, Porto Alegre - RS, Brazil

[b] Centro de Desenvolvimento Tecnológico, Universidade Federal de Pelotas (Center for Technological Development, Federal University of Pelotas - CDTec/UFPel), Rua Gomes Carneiro 01, Pelotas - RS, Brazil

Abstract

Soil moisture, which impacts various hydrological processes, can be estimated from point measurements in a watershed or via remote sensing. As both methods are expensive and complex, efforts have been made to develop empirical models based on data that affect the occurrence of soil moisture. However, these models have been based only on surface-layer data. We present an original approach for investigating regional empirical models of soil moisture, both for the surface (0–10 cm) and subsurface (10–20 cm) layers, and evaluate the main factors which affect the model results. Based on data about the climate, soil properties, topographic features and rainfall, we applied artificial neural network soil-moisture models for a small watershed, in southern Brazil. The models for each layer, with all selected variables, showed Nash-Suitcliffe coefficients of 0.870 and 0.893, respectively, for the surface and subsurface models. We then tested the effects of removing each variable or categories of variables. The most important variables for the surface model were the season, followed by exponential weighted moving average (EWMA) of rainfall. For the subsurface model, the most important variables were the

season (although less so than for the surface model), followed by microporosity. All of the variable categories were important in the surface model. In the subsurface model, the soil-related variables were the most important, whereas the rainfall and topography variables were of little importance. It was possible to estimate soil moisture for both layers with good performance. The subsurface model, which used only the soil- and climate-related variables, explained more of the variance in soil moisture than the other models. The subsurface layer is easier to model, because the variation in moisture that is induced by recent climate and precipitation effects is attenuated by the physical features of the soil which control water infiltration.

Keywords: Surface and subsurface layer; Soil physical properties; Climatic variables; Topographic variables; Rainfall-related variables

2.1 Introduction

Soil moisture is characterized as a key hydrological and ecological variable of the Earth's surface systems (Gao et al., 2013). Above all, it governs the exchange of energy and water between the surface of the earth and the atmosphere, controlling hydrological, meteorological, and ecological processes (Cho and Choi, 2014, Pan et al., 2017). Including soil moisture in hydrological models significantly reduces their uncertainty, enhancing watershed flood prediction (e.g. Alvarez-garreton et al., 2014, Berthet et al., 2009, Massari et al., 2014, Meng et al., 2017, Tayfur et al., 2014, Wooldridge et al., 2003, Zhong et al., 2019). Hydrological models for watershed soil moisture estimation have many potential applications.

However, soil moisture presents high spatial and temporal variability (Gao et al., 2013, Huang et al., 2016, Suo et al., 2018, Zhu et al., 2014), produced by the effects of climate, soil, topography and vegetation (Hagen et al., 2020, Li et al., 2013). Soil properties such as density, organic matter content, texture, structure and macroporosity impact water retention and transport in the soil column (Famiglietti et al., 1998). Features linked to the land cover, root system and plant litter layer impact hydrological aspects such as seepage, surface runoff, interception and evapotranspiration (Jacobs et al., 2004). Topography

plays a key role in determining the spatial distribution of soil moisture. In watersheds, steep parts tend to be dryer than flat parts, due to their lower infiltration rates, faster subsurface drainage, and higher surface runoff (Famiglietti et al., 1998). Further, concave surface areas are more humid than convex areas, due to the accumulation of surface and subsurface lateral flow in the surrounding area (Rosenbaum et al., 2012, Zhu et al., 2014). Aspect (hillslope orientation) affects the sun's angle of incidence, and consequently impacts water evaporation (Famiglietti et al., 1998, Moore et al., 1988), altering soil moisture. Grayson et al. (1997) analysed spatial patterns of water distribution during humid periods (when rainfall exceeds evapotranspiration) and dry periods (when evapotranspiration exceeds rainfall) in two Australian catchment areas. In the humid periods, the water movement was mostly surface and subsurface lateral movement, and was mostly determined by topography; in the dry periods, most of the flows were vertical, and the spatial distribution of soil moisture was determined mostly by the soil properties and topography of highly converging areas, such as highly curved depressions (Grayson et al. 1997).

Soil water content is conventionally measured via sample collection and drying (the gravimetric method). However, although this method is reliable, it is impractical because it requires destructive sampling, and has high costs, both in terms of labour and time (Elshorbagy and Parasuraman, 2008, Topp et al., 1984). Devices such as neutron probes, electromagnetic sensors and heat pulse tracers are used to obtain in situ point-specific soil moisture data (Gao et al., 2013, Robinson et al., 2008). Time Domain Reflectometry (TDR) is a noteworthy method; this approach determines soil moisture by measuring the dielectric constant following an electromagnetic pulse emission (Topp et al., 1984).

In the last decade, the use of remote sensing applied to large areas (river basins larger than 2,500 km^2) has increased, with the launch of projects to study soil moisture, such as Soil Moisture and Oceans Salinity (SMOS) and Soil Moisture Active Passive (SMAP) (McCabe et al., 2017). The use of point-specific measurements via in situ sensors has increased. Nonetheless, there remains a gap in the assessment of intermediate-scale areas, for which information on watershed characteristics, including spatiotemporal soil-moisture

dynamics, is lacking (Robinson et al., 2008, Western et al., 2002). For intermediate scales (subwatersheds or small watersheds of 1–80 km^2; Robinson et al., 2008), the understanding of soil moisture is limited, both by the lack of in situ soil moisture measurements, and because of the complexity of the watershed environments, which are characterized by a range of soil types, diverse topography and multiple land-use types (Hagen et al., 2020). Therefore, the use of data-driven models such as artificial neural networks (ANNs) are an efficient alternative for soil moisture modelling and for examining related problems at small watersheds.

ANNs for modelling soil moisture typically use remote sensing data for large areas (Cui et al., 2016, Hachani et al., 2019, Rodriguez-Fernandez et al., 2015, Santi et al., 2016, Yao et al., 2017), and point-specific data for small catchment areas (smaller than 1 km^2 area), based on meteorological parameters, soil properties, land use and topographic features (Arsoy et al., 2013, Contador et al., 2006, Elshorbagy and Parasuraman, 2008, Oliveira et al., 2021, Yang et al., 2018). However, very few studies have addressed intermediate-scale catchments (Al-mukhtar, 2016, Gill et al., 2006, Oliveira et al., 2017). For instance, Oliveira et al. (2017) used ANNs to analyse spatiotemporal variation in SWC in a 78 km^2 watershed in Brazil, based on climate data, soil physical properties and topographic variables. The results show that it is possible to estimate SWC efficiently (Nash-Sutcliffe statistic (NS) = 0.770) using topographic data, soil physical properties and rainfall. Alternatively, SWC can be estimated via simplified models using rainfall and topographic information, although with less satisfactory performance (NS = 0.65). However, Oliveira et al. (2017) modelled soil moisture for only the surface layer, leaving a knowledge gap that will be addressed by modelling of the subsurface layer.

The primary purpose of this research was to assess the ability of regional empirical soil moisture models to predict both surface and subsurface layer dynamics, using data on climate, soil properties, topographic features, and rainfall, for a small watershed. Further, we evaluated which variables are most important in determining the performance of these models. To do this, we used ANN modelling with the Multilayer Perceptron (MLP) architecture, due to its

relative simplicity and high capacity for approximating nonlinear relationships (Hornik et al., 1989).

2.2 Materials and methods

2.2.1 Study area

The study was performed in the Arroio do Ouro watershed, with an area of 17.17 km^2, in the state of Rio Grande do Sul, Brazil (Figure 2.1). The elevation ranges from 76 to 326 m above sea level; the mean slope is 7.4°, and it can reach up to 30° (Bartels et al., 2021). The region is located at the Pelotas batholith, a plutonic complex which includes granite, gabbro and diorite, located in the Dom Feliciano belt geotectonic unit, in southern Brazil (Philipp et al., 2016). The soils are considered Acrisols and Regosols, distinguished for being shallow and predominantly containing sandy loam (35%−75% sand), based on World Reference Base ratings (FAO, 2014) (Bartels et al., 2016; see also Figure 2.2b). The climate is humid subtropical (Cfa in the Köppen classification), with hot summers and well distributed rainfall throughout the entire year (Peel et al., 2007). Annual rainfall is 1400 ± 299 mm, annual reference evapotranspiration is 1077 ± 33 mm, and mean annual temperature is 18.5 ± 0.5 °C (1971–2018).

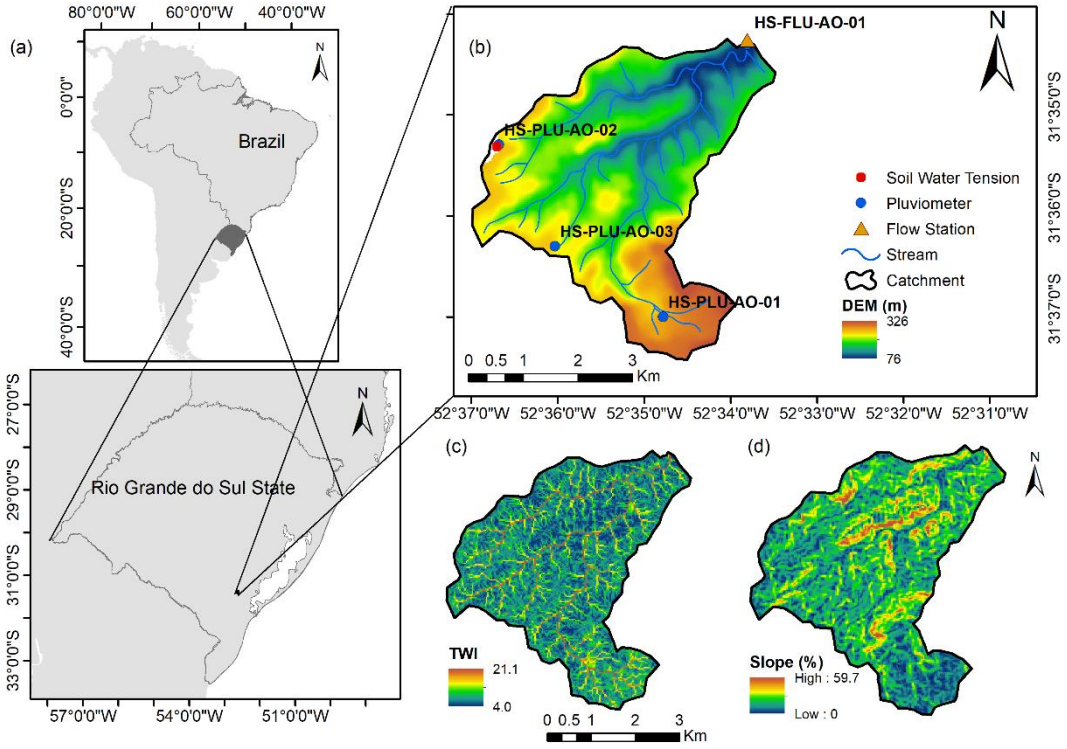

Figure 2.1 - (a) Study area in the State of Rio Grande do Sul, Brazil; (b) Arroio do Ouro watershed showing digital elevation model, streams (blue lines) and the locations of the tensiometer (red point), rain gauges (blue points) and flow station (yellow triangle); (c) Topographic wetness index (TWI); (d) Slope.

Dry/wet variation results from the interaction of precipitation and evapotranspiration (Hu et al., 2018). Thus, drought indices have been widely used for monitoring local dry and wet conditions. We applied two indices – the Standardized Precipitation Index (SPI) (McKee et al., 1993) and the Standardized Precipitation Evapotranspiration Index (SPEI) (Vicente-Serrano et al., 2010) – to evaluate the representativeness of the soil moisture monitoring period, using a long time series (1971–2019). Although we tested these indices at various time scales (e.g., 1, 3, 6, and 12 months; supplementary material section), we analysed only at the one-month scale in this study, because of the strong correlations found with soil moisture (Scaini et al., 2015).

2.2.2 Soil moisture measurement

Surface (0−10 cm) and subsurface (10−20 cm) soil samples were collected at 39 points at the site (Figure 2.2), from 28 February 2018 to 3

September 2018, during ten surveys (Figure 2.3). In each survey, soil samples were collected over four consecutive days (two surveys) and five consecutive days (eight surveys), totalling 24 soil samples per layer at each of the 39 measurement points. In total, 936 samples were collected from each layer. As it was not possible to sample all points in a single day, it was necessary to divide the 39 sampling points into two sets: set A with 18 points, and set B with 21 points (Figure 2.2a).

Gravimetric soil moisture determination (the ratio between water mass and dry soil mass) was performed in a lab, by weighing the wet samples, then drying them in a drying oven at 105 °C for a minimum time of 24h, and weighing the dried samples. The median soil moisture value obtained from triplicate measurements was used in network training and validation, avoiding possible errors associated with extreme values.

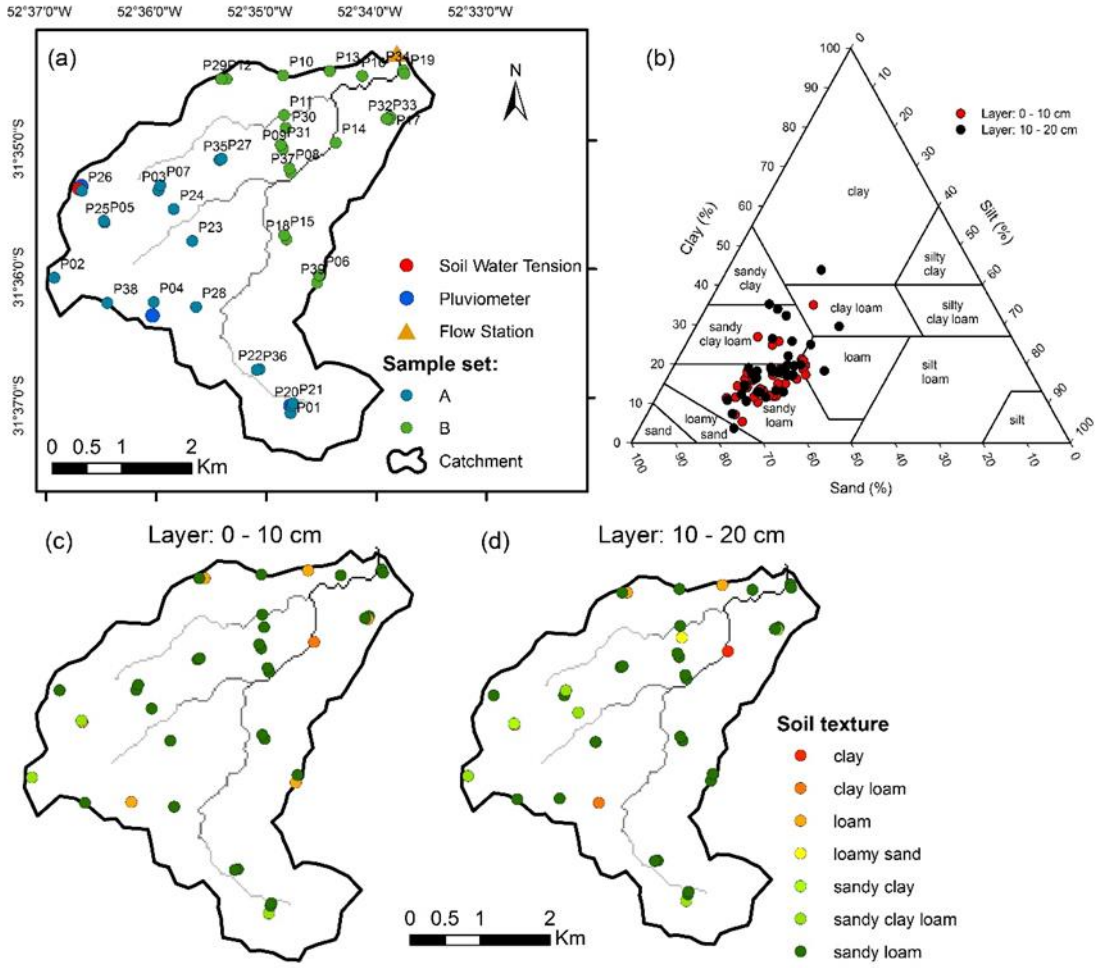

Figure 2.2 - (a) Soil moisture at the 39 monitoring points, divided spatially into two sets (A and B), so that one set could be sampled on one day; (b) Soil

texture at the 39 points at the surface (red dots) and subsurface (black dots); (c, d) Soil texture rating at the 39 points for the surface and subsurface, respectively.

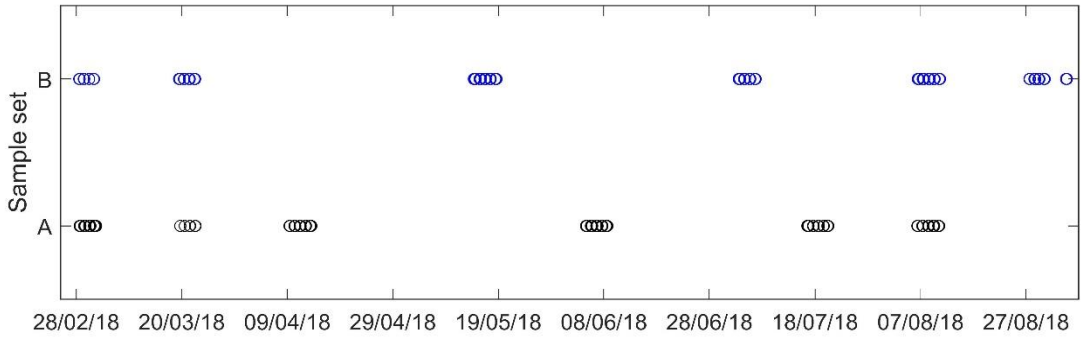

Figure 2.3 - Soil moisture monitoring for the samples from sets A and B, from 28 February to 3 September, 2018. Sets A and B were divided spatially to enable sampling of one set on one day.

2.2.3 Model input variables

In total, 48 input variables were tested using ANN models, to select those variables that improved the estimation of soil moisture spatial and temporal variability. The variables were divided in four categories: (i) Topography (6 variables); (ii) Soil properties and land use and cover (14); (iii) Climatic variables (17); and (iv) rainfall-related variables (11).

2.2.3.1 Topographic variables

Six topographic variables were tested; four reflect point-related features (elevation, slope, distance from sample point to the closest river reach, and difference in elevation between the sampling point and the closest river reach). The two others, terrain curvature and topographic wetness index (TWI), are associated with the water mass, which is proportional to the contributing area, and its momentum, which is proportional to the slope (Contador et al., 2006). TWI was originally drafted by Beven and Kirkby (1979), calculated as follows:

$$TWI = \ln\left(\frac{\alpha}{\tan\beta}\right) \quad (1)$$

where α represents the upstream contribution area per unit contour length (specific area) and β is the local slope.

All topographic variables were extracted from the digital elevation model, with a spatial resolution of 30 m. The topographic variables are described in Table S2.1, and their descriptive statistics are presented in Table 2.1.

Table 2.1 - Topography, climate, and rainfall-related variable categories that were used as input for the artificial neural network models, and the model output (soil moisture), for the surface and subsurface soil layers.

Nº	Variable	Categories	Minimum	Maximum	Mean	Median	SD
1	Elevation (m)		94.00	269.00	188.26	188.00	48.45
2	Slope (%)		1.37	39.17	13.47	10.70	9.15
3	[1]TWI (-)	Topography	4.34	13.37	7.01	6.41	2.00
4	Curvature (-)		-1.32	1.44	0.03	0.12	0.63
5	[2]DTR (m)		15.70	533.50	193.96	157.80	129.68
6	[3]DNR (m)		0.00	84.00	22.59	21.00	20.16
7	[4]Season (-)		-	-	-	-	-
8	Min. air temp. (ºC)		2.40	20.90	11.84	11.10	4.83
9	Max. air temp. (ºC)		9.20	32.60	20.89	21.30	6.39
10	Mean air temp. (ºC)		6.33	25.80	15.91	15.34	5.17
11	Min. Rel. humid. (%)		24.80	99.70	64.00	61.40	18.51
12	Max. Rel. humid. (%)		82.30	100.00	98.91	100.00	3.44
13	Mean Rel. humid. (%)		55.71	100.00	86.14	87.85	10.58
14	Soil Temp. 5 cm (ºC)		9.10	28.30	17.59	16.20	5.48
15	Global solar radiation (cal.cm^{-2} day^{-1})	Climate	27.00	564.70	273.77	260.80	158.34
16	[5]ETo (mm)		0.40	5.00	2.30	2.35	1.32
17	[6]Cum. ETo with 5 days (mm)		2.70	21.20	11.68	10.80	5.00
18	[6] Cum. ETo with 7 days (mm)		6.30	27.90	16.12	14.15	6.79
19	[6] Cum. ETo with 14 days (mm)		15.10	60.10	31.66	27.25	14.26
20	[6] Cum. ETo with 21 days (mm)		23.00	90.30	47.28	40.20	21.49
21	[6] Cum. ETo with 30 days (mm)		38.00	139.70	70.87	60.00	32.34
22	[6] Cum. ETo with 45 days (mm)		60.00	207.80	110.38	86.50	52.06
23	[6] Cum. ETo with 60 days (mm)		83.90	287.20	154.92	131.15	72.24
24	[7] Cum. rainfall with 6 h (mm)		0.00	18.45	1.24	0.00	3.38
25	[7] Cum. rainfall with 12 h (mm)		0.00	26.79	2.33	0.00	5.29
26	[8] Cum. rainfall with 1 day (mm)		0.00	29.73	4.93	0.11	8.01
27	[8] Cum. rainfall with 2 days (mm)	Rainfall	0.00	100.78	11.07	3.27	18.68
28	[8] Cum. rainfall with 3 days (mm)		0.00	145.39	16.80	7.00	25.73
29	[8] Cum. rainfall with 4 days (mm)		0.00	175.27	21.24	11.80	30.32
30	[8] Cum. rainfall with 5 days (mm)		0.00	196.90	26.51	17.54	34.58
31	[8] Cum. rainfall with 10 day (mm)		1.89	198.31	43.94	42.61	37.01

32	[8] Cum. rainfall with 15 days (mm)		10.02	255.66	72.38	61.82	44.31
33	[8] Cum. rainfall with 25 days (mm)		43.89	270.40	124.65	106.35	60.45
34	[9]EWMA of past hour rainfall (mm)		0.00	1.53	0.21	0.06	0.34
-	Soil Moisture (g g^{-1}) – Layer: 0-10 cm	Output	0.013	0.438	0.193	0.192	0.074
-	Soil Moisture (g g^{-1}) – Layer: 10-20 cm		0.014	0.383	0.178	0.179	0.063

Nº: Identification of the respective variable; SD: Standard deviation; 1 Topographic wetness index; 2 Distance from sampled point to the closest river stretch; 3 Difference in elevation between the sampling point and the closest river stretch; 4 Season (summer, 1; autumn, 2; winter, 3); 5 Reference evapotranspiration (ETo); 6 Cumulative Eto over the preceding 5 to 60 days; 7 Cumulative rainfall over the preceding 6 to 12 hours; 8 Cumulative rainfall over the preceding 1 to 25 days; 9EWMA: Exponential weighted moving average.

2.2.3.2 Soil variables

The soil variable category comprises 14 variables: land use and cover; soil bulk density; macroporosity; microporosity; total porosity; clay; silt; total sand content; very coarse sand; coarse sand; medium sand; fine sand; very fine sand; and soil water tension. Except for land use and cover, these variables were collected in three replicates, of which we used the median, from the surface (0−10 cm) and subsurface (10−20 cm) layers at each point (Table S2.2).

Land use and cover was scored as follows: native forest, 1; native grassland, 2; fruit crops, 3; annual crops with vegetable covering, 4; annual crops without vegetable covering, 5; commercial forests, 6. These scores reflect the spatiotemporal variability in land use and cover.

Undisturbed soil samples were collected in metal tubes (0.076 m diameter; 344.1 cm^3 core volume) using a Uhland soil sampler, to determine soil bulk density, total porosity, macroporosity and microporosity. Soil microporosity corresponds to water retained at a pressure potential of 6 kPa (pore diameter equivalent to 50 μm), and macroporosity was calculated as the difference between total porosity and microporosity (Danielson and Sutherland, 1986). Samples were then dried for 24 h at 105 °C to determine soil bulk density (Blake and Hartge, 1986). Mean total porosity was slightly higher for the surface layer than for the subsurface layer. However, the subsurface layer exhibited higher amplitude in variation (between the maximum and minimum

microporosity) than the surface layer (Table 2.2). For the surface layer, native forest had the lowest soil bulk density and highest total porosity.

Disturbed soil samples were air-dried, sieved through a 2 mm sieve, and used to analyse soil granulometry (clay, silt, and sand percentages) using the pipette method (Gee and Bauder, 1986). Sandy loam predominated in both layers (Figure 2.2b). Soil water tension was measured daily throughout the study period using tensiometers installed in the watershed (Figure 2.1b). The tensiometers were installed with two replicates, at depths of 7 cm and 15 cm from the soil surface, to measure the surface and subsurface layers, respectively. As input into the neural network models, we used soil water tensions obtained on the same days as the sample surveys. The amplitude of variation in soil water tension was higher in the surface than in the subsurface layer (Table 2.2).

2.2.3.3 Climatic variables

Seventeen climatic variables, measured daily, were tested as inputs for the ANN models. The season variable was used, based on the season in which the soil moisture samples were collected: summer, 1; autumn, 2; and winter, 3. This approach has been performed with satisfactory results (Oliveira et al., 2017). Air relative humidity and air temperature (minimum, medium, and maximum) were obtained from two automatic stations installed in the watershed (HS-PLU-AO-01 and HS-PLU-AO-03, Figure 2.1b). The other variables – soil temperature at 5 cm depth, global solar radiation and reference evapotranspiration (ETo) – were obtained from a weather station of the Empresa Brasileira de Pesquisa Agropecuária (Brazilian Corporation of Agricultural Research - EMBRAPA), located about 17 km from the watershed (Latitude 31° 41′ S; Longitude 52° 26′ O; elevation: 57 m). ETo was calculated via the Penman-Monteith equation, as recommended by the FAO (Allen et al., 1998). Along with ETo values, another eight input variables were tested in the model (ETo on the day of soil moisture measurement, and the cumulative ETo from day 5 before soil moisture sampling (hereafter “cumulative 5-d Eto”); the same naming convention is then applied to cumulative ETo on days 7, 14, 21, 30, 45, and 60 before soil moisture sampling). The sample surveys were

conducted on days with low and high global solar radiation, which affects ETo; ETo exhibited a large range (0.4 to 5.0 mm day^{-1}) during the monitoring period (Table 2.1).

Table 2.2 - Soil characteristics used as input for the artificial neural network models.

Nº	Variable	Minimum	Maximum	Mean	Median	SD	Minimum	Maximum	Mean	Median	SD
		Layer: 0 - 10 cm					Layer: 10 - 20 cm				
35	[1]Land use and cover (-)	-	-	-	-	-	-	-	-	-	-
36	[2]BD (g cm^{-3})	0.886	1.663	1.401	1.468	0.207	1.064	1.710	1.433	1.449	0.146
37	[3]Macro (cm^3 cm^{-3})	0.050	0.313	0.156	0.132	0.079	0.039	0.305	0.146	0.135	0.074
38	[4]Micro (cm^3 cm^{-3})	0.104	0.413	0.296	0.303	0.071	0.066	0.472	0.281	0.292	0.076
39	[5]TP (cm^3 cm^{-3})	0.356	0.611	0.451	0.430	0.066	0.329	0.574	0.427	0.424	0.052
40	Soil water tension (cm Hg)	0.00	22.00	3.84	2.00	4.34	0.00	9.50	3.26	2.38	2.63
41	Clay (%)	5.37	34.92	16.42	16.19	5.51	3.67	43.82	18.86	17.82	7.87
42	Silt (%)	15.42	31.16	23.10	22.67	4.42	13.90	34.90	22.87	22.38	4.59
43	Total sand (%)	41.03	72.72	60.48	61.73	7.35	34.78	74.73	58.28	58.75	8.88
44	Very coarse sand (%)	2.56	37.79	17.30	15.16	9.31	1.34	37.51	16.29	15.72	9.28
45	Coarse sand (%)	5.69	27.21	14.22	13.62	3.52	4.27	24.54	13.78	13.74	3.50
46	Medium sand (%)	6.97	19.55	11.88	11.56	3.00	6.20	21.78	11.73	10.70	3.58
47	Fine sand (%)	8.11	20.26	13.00	12.16	3.12	3.64	21.66	12.22	11.98	3.33
48	Very fine sand (%)	0.40	9.51	4.07	3.94	2.23	0.52	8.07	4.27	4.38	2.30

Nº: Identification of the respective variable; SD: Standard deviation; [1] Land use and cover (native forest, 1; native grassland, 2; fruit crops, 3; annual crops with vegetable covering, 4; annual crops without vegetable covering, 5; commercial forests, 6); [2] Soil bulk density; [3] Macroporosity; [4] Microporosity; [5] Total porosity.

2.2.3.4 Rainfall variables

We selected 11 rainfall-related variables: cumulative rainfall in the 6 h and 12 h before soil moisture measurement (hereafter “cumulative 6-h rainfall” and “cumulative 12-h rainfall”); cumulative rainfall on day 1 before soil moisture measurement (hereafter “cumulative 1-d rainfall”; the same naming convention is then applied to cumulative rainfall on days 2, 3, 4, 5, 10, 15, and 25 before soil moisture measurement); and the exponential weighted moving average (EWMA) of rainfall. EWMA was introduced by Moore (1980) to represent soil moisture in rainfall-based models. EWMA assigns a higher weight to more recent rainfall events; it has been used (Oliveira et al. 2017) as an important variable in estimating soil moisture via ANNs.

Rainfall data were obtained from three tipping-bucket rain gauges installed in the watershed (Figure 2.1b). We calculated average rainfall over the watershed using the Thiessen polygon method,and used this in the model. Table 2.1 describes the topography, climate, and rainfall variable categories that were used as inputs for the ANN models, as well as the model output (soil moisture). Table 2.2 describes the soil-related variables used as input for the ANN models.

2.2.4 ANN models

ANNs emerged with the artificial neuron concept of McCulloch and Pitts (1943). However, it was only after the 1990s that they were applied with success to hydrology and related areas (ASCE, 2000; Dawson and Wilby, 2001). They achieved relevance following the development by Rumelhart et al. (1986) of the algorithm for training MLP networks; according to this algorithm, the set of artificial neurons is arranged into a layered structure, and the outputs from previous neural layers are used as inputs by the following neurons in determining the next output layer. An MLP network with a three-layer architecture is considered capable of approximating any continuous function to any desired degree of accuracy, if it is appropriately trained and relies on a sufficient number of neurons in the inner layer (Hornik et al., 1989). We chose it for this research because of these features.

The backpropagation algorithm (Rumelhart et al., 1986) and convergence acceleration techniques of Vogl et al. (1988) were applied to network training. However, because of their approximation capabilities, ANNs may be overly adjusted to the data, which would make the model unviable for other applications. To prevent this overfitting, the cross-validation technique (Hecht-Nielsen, 1990) was implemented, with the available dataset divided into three parts, for training, validation, and verification. In this way, one can identify the training cycle in which performance with training samples continues to improve while performance with data other than the training data decreases. Such a cycle indicates model overfitting, and the training of the network should be interrupted. Finally, the trained network is submitted to a verification sample which was not included in the training stage, to guarantee the model's capacity to generalize (Hecht-Nielsen, 1990).

Through systematic sampling, the same frequency distribution of the complete original series was maintained for training, validation, and verification sub-samples. For the training subsample, additional care was taken to ensure the representativeness of the entire data domain (extreme values), both in terms of the input and output variables (soil moisture).

At the initialization of the neural network, synaptic weights are randomly assigned to the neurons, which may result in an unfavourable beginning. Therefore, a series of repetitions is used to identify the ANN whose training results in the best validation performance.

Due to the high number of variables (48) that could be included in the input layer, we adopted an initial method to select the variables to be tested. The selection method departed from the Pearson correlation coefficient (r) between the input variables and soil moisture (Table 2.3). Variables with higher correlations with soil moisture were chosen; among them, those with a correlation among themselves below a given limit (r = 0.9) were selected. Linear correlation applied to variable selection provides an indication of which variables are worth including as inputs in the model for soil moisture estimation. However, using strongly correlated variables duplicates the information used by the model, which confuses the ANNs, often reducing network performance, as observed by Oliveira et al. (2017). We used this method for initial model

selection,and included variables that were not highly correlated with soil moisture, but that are known to be affect soil moisture dynamics.

We used a method first presented by Sari et al. (2017) to estimate the number of inner layer neurons. From an oversized network, the number of inner-layer neurons is progressively reduced until a reduction in its generalization capacity, due to the reduced degrees of freedom, is observed. The lowest number of neurons observed before the reduction in generalization capacity is chosen. This must be assessed using the validation sample, since the verification sample must not be used in the training of synaptic weights or in choosing the ANN architecture (Hecht-Nielsen, 1990).

The ANN models were developed, trained, and verified by the authors using MATLAB® R2012b. In total, 144 ANN models were tested, with different input variable combinations.

2.2.5 Evaluation of model performance

After training, validation and verification, the statistical indicators were calculated based on the errors between the observed and simulated values: mean absolute error (MAE); root mean squared error (RMSE); Nash-Sutcliffe efficiency coefficient (NS); and the quantiles of the error distribution (10, 50, and 90%). MAE, RMSE, and NS are calculated as follows:

$$MAE = \frac{1}{N}\sum_{j=1}^{N}\left|y_j - \hat{y}_j\right| \quad (2)$$

$$RMSE = \sqrt{\frac{1}{N}\sum_{j=1}^{N}(y_j - \hat{y}_j)^2} \quad (3)$$

$$NS = 1 - \sum_{j=1}^{N}(y_j - \hat{y}_j)^2 / \sum_{j=1}^{N}(y_j - \bar{y})^2 \quad (4)$$

where y_j is the *j*th observed variable; $\hat{y}_j$ is the *j*th simulated variable assessed; $\bar{y}$ is the average of all observed values, and *N* is the total number of measurements.

Since the NS coefficient represents the proportion of the variance explained by the model, the difference in NS between the complete model and

a simpler model reflects the proportion of explained variance lost by using the simpler model. Therefore, this difference can be used to quantify comparisons.

2.3 Results

2.3.1 Analysis of correlation with soil moisture

Table 2.3 presents the correlation coefficient (r) between the 48 variables and soil moisture. In both layers, soil moisture was most strongly correlated with microporosity (0.651 and 0.710) and total sand content (−0.624 and −0.671), for the surface and subsurface layers, respectively. The strong positive correlation for microporosity is understandable, because it represents the soil's water retention capacity. The opposite correlation, for the proportion of sand, makes sense because higher sand content improves soil infiltration and reduces its moisture retention capacity.

In terms of topography, soil moisture was most highly correlated with slope, followed by the difference in elevation between the sampling point and the closest river reach (negative correlations), and TWI (positive correlation; Table 2.3). A steep slope increases runoff to lower-lying regions. The highest points in the watershed had lower soil moisture than points at similar elevation as the channel network, reflecting water movement from the top hillslope towards the channel network. Further, as the upstream contributing area increases (resulting in more cumulative flow), the downstream soil moisture increases.

The climatic variables were more strongly correlated with soil moisture in the surface layer than in the subsurface layer. Compared to the climatic variables, the rainfall-related variables were less strongly correlated with soil moisture (Table 2.3). This suggests that these climatic variables affect soil moisture more than rainfall-related variables, especially at the surface layer.

Table 2.3 - Pearson linear correlation (r) between the input variables and soil moisture at the surface (0–10 cm) and subsurface (10–20 cm) layers.

Variable	*r* (0-10 cm)	r (10-20 cm)	Variable	*r* (0-10 cm)	*r* (10-20 cm)
Elevation (m)	0.163	0.155	Min. Rel. humid. (%)	0.207	0.195
Slope (%)	-0.223	-0.321	Max. Rel. humid. (%)	-0.039	-0.038
TWI (-)	0.170	0.222	Rel. humid. (%)	0.148	0.137
Curvature (-)	-0.078	-0.102	Soil Temp. 5 cm (ºC)	-0.334	-0.298
DTR (m)	-0.120	-0.178	Global solar radiation (cal cm^{-2} day^{-1})	-0.338	-0.322
DTR (m)	-0.168	-0.248	ETo (mm)	-0.332	-0.308
Land use and cover (-)	-0.419	-0.271	Cum. ETo of 5 days (mm)	-0.369	-0.349
BD (g cm^{-3})	-0.533	-0.442	Cum. ETo of 7 days (mm)	-0.379	-0.354
Macro (cm^3 cm^{-3})	-0.162	-0.371	Cum. ETo of 14 days (mm)	-0.385	-0.370
Micro (cm^3 cm^{-3})	0.651	0.710	Cum. ETo of 21 days (mm)	-0.400	-0.384
TP (cm^3 cm^{-3})	0.503	0.507	Cum. ETo of 30 days (mm)	-0.408	-0,385
Soil water tension (cm Hg)	-0,344	-0,390	Cum. ETo of 45 days (mm)	-0,419	-0,390
Clay (%)	0.492	0.557	Cum. ETo of 60 days (mm)	-0.416	-0.377
Silt (%)	0.422	0.342	Cum. rainfall of 6 h (mm)	0.148	0.151
Total sand (%)	-0.624	-0.671	Cum. rainfall of 12 h (mm)	0.229	0.232
Very Coarse sand (%)	-0.578	-0.648	Cum. rainfall of 1 day (mm)	0.256	0.256
Coarse sand (%)	-0.126	-0.193	Cum. rainfall of 2 days (mm)	0.233	0.214
Medium sand (%)	0.096	0.054	Cum. rainfall of 3 days (mm)	0.234	0.211
Fine sand (%)	0.190	0.134	Cum. rainfall of 4 days (mm)	0.220	0.195
Very Fine sand (%)	0.169	0.038	Cum. rainfall of 5 days (mm)	0.205	0.175
Season (-)	0.402	0.361	Cum. rainfall of 10 days (mm)	0.164	0.160
Min. air temp. (ºC)	-0.230	-0.197	Cum. rainfall of 15 days (mm)	0.279	0.260
Max. air temp. (ºC)	-0.276	-0.252	Cum. rainfall of 25 days (mm)	0.251	0.230
Mean air temp. (ºC)	-0.266	-0.236	EWMA of past hour rainfall (mm)	0.275	0.264

2.3.2 Temporal and spatial soil moisture variation in the watershed

During the monitoring period (February to September 2018), soil moisture ranged from 0.013 to 0.438 g g^{-1} for the surface and 0.014 to 0.383 g g^{-1} for the subsurface, presenting very similar mean values throughout the period (Table 2.1). Average soil gravimetric moisture was lowest during the first week of surveys, at 0.123 g g^{-1} for the surface and 0.114 g g^{-1} for the subsurface.

Temporal soil moisture variation was influenced by rainfall and evapotranspiration seasonality (Figure 2.4a). From summer to the end of autumn (21 December 2017 to 20 June 2018), there was 605.2 mm cumulative rainfall and 624.2 mm cumulative ETo. In the winter (21 June to 22 September

2018), cumulative rainfall was 646.8 mm, while ETo was only 156.8 mm. In both layers, soil moisture was lowest during the first five surveys (summer and autumn; Figure 2.4b, c), presenting averages of 0.167 g g^{-1} for the surface and 0.159 g g^{-1} for the subsurface. In winter, average soil moisture was higher, at 0.218 g g^{-1} for the surface and 0.195 g g^{-1} for the subsurface, respectively.

These findings reflect the fact that soil moisture responds to rainfall (which raises it) and evapotranspiration (which lowers it). SPI (SPEI) ranged from −1.0 to 1.56 (−1.1 to 1.6) at the one-month time scale (Figs S1 and S2). SPI and SPEI can be classified as near-normal (−0.99 to 0.99), moderately wet (1.0 to 1.49), and severely wet (1.50 to 1.99). For the period 1971 to 2019, the proportions of samples falling into these categories, for SPI (SPEI), were 70% (65%) for near-normal, 10.0% (10.5%) for moderately wet, and 4.1% (5.8%) for severely wet (Figure S2.3). Overall, the frequency of SPI (SPEI) explained 81% (80%) of the variation in the time series. This indicates that the conditions during the monitoring period were near-normal, both in terms of dry and wet conditions.

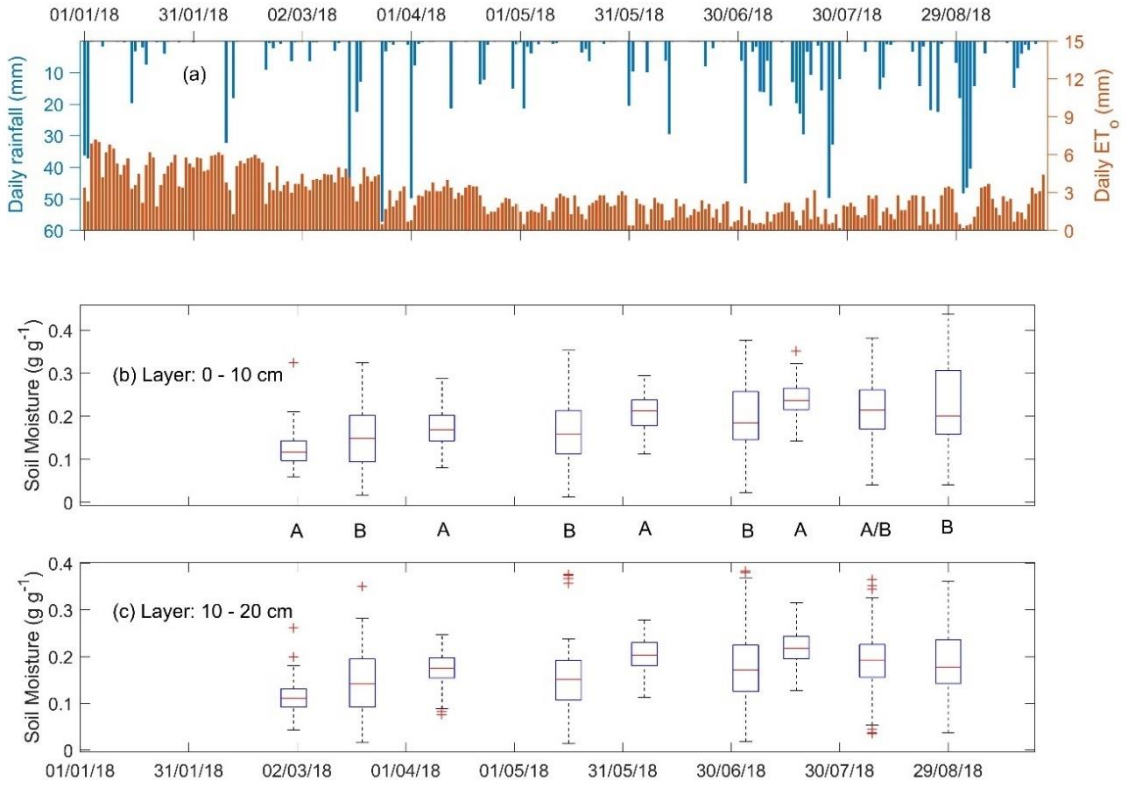

Figure 2.4 - (a) Rainfall and reference evapotranspiration (ETo) variation during the study period. Box-plot of gravimetric moisture measurements for the ten surveys at (b) the surface layer (0–10 cm) and (c) the subsurface layer (10–20 cm). A, B, and A/B: group of points displayed, according to Figure 2.2a. Box

edges: 25th and 75th percentiles; Central line: median; Whiskers: lower and upper non-divergent limits; Crosses: outliers.

High soil moisture was observed even during the driest period (the first five weeks), and low soil moisture even during the wet period (the last four weeks), particularly in the subsurface (Figure 2.4b, c). This becomes more evident when comparing the two sets of sample points: set A points have lower soil moisture variability than set B points, in both layers (Figure 2.5). Point P14 had the highest median surface and subsurface soil moisture (at 0.322 and 0.357 g g^{-1}, respectively; Figure 2.5b, d). This point had the highest proportion of clay, and highest microporosity, in the surface layer (Table S2.2). In contrast, point P30 had the lowest median soil moisture (0.038 and 0.031 g g^{-1}), lowest proportion of clay and lowest microporosity, in both layers. This reflects the importance of soil granulometry and porosity for water retention.

Topography and land use and cover may also explain the differences in soil moisture between sample sets A and B. For both layers, spatial heterogeneity of soil moisture was higher in set B (CV = 0.44) than in set A (CV = 0.29). The average slope of set B points (17.5%) was higher than that of set A points (8.8%). Further, land use and cover affected soil moisture: points in native forest had greater variability (CV = 0.35) than those in grassland (CV = 0.28). One-third of the area of sample set B is native forest.

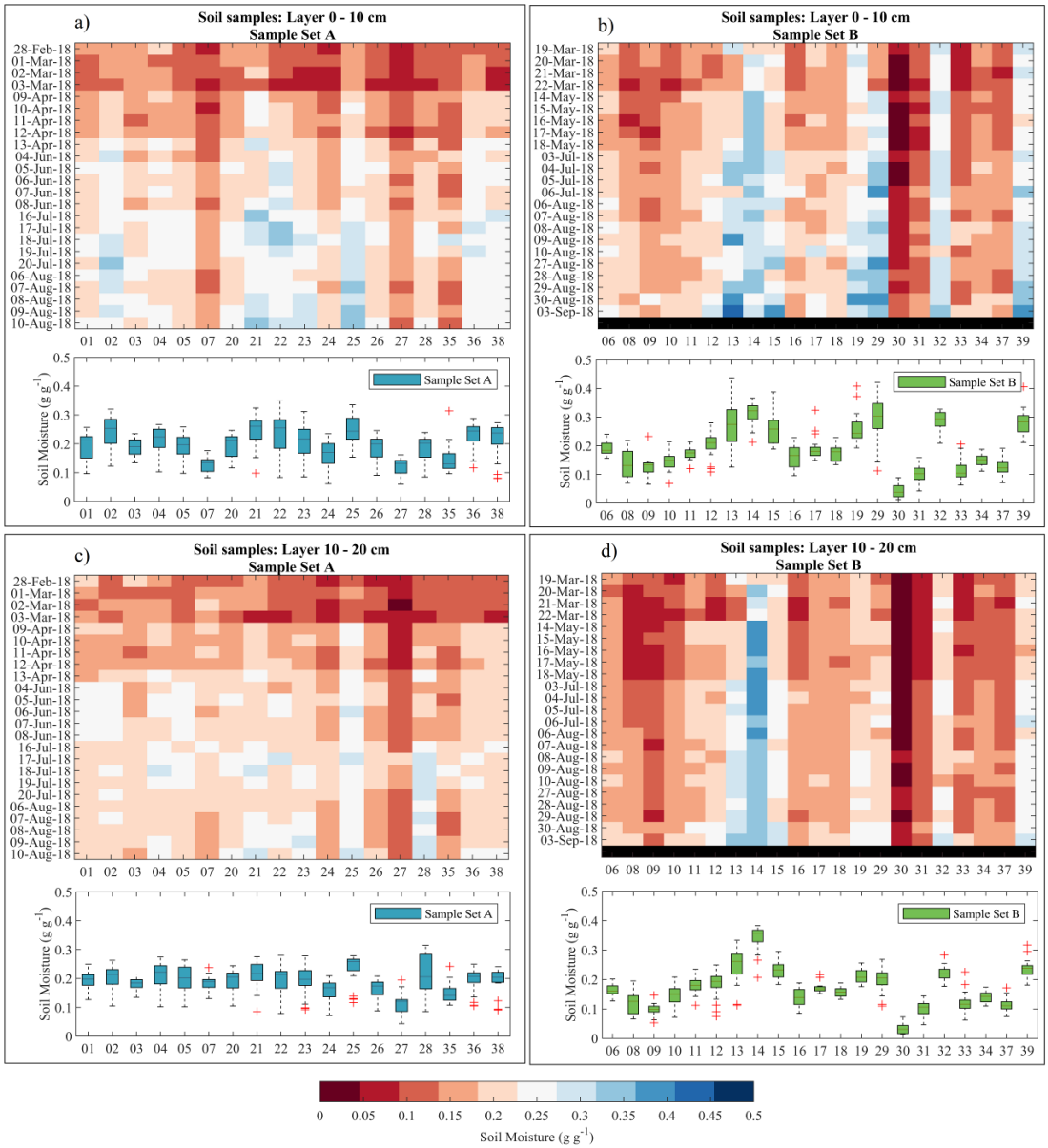

Figure 2.5 - Spatial and temporal distribution of soil moisture for the 39 measurement points. (a, b) Surface-layer soil samples from sets A and B, respectively; (c, d) Subsurface soil samples from sets A and B, respectively. The numbers on the x-axes indicate the soil sampling points.

2.3.3 Soil moisture estimation via ANN models

We used one-third of the records from each subsample for cross-validation training, and the same training configuration was used for all models (20 repetitions and a maximum of 90,000 cycles). Starting with an oversized initial network, with 20 neurons in the hidden layer, each model was tested to determine its optimal complexity (Section 2.2.4). All models whose complexity

was researched resulted with up to six neurons in the inner layer. Since, in all cases, the possible excess of complexity was contained by means of cross-validation, the number of six neurons was adopted as a reasonable standard for the final complexity of all models.

By assessing their linear correlations (Section 2.2.4), we selected 14 variables for the surface and 15 for the subsurface. We then tested the effects of including or removing certain variables. The initial selection of input variables had the greatest impact in selecting the best models for each layer (Table S2.3). The best models contained more topographical variables and fewer soil-related variables. Tables S2.4 and S2.5 present data on model performance evaluation during network verification, for the 39 models analysed.

For the subsequent analysis, we used the verification subsample (one-third of the samples). The main models for this stage of the analysis had NS coefficients ranging from 0.477 to 0.887 for the surface and 0.213 to 0.893 for the subsurface (Table 2.4). The two best models were M38 (surface, with 11 network input variables) and M49 (subsurface, with 13 network input variables), representing all of the variable categories (topography, soil, climate, and rainfall; Table S2.4). Model M38 (NS = 0.870) had the following input variables: elevation, slope, TWI, land use and cover, soil bulk density, microporosity, total sand content, season, cumulative 6-h rainfall, EWMA, and cumulative 7-d ETo (model statistics, in g g^{-1}: RMSE = 0.026, MAE = 0.02, E10 = −0.03, E50 = 0.001, and E90 = 0.033; Figure 2.6a, Table 2.4). The symmetrical error distribution (E10 versus E90), its MAE, and the E50 close to zero, indicates good neural network adjustment during the verification stage.

In contrast, model M49 (the best subsurface model; N<u>S</u> = 0.893) included soil water tension and clay percentage; further, rather than cumulative 7-d ETo, it included cumulative 45-d ETo; and rather than cumulative 6-h rainfall, it included cumulative 24-h rainfall (model statistics, in g g^{-1}: RMSE = 0.020, MAE = 0.015, E10 = −0.021, E50 = 0.0002, and E90 = 0.025 (Figure 2.6b, Table 2.4). M49 also had symmetrically distributed errors, with low MAE and E50 values, indicating good neural network adjustment, even better than for the surface model (M38).

The good verification performance of both M38 and M49 demonstrates that ANNs can be used to model soil moisture, and to make predictions even for

situations not presented during training, thus confirming their capacity to generalize. Given that M49 presented better verification performance statistics, the performance statistics cannot be used alone to compare the surface and subsurface models. Nonetheless, it may be important to address large differences in model performance statistics, particularly in NS.

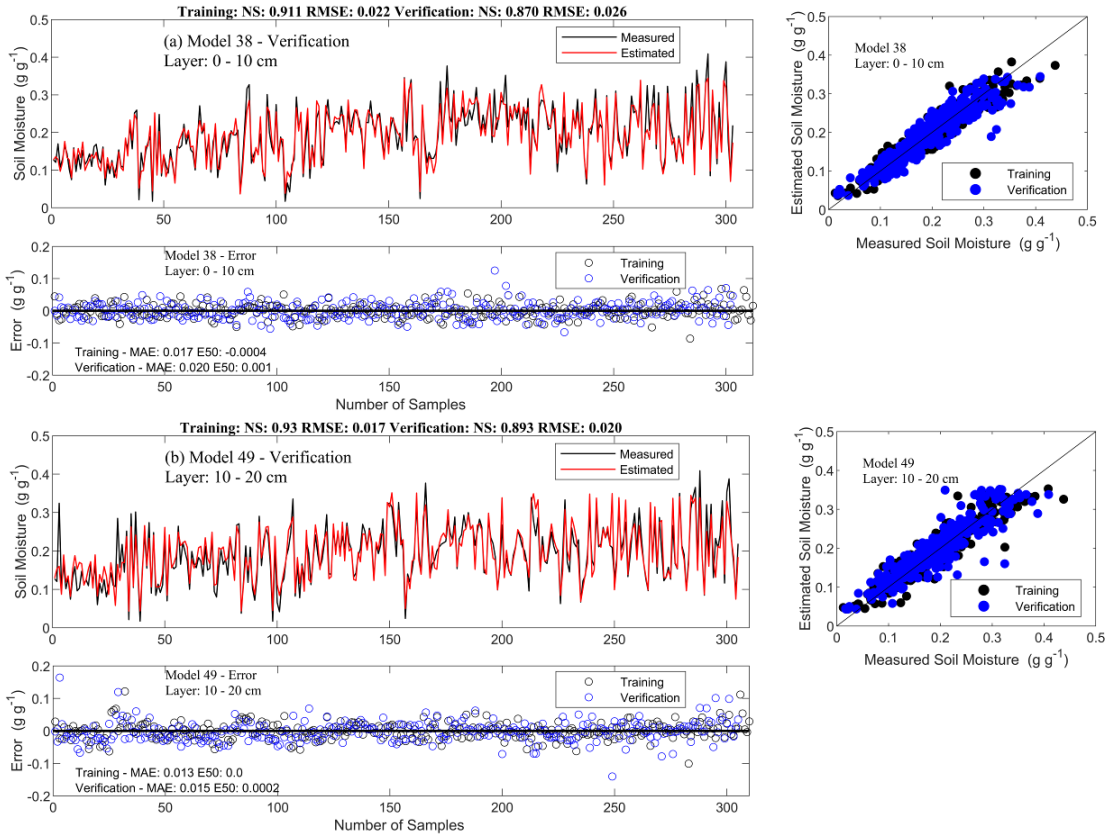

Figure 2.6 - Model performance during the verification process. (a) Model M38, surface layer; (b) Model M49, subsurface layer. Soil moisture measurements and estimates in relation to the ideal adjusted values (1:1 line) for training (black circles) and verification (blue circles) for both models. Error: difference between the measurements and estimates for training (black circles) and verification (blue circles) for both models.

Table 2.4 - Statistical verification performance of the best models for the surface and subsurface layers.

Model	38	51	52	53	54	55	56	49	64	65	66	67	68	69
Layer	Surface (0-10 cm)							Subsurface (10-20 cm)						
J[1]	18273	62377	48001	16781	13005	34215	5852	16618	61888	49176	3784	53695	13096	1193
Input variables[2]	1, 2, 3, 35, 36, 38, 43, 7, 24, 34, 18	35, 36, 38, 43, 7, 24, 34, 18	1, 2, 3, 7, 24, 34, 18	1, 2, 3, 35, 36, 38, 43, 24, 34	1, 2, 3, 35, 36, 38, 43, 7, 18	1, 2, 3, 35, 36, 38, 43	35, 7, 24, 34, 18	1, 2, 3, 35, 36, 38, 40, 41, 43, 7, 26, 34, 22	35, 36, 38, 40, 41, 43, 7, 26, 34, 22	1, 2, 3, 7, 26, 34, 22	1, 2, 3, 35, 36, 38, 40, 41, 43, 26, 34	1, 2, 3, 35, 36, 38, 40, 41, 43, 7, 22	1, 2, 3, 35, 36, 38, 41, 43	35, 40, 7, 26, 34,22
	Verification													
E10	-0.03	-0.033	-0.038	-0.046	-0.036	-0.054	-0.061	-0.021	-0.029	-0.042	-0.027	-0.025	-0.045	-0.07
E50	0.001	0.0014	-0.003	0.0033	-0.0045	0	0.0033	0.0002	0.0025	-0.0005	0.0044	-0.0013	0.0018	0.0036
E90	0.033	0.041	0.046	0.064	0.036	0.049	0.063	0.025	0.03	0.043	0.041	0.028	0.047	0.057
MAE	0.02	0.023	0.027	0.035	0.023	0.034	0.04	0.015	0.018	0.026	0.021	0.017	0.03	0.043
RMSE	0.026	0.031	0.035	0.045	0.031	0.044	0.052	0.020	0.024	0.034	0.027	0.022	0.040	0.055
NS	0.870	0.824	0.770	0.617	0.824	0.635	0.497	0.893	0.858	0.708	0.816	0.880	0.594	0.224

[1]J: number of cycles used in model selection. [2] Input variables: 1, elevation; 2, Slope; 3, TWI; 7, Season; 18, Cumulative 7-day ETo; 22, Cumulative 45-day ETo; 24, Cumulative 6-h rainfall; 26, Cumulative 1-day rainfall; 34, EWMA of rainfall in the hour before sampling; 35, Land use and cover; 36, Soil bulk density; 38, Microporosity; 40, Soil water tension; 41, Clay; 43, Total Sand.

2.3.3.1 Importance of input variables in the ANN models

For the surface model (M38), removing the season variable caused the largest reduction in network predictive capacity, reducing NS by 0.076, producing a model with NS = 0.794, RMSE = 0.033 g g^{-1}, MAE = 0.026 g g^{-1}. EWMA of rainfall in the hour before sampling was the second most important input variable: its removal reduced the model's predictive capacity, reducing NS by 0.053, producing a model with NS = 0.817, RMSE = 0.031 g g^{-1}, MAE = 0.023 g g^{-1}. Therefore, EWMA and its interactions with the other variables were important predictive factors, although without a strong linear relationship with soil moisture.

For the subsurface layer model (M49), removing microporosity and the season variable caused the largest reductions in predictive performance (NS = 0.846 and 0.842, RMSE = 0.025 for both, with NS reductions of 0.047 and 0.051 g g^{-1}, MAE = 0.019 and 0.018 g g^{-1}, respectively). These findings indicate that, for the subsurface soil moisture, microporosity is as important as the season variable. Further, the season variable was less important in the subsurface model than in the surface model. These results highlight the relevance of easily obtainable input variables for predicting both surface and subsurface soil moisture.

2.3.3.2 Importance of the variable categories for the best models

The performance statistics of the M38 and M49 models, and of those obtained by removing all of the variables in each of the four variable categories, are shown in Figure 2.7. The reductions in NS are relative to the complete models.

Removing the topographic variables reduced the verification performance of both models, noticeably increasing the dispersion of errors, with reductions in NS of 0.046 (M51, surface) and 0.035 (M64, subsurface).

Removing soil-related variables caused larger reductions in performance than removing topography-related variables, reducing NS by 0.100 (M52, surface) and 0.185 (M65, subsurface). This indicates that soil-related variables affected the subsurface model more than the surface model. M52 and M65 had

similar E10 and E90 values: E10 was slightly higher in M65 (−0.042 g g^{-1}) than in M52 (−0.038 g g^{-1}).

Removing climate-related variables reduced the predictive performance of the surface and subsurface models (M53 and M66, respectively). For the surface model, removing climatic variables had more effect than removing the other variable categories, reducing NS by 0.253; for the subsurface model, the reduction in NS was lower, at 0.077. The errors were larger, and the error distribution was more asymmetric, for M53 (E10 = −0.046 g g^{-1}, E90 = 0.064 g g^{-1}) than for M66 (E10 = −0.027 g g^{-1}, E90 = 0.041 g g^{-1}). M53 tended to overestimate low soil moisture values and underestimate high soil moisture values (Figure 2.7).

Removing rainfall-related variables reduced model performance less for the subsurface model (M67) than for the surface model (M54), with NS reductions of 0.013 and 0.046, respectively. Although both models had symmetrical error distributions, the errors more dispersed for M54 (E10 = −0.036 g g^{-1}, E90 = 0.036 g g^{-1}) than for M67 (E10 = −0.025 g g^{-1}, E90 = 0.028 g g^{-1}).

In summary, although all four variable categories are important for the surface model, those related to climate are the most important, followed by those related to soil. For the subsurface model, soil-related variables are the most important, followed by those related to climate; rainfall and topographical variables are of little importance for the subsurface model.

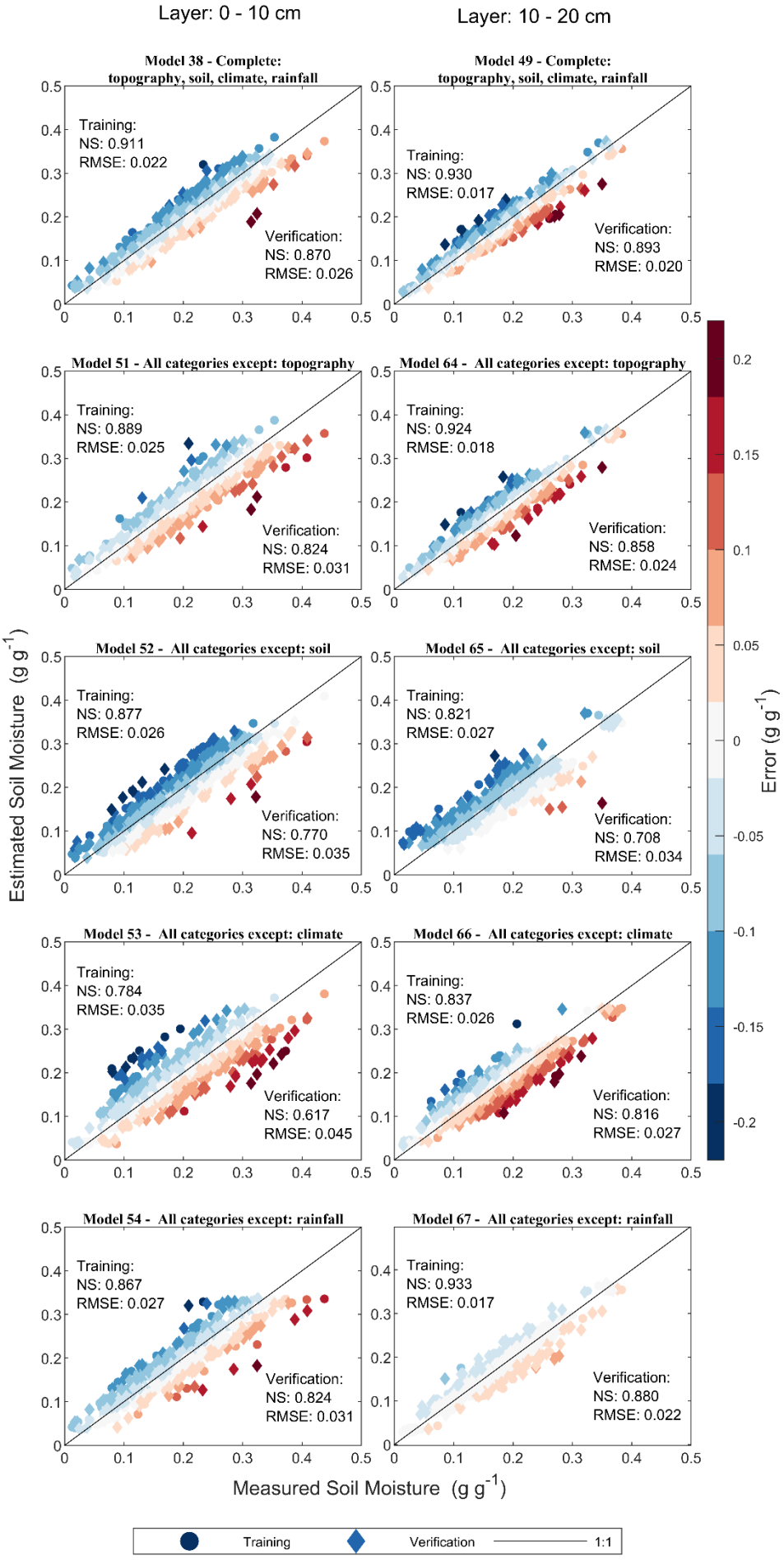
Layer: 0 - 10 cm
Layer: 10 - 20 cm
Model 38 - Complete: topography, soil, climate, rainfall
Training: NS: 0.911 RMSE: 0.022
Verification: NS: 0.870 RMSE: 0.026
Model 49 - Complete: topography, soil, climate, rainfall
Training: NS: 0.930 RMSE: 0.017
Verification: NS: 0.893 RMSE: 0.020
Model 51 - All categories except: topography
Training: NS: 0.889 RMSE: 0.025
Verification: NS: 0.824 RMSE: 0.031
Model 64 - All categories except: topography
Training: NS: 0.924 RMSE: 0.018
Verification: NS: 0.858 RMSE: 0.024
Model 52 - All categories except: soil
Training: NS: 0.877 RMSE: 0.026
Verification: NS: 0.770 RMSE: 0.035
Model 65 - All categories except: soil
Training: NS: 0.821 RMSE: 0.027
Verification: NS: 0.708 RMSE: 0.034
Model 53 - All categories except: climate
Training: NS: 0.784 RMSE: 0.035
Verification: NS: 0.617 RMSE: 0.045
Model 66 - All categories except: climate
Training: NS: 0.837 RMSE: 0.026
Verification: NS: 0.816 RMSE: 0.027
Model 54 - All categories except: rainfall
Training: NS: 0.867 RMSE: 0.027
Verification: NS: 0.824 RMSE: 0.031
Model 67 - All categories except: rainfall
Training: NS: 0.933 RMSE: 0.017
Verification: NS: 0.880 RMSE: 0.022
Estimated Soil Moisture (g g-1)
Measured Soil Moisture (g g-1)
Error (g g-1)
0.2
0.15
0.1
0.05
0
-0.05
-0.1
-0.15
-0.2
Training
Verification
1:1

Figure 2.7 - Model performance testing by removing each variables category (topography, soil, climate and rainfall). The 1:1 line depicts the ideal adjusted values. For soil moisture, the colder (blue) and hotter (red) colors depict higher negative errors (overestimates) and higher positive errors (underestimates), respectively.

2.3.3.3 Importance of spatial and temporal variables for the best models

The input variables were separated based on spatial features (for elevation, slope, TWI, land use and cover, soil bulk density, microporosity, clay content, and total sand content) and temporal features (land use and cover, soil water tension, climate, cumulative 6-h rainfall, cumulative 1-day rainfall, EWMA of rainfall in the hour before sampling, and cumulative 7-day and 45-day ETo). Because it is a spatial variable with patterns that change over time, land use and cover was considered as both spatial and temporal. Not surprisingly, excluding either the spatial or temporal information from the models reduced their predictive potential (Figure 2.8, Tables S2.4 and S2.5).

Removing the spatial features from the models reduced the predictive performance of the subsurface model (M69) more than that of the surface model (M56). Although they had similar median errors (E50 = 0.0036 and 0.0033 g g^{-1} for M69 and M56, respectively), the error distribution of M69 was more asymmetrical (E10 = −0.07 g g^{-1}, E90 = 0.057 g g^{-1}) than that of M56 (E10 = −0.061 g g^{-1}, E90 = 0.063 g g^{-1}). This confirms our earlier finding that removing the soil-related variables reduces predictive performance more for the subsurface model than the surface model.

Removing temporal variables similarly reduces the predictive performance of both the subsurface model (M68: NS = 0.594, RMSE = 0.040 g g^{-1}, and MAE = 0.03 g g^{-1}) and the surface model (M55: NS = 0.635, RMSE = 0.044 g g^{-1} and MAE = 0,034 g g^{-1}). The errors of M55 were larger and more asymmetrically distributed (E10 = −0.054g g^{-1}, E90 = 0.049 g g^{-1}) than those of M68 (E10 = −0.045 g g^{-1}, E90 = 0.047 g g^{-1}). Although the climate and rainfall-related variables had little influence on the performance of the subsurface model, removing all of the temporal variables (climate and rainfall-related variables, land use and cover, and soil water tension) reduced the model's predictive

performance. This is because the soil-related variables have a strong influence on model performance.

For the surface model, removing spatial variables reduced predictive performance more than removing temporal variables. However, the effect of removing spatial variables was less strong for the surface than for the subsurface model. Although spatial variables are important for the surface model, they have a larger effect on the subsurface model (M69). This provides further evidence that the climatic variables are more relevant to the performance of the surface model.

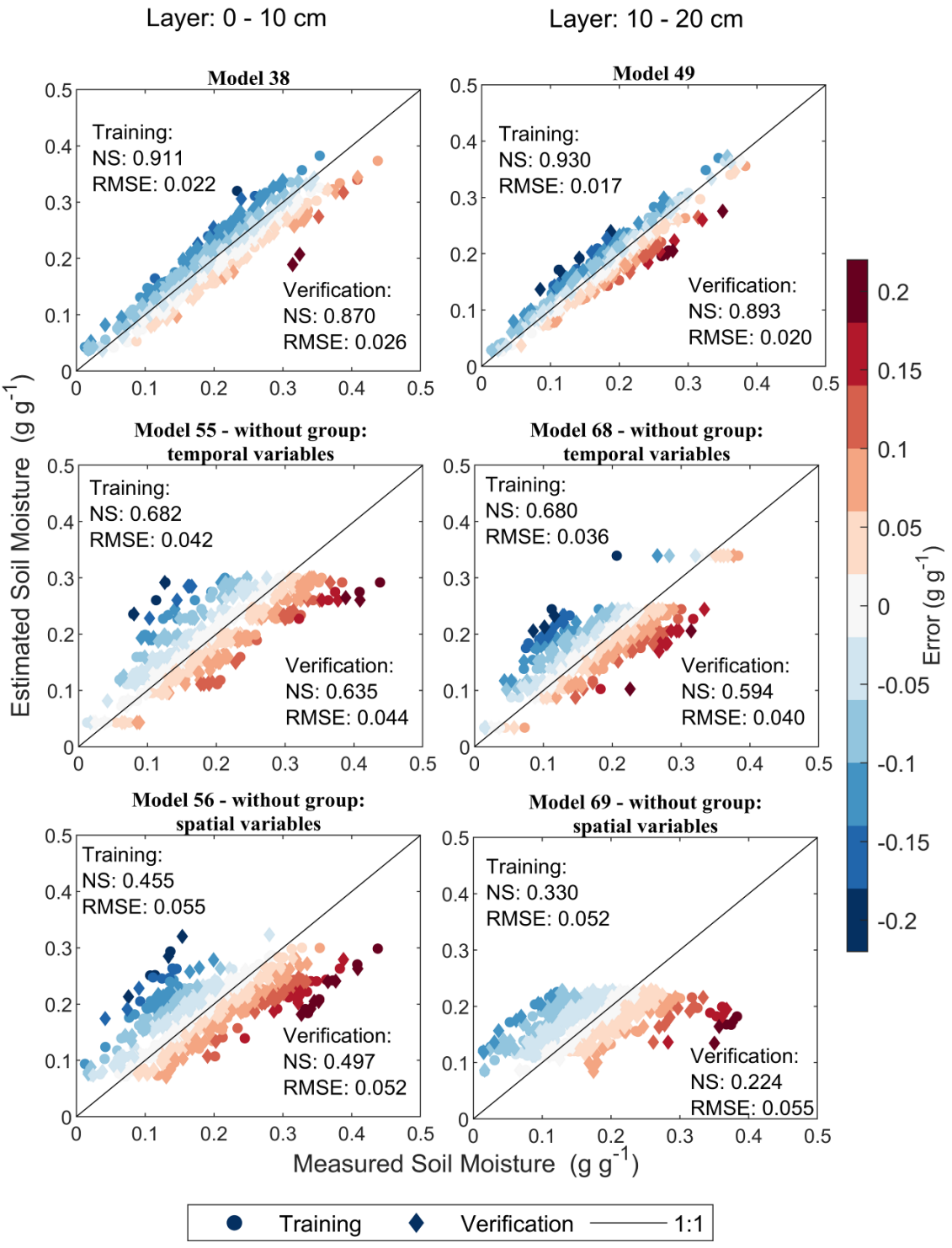

Figure 2.8 - Model performance following removal of temporal and spatial variables. The 1:1 line depicts the ideal adjusted values. For soil moisture, the colder (blue) and hotter (red) colors depict higher negative errors (overestimates) and higher positive errors (underestimates), respectively.

2.4 Discussion

The effects of topography, soil, climate, land use, and land cover on soil moisture have been widely investigated (e.g. Hu and Cheng, 2014; Korres et al., 2015; Liang, 2017; Yang et al., 2017). In the studied watershed, for both layers, spatial heterogeneity of soil moisture was higher for set B than set A samples, which can be attributed to the higher average slope of set B. Further, the higher CV of soil moisture for the native forest than for the grassland indicates that land use and cover also influenced soil moisture variability. The greater heterogeneity of soil moisture on steep slopes and in native forest is consistent with previous findings (Korres et al., 2015; Yang et al., 2017).

All four of the input variable categories (topography, soil, climate, and rainfall) were included in the best-performing ANN-based soil moisture models (M38 and M49). This reflects the complex spatiotemporal dynamics that determine soil moisture, at the watershed scale. The fact that variables with low linear correlations with soil moisture (e.g., elevation, EWMA; Table 2.3) were included in the best models indicates that even low-correlation variables can affect ANN performance. This is because ANNs build nonlinear relationships among input and output variables (Oliveira et al., 2017).

Both of the best-performing models (M38 and M49, for surface and subsurface, respectively) performed well during the verification stage. The slightly superior performance of the subsurface model probably reflects the fact that the soil moisture has lower coefficients of variation in this layer. Similarly, Contador et al. (2006) obtained good results when using ANN modelling to estimate soil moisture in a Spanish watershed, emphasizing the effects of changes in land cover on soil moisture. Further, Kornelsen and Coulibaly (2014) reported that ANNs can explain nonlinear soil moisture dynamics; however, they achieved good results for deeper layers only when using surface soil moisture as a network input. Using the same variable categories that we used, Oliveira et al. (2017) also achieved good results, for a watershed of the same climatic type but with very different land use, land cover, soil hydro-physical features, and topography. In the present study, cumulative 6-h rainfall was more important in predicting surface soil moisture, whereas cumulative 24-h rainfall was more important in predicting subsurface soil moisture, indicating that

rainfall affected surface soil moisture faster than subsurface soil moisture. Similarly, cumulative 7-day ETo was more important for the surface model, whereas cumulative 45-day Eto was more important for the subsurface model, indicating that the surface soil dries out faster than the subsurface soil. This suggests that surface soil moisture responds to the most recent rainfall and climatic conditions, whereas subsurface soil moisture is attenuated by the soil's hydro-physical features, which control water infiltration and delay the effects of rainfall and climate conditions, as observed by Lv et al. (2019). Furthermore, the linkage of soil moisture in surface and subsurface is dependent on the kind of transition between soil horizons (Hagen et al., 2020). Water reallocation to greater depths causes soil moisture to be more stable at greater depths (Rosenbaum et al., 2012).

Excluding the input variable categories had different effects on the performance of the surface and subsurface ANN models. In both layers, excluding the soil-related variables caused greater loss of performance than removing the topographic variables. Gwak and Kim (2017) and Hu and Cheng (2014) report that soil-related properties are more important than topography in determining the soil moisture distribution. Various other studies have reported that topography, land use and land cover are essential in characterizing catchment-scale soil moisture variability (Liang, 2017; Yang et al., 2017; Yu et al., 2018).

For the surface layer, climate-related variables were more important than topography, soil, and rainfall-related variables in predicting soil moisture. This probably related to the observed differences in cumulative rainfall and ETo between dry periods (summer and autumn) and humid periods (winter). By assigning a numeric value to each season, this information is indirectly included in the model. Further, for small watersheds, it has been reported that changes in soil moisture over time may influence processes which control spatial patterns of soil moisture (e.g. Hu and Cheng, 2014; Liang, 2017; Western et al., 2004). In this context, for a small watershed in Germany, Rosenbaum et al. (2012) observed that temporal changes in the surface layer (0–5 cm) were strongly influenced by climatic forcing.

Consistent with Oliveira et al. (2017), we found that including simple, accessible, and low cost variables (such as land use and cover, and season)

improved network performance in estimating soil moisture. Excluding rainfall-related variables caused small losses in predictive performance, especially for the subsurface layer. This is consistent with other experimental and modelling studies. For instance, Metzger et al. (2017), in a forest-parcel experiment, observed that soil wetting and rainfall patterns were weakly associated; they attributed this to the rapid drying of soil after rainfall, with dry soil being the stable condition over time. Using a Richards equation-derived 3D model for a hillslope, Coenders-Gerrits et al. (2013) observed that rainfall influences soil moisture predictions, but only during and shortly after a rainfall event, with bedrock topography being the limiting factor most of the time.

2.5 Conclusions

For a small watershed, we investigated the capacity of ANN models to predict regional soil moisture, both for surface and subsurface layers, and evaluated the main driving factors. The models were configured using inputs in four categories (topography, soil properties, climate, and rainfall) and were classified as spatial (having invariant physical characteristics) and temporal (varying over time, such as rainfall and ETo).

For both layers, the complete models showed excellent performance. We then evaluated model performance by removing each one of the variables, categories, or spatiotemporal classes, in turn. The most important variable for the surface model was climate, followed by the EWMA of rainfall. For the subsurface model, climate was also the most important variable (although less so than for the surface model), followed by microporosity. Although all four categories were important for the surface model, the most important was climate, followed by soil properties. For the subsurface model, the most important categories were soil properties, followed by climate; rainfall and topography were of little importance. For both layers, the models were more sensitive to exclusion of spatial than of temporal variables.

In conclusion, it is possible to estimate soil moisture for both layers with good performance, using the selected variables, which represent the physical conditions affecting soil moisture. However, the surface model requires more input variables to achieve good performance. In contrast, for the subsurface

model, more variance in soil moisture can be explained using only soil and climate-related variables (in particular, season and microporosity). This is because the most recent rainfall and climate conditions determine changes in surface soil moisture, whereas subsurface soil moisture is attenuated by soil properties, which control water infiltration and delay the effects of rainfall and climate.

Acknowledgments

We thank NEPE-HidroSedi at the Federal University of Pelotas (UFPel) for providing facilities to perform laboratory analyses and field surveys, and the Agricultural Meteorology Laboratory of the Brazilian Corporation of Agricultural Research (EMBRAPA) for providing the meteorological data used in this study.

Funding

We thank the National Council for Scientific and Technological Development (CNPq) for financing a PhD fellowship [grant number 141235/2017-9] for the first author, and research productivity fellowships for the second and third authors. The funders had no role in study design; in the collection, analysis and interpretation of data; in the writing of the report; or in the decision to submit the article for publication.

References

Al-mukhtar, M., 2016. Modelling the root zone soil moisture using artificial neural networks , a case study. Environ. Earth Sci. 75, 1–12. https://doi.org/10.1007/s12665-016-5929-2

Alvarez-garreton, C., Ryu, D., Western, A.W., Crow, W.T., Robertson, D.E., 2014. The impacts of assimilating satellite soil moisture into a rainfall – runoff model in a semi-arid catchment. J. Hydrol. 519, 2763–2774. https://doi.org/10.1016/j.jhydrol.2014.07.041

Arsoy, S., Ozgur, M., Keskin, E., Yilmaz, C., 2013. Geoderma Enhancing TDR based water content measurements by ANN in sandy soils. Geoderma 195–196, 133–144. https://doi.org/10.1016/j.geoderma.2012.11.019

Bartels, G.K., Castro, N.M. dos R., Collares, G.L., Fan, F.M., 2021. Performance of bedload transport equations in a mixed bedrock–alluvial

channel environment. Catena 199, 105108. https://doi.org/10.1016/j.catena.2020.105108

Bartels, G.K., Terra, V.S.S., Cassalho, F., Lima, L.S., Reinert, D.J., Collares, G.L., 2016. Spatial variability of soil physical and hydraulic properties in the southern Brazil small watershed. African J. Agric. 11, 5036–5042. https://doi.org/10.5897/AJAR2016.11812

Berthet, L., Andréassian, V., Perrin, C., Javelle, P., 2009. How crucial is it to account for the antecedent moisture conditions in flood forecasting ? Comparison of event-based and continuous approaches on 178 catchments. Hydrol. Earth Syst. Sci. 13, 819–831. https://doi.org/https://doi.org/10.5194/hess-13-819-2009

Beven, K.J., Kirkby, M.J., 1979. A physically based, variable contributing area model of basin hydrology. Hydrol. Sci. Bull. 24, 43–69. https://doi.org/10.1080/02626667909491834

Blake, G.R., Hartge, K.H., 1986. Bulk Density, in: Klute, A. (Ed.), Methods of Soil Analysis, Part 1. Physical and Mineralogical Methods. Madison, pp. 363–375.

Cho, E., Choi, M., 2014. Regional scale spatio-temporal variability of soil moisture and its relationship with meteorological factors over the Korean peninsula. J. Hydrol. 516, 317–329. https://doi.org/10.1016/j.jhydrol.2013.12.053

Coenders-Gerrits, A.M.., Hopp, L., Savenije, H.H.., Pfister, L., 2013. The effect of spatial throughfall patterns on soil moisture patterns at the hillslope scale. Hydrol. Earth Syst. Sci. 17, 1749–1763. https://doi.org/10.5194/hess-17-1749-2013

Contador, J.F.L., Maneta, M., Schnabel, S., 2006. Prediction of Near-Surface Soil Moisture at Large Scale by Digital Terrain Modeling and Neural Networks. Environ. Monit. Assess. 121, 213–232. https://doi.org/10.1007/s10661-005-9116-2

Cui, Y., Long, D., Hong, Y., Zeng, C., Zhou, J., Han, Z., Liu, R., Wan, W., 2016. Validation and reconstruction of FY-3B/MWRI soil moisture using an artificial neural network based on reconstructed MODIS optical products over the Tibetan Plateau. J. Hydrol. 543, 242–254. https://doi.org/10.1016/j.jhydrol.2016.10.005

Danielson, R.E., Sutherland, P.L., 1986. Porosity, in: Klute, A. (Ed.), Methods of Soil Analysis, Part 1. Physical and Mineralogical Methods. Madison, pp. 443–461.

Elshorbagy, A., Parasuraman, K., 2008. On the relevance of using artificial neural networks for estimating soil moisture content. J. Hydrol. 362, 1–18. https://doi.org/10.1016/j.jhydrol.2008.08.012

Famiglietti, J.S., Rudnicki, J.W., Rodell, M., 1998. Variability in surface moisture content along a hillslope transect : Rattlesnake Hill , Texas. J. Hydrol. 210, 259–281. https://doi.org/10.1016/S0022-1694(98)00187-5

Food and Agriculture Organization of the United Nations, 2014. World reference base for soil resources 2014: International soil classification system for

naming soils and creating legends for soil maps. FAO, Rome.

Gao, X., Wu, P., Zhao, X., Wang, J., Shi, Y., Zhang, B., 2013. Estimation of spatial soil moisture averages in a large gully of the Loess Plateau of China through statistical and modeling solutions. J. Hydrol. 486, 466–478. https://doi.org/10.1016/j.jhydrol.2013.02.026

Gee, G.W., Bauder, J.W., 1986. Particle-size Analysis, in: Klute, A. (Ed.), Methods of Soil Analysis, Part 1. Physical and Mineralogical Methods. Madison, pp. 383–411.

Gill, M.K., Asefa, T., Kemblowski, M.W., McKee, M., 2006. SOIL MOISTURE PREDICTION USING SUPPORT VECTOR MACHINES. J. Am. Water Resour. Assoc. 42, 1033–1046. https://doi.org/10.1111/j.1752-1688.2006.tb04512.x

Grayson, R.B., Western, A.W., Chiew, F.H.S., Blöschl, G., 1997. Preferred states in spatial soil moisture patterns : Water Resour. Res. 33, 2897–2908.

Gwak, Y., Kim, S., 2017. Factors affecting soil moisture spatial variability for a humid forest hillslope. Hydrol. Process. 31, 431–445. https://doi.org/10.1002/hyp.11039

Hachani, A., Ouessar, M., Paloscia, S., Santi, E., Pettinato, S., 2019. Soil moisture retrieval from Sentinel-1 acquisitions in an arid environment in Tunisia: application of Artificial Neural Networks techniques. Int. J. Remote Sens. 40, 9159–9180. https://doi.org/10.1080/01431161.2019.1629503

Hagen, K., Berger, A., Gartner, K., Geitner, C., Kofler, T., Kogelbauer, I., Kohl, B., Markart, G., Meißl, G., Niedertscheider, K., 2020. Event-based dynamics of the soil water content at Alpine sites (Tyrol, Austria). CATENA 194, 104682. https://doi.org/10.1016/j.catena.2020.104682

Hecht-Nielsen, R., 1990. Neurocomputing. Addison - Wesley Publishing Company, Boston.

Hornik, K., Stinchcombe, M., White, H., 1989. Multilayer feedforward networks are universal approximators. Neural Networks 2, 359–366. https://doi.org/10.1016/0893-6080(89)90020-8

Hu, Q., Pan, F., Pan, X., Hu, L., Wang, X., Yang, P., Wei, P., Pan, Z., 2018. Dry-wet variations and cause analysis in Northeast China at multi-time scales. Theor. Appl. Climatol. 133, 775–786. https://doi.org/10.1007/s00704-017-2222-6

Hu, W., Cheng, B., 2014. Revealing the relative influence of soil and topographic properties on soil water content distribution at the watershed scale in two sites. J. Hydrol. 516, 107–118. https://doi.org/10.1016/j.jhydrol.2013.10.002

Huang, X., Shi, Z.H., Zhu, H.D., Zhang, H.Y., Ai, L., Yin, W., 2016. Soil moisture dynamics within soil pro fi les and associated environmental controls. Catena 136, 189–196. https://doi.org/10.1016/j.catena.2015.01.014

Jacobs, J.M., Mohanty, B.P., Hsu, E., Miller, D., 2004. SMEX02 : Field scale variability , time stability and similarity of soil moisture. Remote Sens. Environ. 92, 436–446. https://doi.org/10.1016/j.rse.2004.02.017

Kornelsen, K.C., Coulibaly, P., 2014. Root-zone soil moisture estimation using data-driven methods. Water Resour. Res. 50, 2946–2962. https://doi.org/10.1002/2013WR014127

Korres, W., Reichenau, T.G., Fiener, P., Koyama, C.N., Bogena, H.R., Cornelissen, T., Baatz, R., Herbst, M., Diekkrüger, B., Vereecken, H., Schneider, K., 2015. Spatio-temporal soil moisture patterns – A meta-analysis using plot to catchment scale data. J. Hydrol. 520, 326–341. https://doi.org/10.1016/j.jhydrol.2014.11.042

Korres, W., Reichenau, T.G., Schneider, K., 2013. Patterns and scaling properties of surface soil moisture in an agricultural landscape : An ecohydrological modeling study. J. Hydrol. 498, 89–102. https://doi.org/10.1016/j.jhydrol.2013.05.050

Li, X., Zhang, S., Peng, H., Hu, X., Ma, Y., 2013. Agricultural and Forest Meteorology Soil water and temperature dynamics in shrub-encroached grasslands and climatic implications : Results from Inner Mongolia steppe ecosystem of north. Agric. For. Meteorol. 171–172, 20–30. https://doi.org/10.1016/j.agrformet.2012.11.001

Liang, W.L., 2017. Analysis of the contributions of topographic, soil, and vegetation features on the spatial distributions of surface soil moisture in a steep natural forested headwater catchment. Hydrol. Process. 31, 3796–3809. https://doi.org/10.1002/hyp.11290

Lv, L., Liao, K., Zhou, Z., Zhu, Q., Shen, C., 2019. Catena Determining hot moments / spots of hillslope soil moisture variations based on high-resolution spatiotemporal soil moisture data. Catena 173, 150–161. https://doi.org/10.1016/j.catena.2018.10.012

Massari, C., Brocca, L., Moramarco, T., Tramblay, Y., Lescot, J.D., 2014. Advances in Water Resources Potential of soil moisture observations in flood modelling : Estimating initial conditions and correcting rainfall. Adv. Water Resour. 74, 44–53. https://doi.org/10.1016/j.advwatres.2014.08.004

McCabe, M.F., Rodell, M., Alsdorf, D.E., Miralles, D.G., Uijlenhoet, R., Wagner, W., Lucieer, A., Houborg, R., Verhoest, N.E.C., Franz, T.E., Shi, J., Gao, H., Wood, E.F., 2017. The Future of Earth Observation in Hydrology. Hydrol. Earth Syst. Sci. Discuss. 21, 1–55. https://doi.org/10.5194/hess-2017-54

McKee, T.B., Doesken, N.., Kleist, J., 1993. THE RELATIONSHIP OF DROUGHT FREQUENCY AND DURATION TO TIME SCALES, in: 8th Conference on Applied Climatology. Anaheim, California, pp. 179–184. https://doi.org/10.1002/joc.846

Meng, S., Xie, X., Liang, S., 2017. Assimilation of soil moisture and streamflow observations to improve flood forecasting with considering runoff routing lags. J. Hydrol. 550, 568–579. https://doi.org/10.1016/j.jhydrol.2017.05.024

Metzger, J.C., Wutzler, T., Valle, N.D., Grauer, C., Lehmann, R., Roggenbuck, M., Schelhorn, D., Weckmüller, J., Küsel, K., Uwe, K., Susan, T., Hildebrandt, A., 2017. Vegetation impacts soil water content patterns by shaping canopy water fluxes and soil properties. Hydrol. Process. 31, 3783–3795. https://doi.org/10.1002/hyp.11274

Moore, I.D., Burch, G.J., Mackenzie, D.H., 1988. Topographic Effects on the Distribution of Surface Soil Water and the Location of Ephemeral Gullies. Trans. ASAE 31, 1098–1107. https://doi.org/10.13031/2013.30829

Moore, R.J., 1980. Real-time Forecasting of Flood Events Using Transfer Function Noise Models: report, Part 2. Institute of Hydrology, Wallingford.

Oliveira, M.H.C., Sari, V., Castro, N.M. dos R., Pedrollo, O.C., 2017. Estimation of soil water content in watershed using artificial neural networks. Hydrol. Sci. J. 62, 2120–2138. https://doi.org/10.1080/02626667.2017.1364844

Oliveira, V.A., Rodrigues, A.F., Morais, M.A.V., Terra, M. de C.N.S., Guo, L., Mello, C.R., 2021. Spatiotemporal modelling of soil moisture in an Atlantic forest through machine learning algorithms. Eur. J. Soil Sci. ejss.13123. https://doi.org/10.1111/ejss.13123

Pan, X., Kornelsen, K.C., Coulibaly, P., 2017. Estimating Root Zone Soil Moisture at Continental Scale Using Neural Networks. JAWRA J. Am. Water Resour. Assoc. 53, 220–237. https://doi.org/10.1111/1752-1688.12491

Peel, M.C., Finlayson, B.L., McMahon, T.A., 2007. Updated world map of the Köppen-Geiger climate classificatio. Hydrol. Earth Syst. Sci. 1, 1633–1644. https://doi.org/10.1127/0941-2948/2006/0130

Philipp, R.P., Bom, F.M., Pimentel, M.M., Junges, S.L., Zvirtes, G., 2016. SHRIMP U-Pb age and high temperature conditions of the collisional metamorphism in the V??rzea do Capivarita Complex: Implications for the origin of Pelotas Batholith, Dom Feliciano Belt, southern Brazil. J. South Am. Earth Sci. 66, 196–207. https://doi.org/10.1016/j.jsames.2015.11.008

Robinson, D.A., Campbell, C.S., Hopmans, J.W., Hornbuckle, B.K., Jones, S.B., Knight, R., Ogden, F., Selker, J., Wendroth, O., 2008. Soil Moisture Measurement for Ecological and Hydrological Watershed-Scale Observatories: A Review. Vadose Zo. J. 7, 358–389. https://doi.org/10.2136/vzj2007.0143

Rodriguez-Fernandez, N.J., Aires, F., Richaume, P., Kerr, Y.H., Prigent, C., Kolassa, J., Cabot, F., Jimenez, C., Mahmoodi, A., Drusch, M., 2015. Soil Moisture Retrieval Using Neural Networks: Application to SMOS. IEEE Trans. Geosci. Remote Sens. 53, 5991–6007. https://doi.org/10.1109/TGRS.2015.2430845

Rosenbaum, U., Bogena, H.R., Herbst, M., Huisman, J.A., Peterson, T.J., Weuthen, A., Western, A.W., Vereecken, H., 2012. Seasonal and event dynamics of spatial soil moisture patterns at the small catchment scale. Water Resour. Res. 48, 1–22. https://doi.org/10.1029/2011WR011518

Rumelhart, D.E., Hinton, G.E., Williams, R.J., 1986. Learning representations by back-propagating errors. Nature 323, 533–536. https://doi.org/10.1038/323533a0

Santi, E., Paloscia, S., Pettinato, S., Fontanelli, G., 2016. Application of artificial neural networks for the soil moisture retrieval from active and passive microwave spaceborne sensors. Int. J. Appl. Earth Obs. Geoinf. 48, 61–73. https://doi.org/10.1016/j.jag.2015.08.002

Sari, V., dos Reis Castro, N.M., Pedrollo, O.C., 2017. Estimate of Suspended Sediment Concentration from Monitored Data of Turbidity and Water Level Using Artificial Neural Networks. Water Resour. Manag. 31, 4909–4923. https://doi.org/10.1007/s11269-017-1785-4

Scaini, A., Sánchez, N., Vicente-Serrano, S.M., Martínez-Fernández, J., 2015. SMOS-derived soil moisture anomalies and drought indices: a comparative analysis using in situ measurements. Hydrol. Process. 29, 373–383. https://doi.org/10.1002/hyp.10150

Suo, L., Huang, M., Zhang, Y., Duan, L., Shan, Y., 2018. Soil moisture dynamics and dominant controls at different spatial scales over semiarid and semi-humid areas. J. Hydrol. 562, 635–647. https://doi.org/10.1016/j.jhydrol.2018.05.036

Tayfur, G., Zucco, G., Brocca, L., Moramarco, T., 2014. Coupling soil moisture and precipitation observations for predicting hourly runoff at small catchment scale. J. Hydrol. 510, 363–371. https://doi.org/10.1016/j.jhydrol.2013.12.045

Topp, G.C., Davis, J.L., Bailey, W.G., Zebchuk, W.D., 1984. The measurement of soil water content using a portable TDR hand probe. Can. J. Soil Sci. 64, 313–321.

Vicente-Serrano, S.M., Beguería, S., López-Moreno, J.I., 2010. A multiscalar drought index sensitive to global warming: The standardized precipitation evapotranspiration index. J. Clim. 23, 1696–1718. https://doi.org/10.1175/2009JCLI2909.1

Vogl, T.P., Mangis, J.K., Rigler, A.K., Zink, W.T., Alkon, D.L., 1988. Accelerating the convergence of the back-propagation method. Biol. Cybern. 59, 257–263. https://doi.org/10.1007/BF00332914

Western, A.W., Grayson, R.B., Blöschl, G., 2002. Scaling of Soil Moisture: A Hydrologic Perspective. Annu. Rev. Earth Planet. Sci. 30, 149–180. https://doi.org/10.1146/annurev.earth.30.091201.140434

Western, A.W., Zhou, S., Grayson, R.B., Wilson, D.J., Mcmahon, T.A., 2004. Spatial correlation of soil moisture in small catchments and its relationship to dominant spatial hydrological processes. J. Hydrol. 286, 113–134. https://doi.org/10.1016/j.jhydrol.2003.09.014

Wooldridge, S.A., Kalma, J.D., Walker, J.P., 2003. Importance of soil moisture measurements for inferring parameters in hydrologic models of low-yielding ephemeral catchments. Environ. Model. Softw. 18, 35–48.

Yang, J., Feng, J., He, Z., 2018. Improving soil heat and moisture forecasting for arid and semi-arid regions : A comparative study of four mathematical algorithms. Arid L. Res. Manag. 32, 149–169. https://doi.org/10.1080/15324982.2017.1408716

Yang, Y., Dou, Y., Liu, D., An, S., 2017. Spatial pattern and heterogeneity of soil moisture along a transect in a small catchment on the Loess Plateau. J. Hydrol. 550, 466–477. https://doi.org/10.1016/j.jhydrol.2017.05.026

Yao, P., Shi, J., Zhao, T., Lu, H., Al-Yaari, A., 2017. Rebuilding Long Time Series Global Soil Moisture Products Using the Neural Network Adopting

the Microwave Vegetation Index. Remote Sens. 9, 35. https://doi.org/10.3390/rs9010035

Yu, B., Liu, G., Liu, Q., Wang, X., Feng, J., Huang, C., 2018. Soil moisture variations at different topographic domains and land use types in the semi-arid Loess Plateau, China. CATENA 165, 125–132. https://doi.org/10.1016/j.catena.2018.01.020

Zhong, M., Jiang, T., Hong, Y., Yang, X., 2019. Performance of multi-level association rule mining for the relationship between causal factor patterns and flash flood magnitudes in a humid area. Geomatics, Nat. Hazards Risk 10, 1967–1987. https://doi.org/10.1080/19475705.2019.1655102

Zhu, H.D., Shi, Z.H., Fang, N.F., Wu, G.L., Guo, Z.L., Zhang, Y., 2014. Soil moisture response to environmental factors following precipitation events in a small catchment. Catena 120, 73–80. https://doi.org/10.1016/j.catena.2014.04.003

Appendix A. Supplementary data

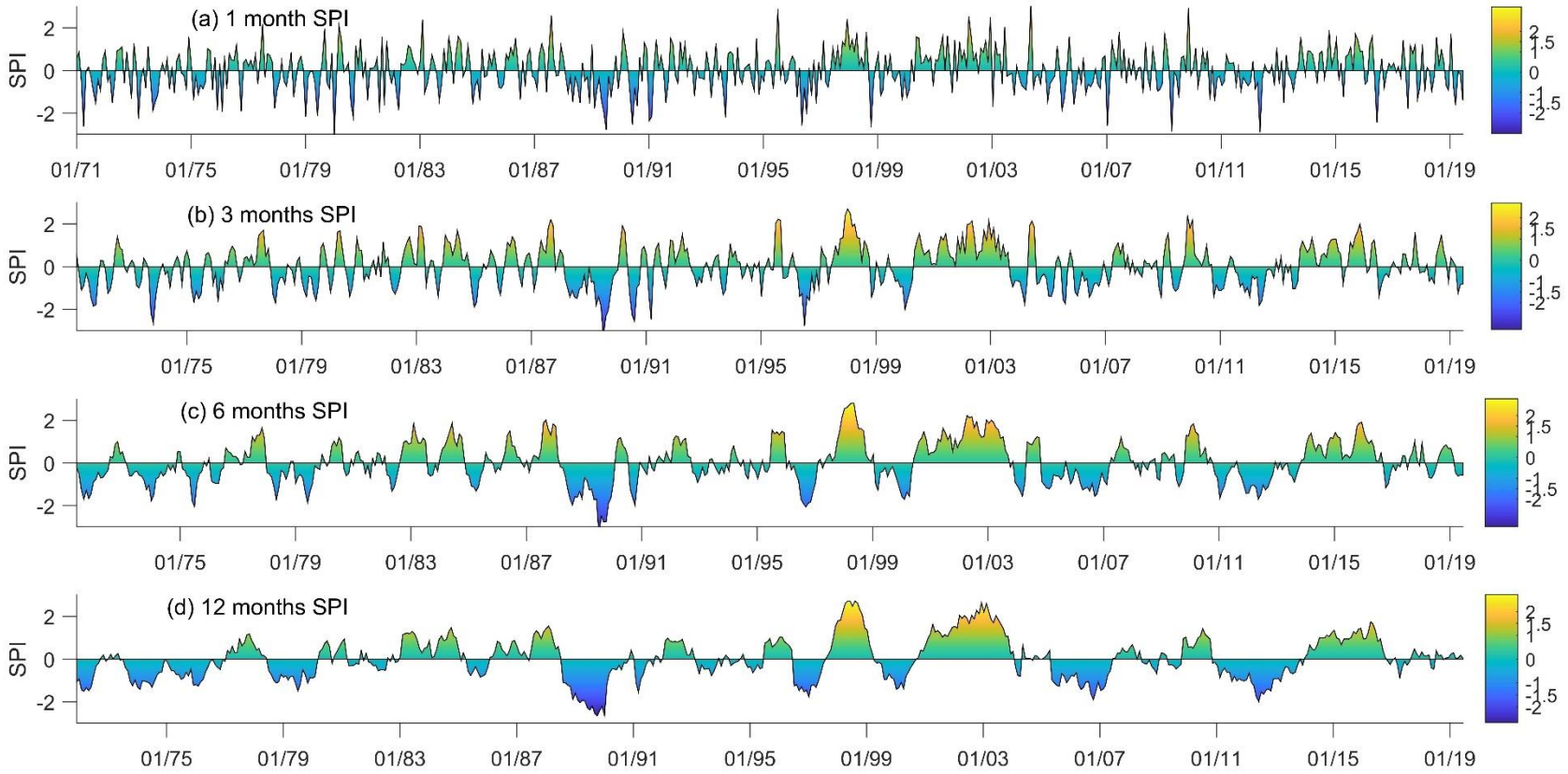

Figure S2.1 - The 1-, 3-, 6-, and 12-month SPIs in the Arroio do Ouro watershed (1971–2019).

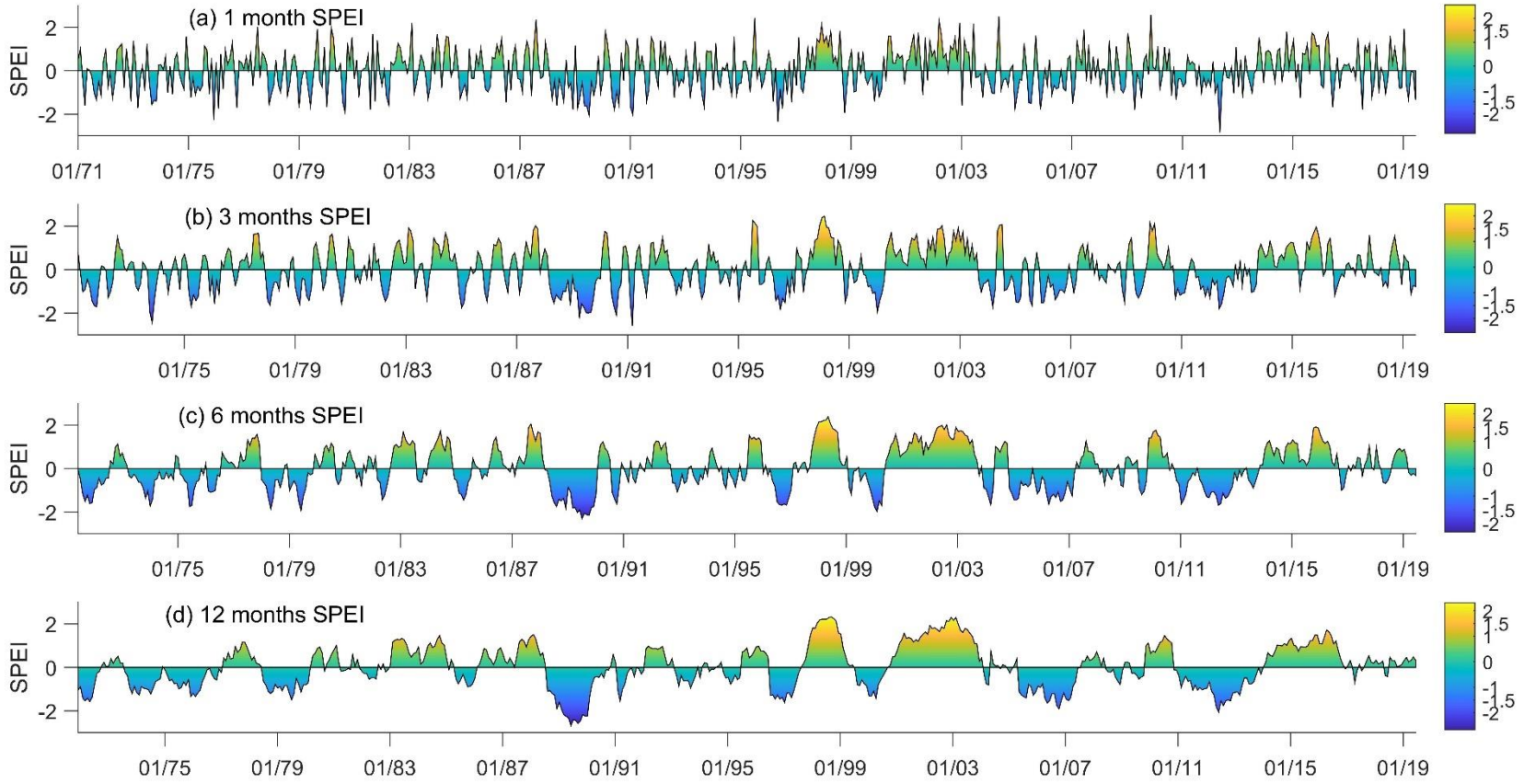

Figure S2.2 - The 1-, 3-, 6-, and 12-month SPEIs in the Arroio do Ouro watershed (1971–2019).

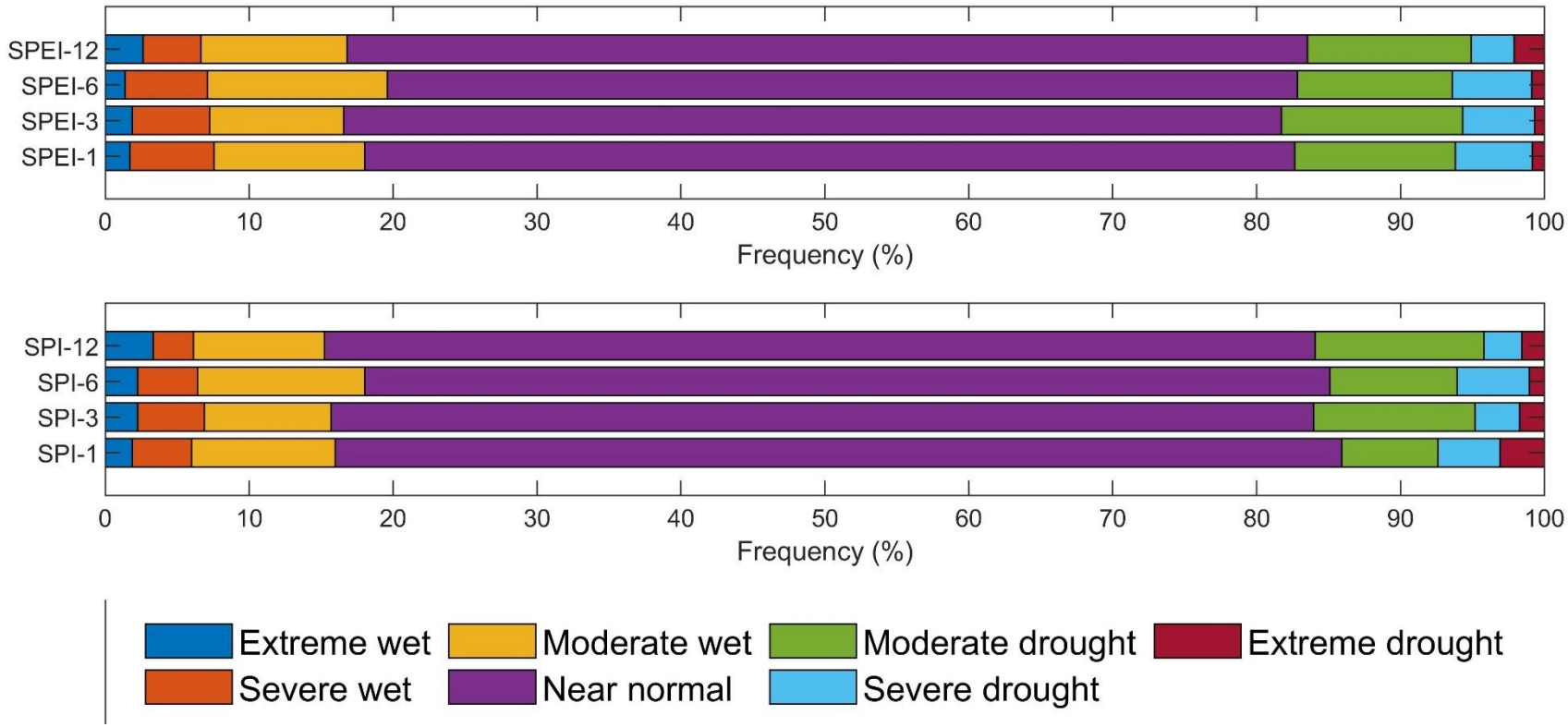

Figure S2.3 - Frequencies of drought and wetness in different categories at 1-, 3-, 6-, and 12-month SPEI/SPI in the Arroio do Ouro watershed (1971–2019).

Table S2.1 - Topographic variables of the 39 soil moisture monitoring points.

	Coordinates		Group topographic variables					
Point	North (m)	East (m)	DEM (m)	Slope (%)	TWI	Curvature	DTR (m)	DNR (m)
P01	6500807.035	350189.819	262.0	12.3	6.9	0.01	100.9	4.0
P02	6502754.349	346798.502	242.0	10.7	5.6	0.05	233.6	26.0
P03	6504008.686	348293.163	205.0	5.5	7.7	0.05	321.6	20.0
P04	6502403.456	348222.575	230.0	3.1	6.9	0.10	233	26.0
P05	6503569.989	347508.669	215.0	5.5	8.1	0.58	138.6	6.0
P06	6502789.537	350603.013	210.0	28.1	5.8	0.16	348.2	30.0
P07	6504084.511	348318.903	206.0	9.9	6.4	0.07	297.5	25.0
P08	6504325.972	350172.712	134.0	30.1	4.6	-0.32	108.4	18.0
P09	6504604.935	350079.739	184.0	21.8	5.6	0.10	404.5	68.0
P10	6505665.007	350084.702	193.0	6.6	6.8	0.12	533.5	84.0
P11	6505091.14	350095.592	121.0	16.8	10.0	-0.24	24.2	4.0
P12	6505611.122	349194.406	205.0	13.5	6.1	0.17	341.6	35.0
P13	6505725.351	350752.534	153.0	20.5	5.7	0.48	204.1	41.0
P14	6504696.698	350839.618	112.0	2.6	9.1	-0.12	29.4	4.0
P15	6503366.146	350097.106	148.0	14.5	7.8	0.06	15.7	1.0
P16	6505653.88	351220.098	113.0	10.0	5.7	-0.09	149.2	15.0
P17	6505067.99	351623.338	165.0	9.6	5.7	0.16	170.6	31.0
P18	6503308.791	350124.565	152.0	11.2	12.2	-0.03	32.3	1.0
P19	6505689.081	351825.098	106.0	34.5	6.4	0.06	80.5	13.0
P20	6500914.878	350214.38	269.0	6.6	7.7	0.10	65.3	4.0
P21	6500952.001	350225.455	266.0	6.1	13.4	0.00	27.3	1.0
P22	6501439.094	349745.787	249.0	1.4	10.4	0.26	187.01	0.0
P23	6503282.877	348779.105	170.0	5.8	8.6	-0.52	50.1	2.0
P24	6503743.397	348511.693	181.0	17.0	5.2	0.07	156.4	16.0
P25	6503548.886	347520.597	220.0	6.6	6.1	0.48	132.7	8.0
P26	6504007.535	347194.189	246.0	3.9	6.7	0.05	271.1	21.0
P27	6504464.924	349200.807	180.0	21.2	6.6	-0.12	296.4	34.0
P28	6502334.821	348832.555	214.0	9.2	5.8	0.20	217.8	23.0
P29	6505610.806	349270.01	207.0	15.4	5.3	0.26	290.7	37.0
P30	6504910.426	350123.016	154.0	23.9	5.5	-0.09	148.2	32.0
P31	6504664.785	350050.575	180.0	11.7	5.5	0.16	338.6	56.0
P32	6505029.124	351608.249	166.0	6.8	6.1	0.11	149.1	32.0
P33	6505041.239	351570.022	161.0	21.2	5.6	0.01	112.5	27.0
P34	6505737.402	351809.307	94.0	39.2	4.3	-0.05	63.8	4.0
P35	6504447.271	349171.153	188.0	21.1	6.9	-0.05	317.9	42.0
P36	6501430.364	349703.72	249.0	2.4	9.9	0.34	157.8	3.0
P37	6504268.403	350195.415	119.0	9.2	8.7	0.00	48.5	3.0
P38	6502392.971	347559.263	233.0	10.3	6.4	0.15	362.9	24.0
P39	6502680.937	350574.069	240.0	19.6	5.7	0.14	403.1	60.0

TWI: topographic wetness index; DTR: distance from sampled point to the closest river stretch; DNR: difference in elevation between the sampling point and the closest river stretch.

Table S2.2 - Soil-related variables of the 39 soil moisture monitoring points in the surface layer (0-10 cm) and subsurface layer (10-20 cm).

Point	Land use and cover	BD ($g\ cm^{-3}$)	Macro ($cm^3\ cm^{-3}$)	Micro ($cm^3\ cm^{-3}$)	TP ($cm^3\ cm^{-3}$)	Total sand (%)	Clay (%)	Silt (%)	BD ($g\ cm^{-3}$)	Macro ($cm^3\ cm^{-3}$)	Micro ($cm^3\ cm^{-3}$)	TP ($cm^3\ cm^{-3}$)	Total sand (%)	Clay (%)	Silt (%)
		Surface layer (0-10 cm)							Subsurface layer (10-20 cm)						
P01	4	1.54	0.050	0.348	0.397	55.4	24.8	19.7	1.63	0.097	0.232	0.329	49.7	33.9	16.4
P02	2	1.47	0.083	0.329	0.412	53.5	25.7	20.8	1.06	0.229	0.292	0.521	48.6	32.2	19.2
P03	4/5	1.64	0.050	0.325	0.375	59.0	15.0	26.0	1.46	0.118	0.259	0.377	57.5	17.8	24.7
P04	2	1.28	0.132	0.349	0.481	50.3	20.8	28.8	1.26	0.236	0.256	0.493	54.6	19.7	25.7
P05	4/5	1.53	0.096	0.296	0.392	57.7	26.9	15.4	1.52	0.111	0.282	0.392	51.0	35.1	13.9
P06	2	1.52	0.130	0.282	0.412	63.8	13.6	22.6	1.47	0.120	0.259	0.379	64.2	12.8	23.0
P07	6	1.50	0.180	0.245	0.425	61.7	11.9	26.4	1.31	0.051	0.399	0.450	50.5	25.7	23.8
P08	6	1.30	0.270	0.269	0.540	66.2	15.3	18.4	1.45	0.098	0.317	0.415	66.9	14.3	18.8
P09	1	1.32	0.313	0.182	0.495	66.6	14.0	19.4	1.27	0.142	0.349	0.491	66.9	14.6	18.5
P10	3	1.51	0.149	0.232	0.382	63.3	17.7	18.9	1.32	0.141	0.320	0.461	63.7	17.5	18.8
P11	2	1.54	0.115	0.308	0.423	66.2	11.6	22.2	1.43	0.147	0.298	0.445	55.9	17.0	27.1
P12	3	1.51	0.099	0.302	0.401	56.7	18.8	24.6	1.42	0.039	0.394	0.433	58.7	18.0	23.3
P13	1	0.99	0.275	0.316	0.591	51.6	17.2	31.2	1.60	0.052	0.313	0.364	46.9	18.2	34.9
P14	4	1.37	0.067	0.413	0.480	41.0	34.9	24.0	1.52	0.071	0.335	0.406	34.8	43.8	21.4
P15	1	1.15	0.128	0.391	0.520	66.0	10.3	23.7	1.40	0.135	0.295	0.430	60.5	13.2	26.3
P16	4	1.63	0.090	0.266	0.356	72.7	7.2	20.1	1.71	0.040	0.385	0.424	73.3	7.4	19.4
P17	4/5	1.54	0.067	0.321	0.388	64.6	15.7	19.7	1.27	0.156	0.302	0.458	63.2	16.4	20.4
P18	2	1.49	0.153	0.265	0.417	62.6	11.9	25.5	1.49	0.172	0.245	0.416	63.6	11.6	24.9
P19	1	1.06	0.261	0.295	0.556	57.4	15.0	27.7	1.46	0.166	0.237	0.403	58.9	12.9	28.2
P20	2	1.41	0.173	0.301	0.474	68.6	14.4	17.0	1.29	0.129	0.339	0.468	63.1	17.6	19.3
P21	1	1.06	0.204	0.336	0.540	64.7	17.8	17.5	1.31	0.269	0.190	0.459	63.8	19.0	17.3
P22	4/5	1.44	0.058	0.396	0.454	58.6	19.1	22.3	1.54	0.221	0.181	0.402	58.8	18.9	22.4

(continued on next page)

Table S2.2 (Continued).

Point	Land use and cover	BD (g cm^{-3})	Macro (cm^3 cm^{-3})	Micro (cm^3 cm^{-3})	TP (cm^3 cm^{-3})	Total sand (%)	Clay (%)	Silt (%)	BD (g cm^{-3})	Macro (cm^3 cm^{-3})	Micro (cm^3 cm^{-3})	TP (cm^3 cm^{-3})	Total sand (%)	Clay (%)	Silt (%)
		Surface layer (0-10 cm)							Subsurface layer (10-20 cm)						
P23	4/5	1.41	0.106	0.385	0.491	54.6	16.8	28.6	1.14	0.103	0.472	0.574	54.5	17.2	28.3
P24	4/5	1.51	0.135	0.275	0.410	64.1	16.6	19.3	1.51	0.145	0.224	0.369	54.6	26.4	19.0
P25	2	1.39	0.080	0.378	0.458	50.5	21.3	28.3	1.15	0.237	0.273	0.509	46.6	24.9	28.5
P26	4/5	1.52	0.107	0.303	0.410	61.1	11.8	27.1	1.60	0.059	0.294	0.353	55.8	17.5	26.7
P27	2	1.57	0.232	0.198	0.430	72.6	11.4	16.1	1.29	0.220	0.254	0.474	72.7	10.8	16.5
P28	4/5	1.66	0.093	0.329	0.422	54.2	16.2	29.6	1.62	0.100	0.251	0.350	37.9	29.5	32.6
P29	1	0.89	0.289	0.294	0.583	50.5	19.6	29.9	1.42	0.167	0.290	0.457	51.5	19.8	28.7
P30	6	1.66	0.270	0.104	0.374	72.0	5.4	22.7	1.56	0.291	0.066	0.357	74.7	3.7	21.6
P31	4/5	1.49	0.250	0.132	0.382	70.4	11.5	18.0	1.43	0.305	0.148	0.453	68.8	12.2	19.0
P32	1	0.90	0.276	0.335	0.611	50.7	20.8	28.5	1.50	0.236	0.166	0.402	53.2	22.0	24.8
P33	4/5/6	1.41	0.192	0.244	0.436	66.0	16.1	17.9	1.55	0.092	0.304	0.397	63.6	16.3	20.2
P34	2	1.58	0.096	0.303	0.399	63.3	13.3	23.4	1.52	0.253	0.181	0.434	64.8	12.9	22.3
P35	1	1.37	0.239	0.227	0.466	64.2	16.3	19.5	1.40	0.204	0.240	0.444	62.3	18.2	19.6
P36	2	1.41	0.097	0.348	0.444	59.2	17.2	23.7	1.42	0.130	0.337	0.467	58.8	18.1	23.1
P37	4/5	1.58	0.217	0.178	0.395	68.5	10.5	21.0	1.58	0.060	0.318	0.378	68.5	10.7	20.9
P38	4/5	1.41	0.074	0.368	0.442	56.9	17.6	25.6	1.45	0.087	0.328	0.415	56.8	18.4	24.9
P39	1	1.09	0.174	0.361	0.535	51.5	18.6	29.9	1.58	0.068	0.322	0.390	53.1	19.5	27.4

Land use and cover (native forest, 1; native grassland, 2; fruit crops, 3; annual crops with vegetable covering, 4; annual crops without vegetable covering, 5; commercial forests, 6); BD: soil bulk density; Macro: Macroporosity; Micro: microporosity; TP: total porosity;

Table S2.3 - Variables selected through the initial method of linear correlations for the surface (MI-SS) and for the subsurface (MI-SB) layers. Variables selected on the best surface (MM-SS) and subsurface (MM-SB) models.

Variable	MI - SS	MI - SB	MM-SS	MM-SB	Variable	MI - SS	MI - SB	MM-SS	MM-SB
Elevation (m)			X	X	Min. Rel. humid. (%)				
Slope (%)		X	X	X	Max. Rel. humid. (%)				
TWI (-)			X	X	Rel. humid. (%)				
Curvature (-)					Soil Temp. 5 cm (ºC)				
DTR (m)					Global solar radiation (cal cm^{-2} day^{-1})	X	X		
DTR (m)					ETo (mm)				
Land use and cover	X	X	X	X	Cum. ETo of 5 days (mm)				
BD (g cm^{-3})	X	X	X	X	Cum. ETo of 7 days (mm)			X	
Macro (cm^3 cm^{-3})		X			Cum. ETo of 14 days (mm)				
Micro (cm^3 cm^{-3})	X	X	X	X	Cum. ETo of 21 days (mm)				
TP (cm^3 cm^{-3})		X			Cum. ETo of 30 days (mm)				
Soil water tension (cm Hg)	X	X		X	Cum. ETo of 45 days (mm)	X	X		X
Clay (%)	X	X		X	Cum. ETo of 60 days (mm)				
Silt (%)	X	X			Cum. rainfall of 6 h (mm)			X	
Total sand (%)	X	X	X	X	Cum. rainfall of 12 h (mm)				
Very Coarse sand (%)	X	X			Cum. rainfall of 1 day (mm)	X			X
Coarse sand (%)					Cum. rainfall of 2 days (mm)				
Medium sand (%)					Cum. rainfall of 3 days (mm)				
Fine sand (%)					Cum. rainfall of 4 days (mm)				
Very Fine sand (%)					Cum. rainfall of 5 days (mm)				
Season (-)			X	X	Cum. rainfall of 10 days (mm)				
Min. air temp. (ºC)					Cum. rainfall of 15 days (mm)	X	X		
Max. air temp. (ºC)	X				Cum. rainfall of 25 days (mm)	X			
Mean air temp. (ºC)					EWMA of past hourly rainfall (mm)		X	X	X

Table S2.4 - Statistical verification performance of the selected models for surface layer (0-10 cm).

Model	38	40	41	42	43	44	45	46	47	48	49	50	51	52	53	54	55	56
J[1]	18273	25024	2702	12649	57890	19391	29947	5839	2385	5166	18071	14351	62377	48001	16781	13005	34215	5852
Input variables[2]	1, 2, 3, 35, 36, 38, 43, 7, 24, 34, 18	2, 3, 35, 36, 38, 43, 7, 24, 34, 18	1, 3, 35, 36, 38, 43, 7, 24, 34, 18	1, 2, 35, 36, 38, 43, 7, 24, 34, 18	1, 2, 3, 36, 38, 43, 7, 24, 34, 18	1, 2, 3, 35, 38, 43, 7, 24, 34, 18	1, 2, 3, 35, 36, 43, 7, 24, 34, 18	1, 2, 3, 35, 36, 38, 7, 24, 34, 18	1, 2, 3, 35, 36, 38, 43, 24, 34, 18	1, 2, 3, 35, 36, 38, 43, 7, 34, 18	1, 2, 3, 35, 36, 38, 43, 7, 24, 18	1, 2, 3, 35, 36, 38, 43, 7, 24, 34	35, 36, 38, 43, 7, 24, 34, 18	1, 2, 3, 7, 24, 34, 18	1, 2, 3, 35, 36, 38, 43, 24, 34	1, 2, 3, 35, 36, 38, 43, 7, 18	1, 2, 3, 35, 36, 38, 43,	35, 7, 24, 34, 18
Verification																		
E10	-0.03	-0.029	-0.033	-0.029	-0.03	-0.034	-0.03	-0.033	-0.037	-0.029	-0.035	-0.034	-0.033	-0.038	-0.046	-0.036	-0.054	-0.061
E50	0.001	0.0014	-0.0041	-0.002	0.0017	-0.0006	-0.0018	0.0003	-0.0018	-0.0014	-0.0019	0.0004	0.0014	-0.003	0.0033	-0.0045	0	0.0033
E90	0.033	0.033	0.038	0.034	0.043	0.035	0.035	0.033	0.04	0.035	0.032	0.036	0.041	0.046	0.064	0.036	0.049	0.063
MAE	0.02	0.019	0.023	0.021	0.023	0.023	0.021	0.021	0.026	0.021	0.023	0.022	0.023	0.027	0.035	0.023	0.034	0.04
RMSE	0.026	0.026	0.030	0.027	0.031	0.029	0.028	0.027	0.033	0.027	0.031	0.029	0.031	0.035	0.045	0.031	0.044	0.052
NS	0.87	0.877	0.836	0.863	0.82	0.842	0.851	0.863	0.794	0.858	0.817	0.844	0.824	0.77	0.617	0.824	0.635	0.497

[1]J: number of cycles used in model selection.

[2]Input variables: 1: elevation; 2: Slope; 3: TWI; 7: Season; 15: Global solar radiation; 18: Cumulative 7-day ETo ; 22: Cumulative 45-day ETo ; 24: Cumulative 6-h rainfall; 26: Cumulative 1-day rainfall; 32: Cumulative 15-day rainfall; 34: EWMA of rainfall in the hour before sampling; 35: Land use and cover; 36: Soil bulk density; 37: Macroporosity; 38: Microporosity; 39: Total Porosity; 40: Soil water tension; 41: Clay; 42: Silt; 43: Total Sand; 44: Very Coarse sand.

Table S2.5 - Statistical verification performance of the selected models for subsurface layer (10-20 cm).

Model	01	49	51	52	53	54	55	56	57	58	59	60	61	62	63	64	65	66	67	68	69
J[1]	31916	16618	14407	18609	11753	3560	15939	13165	21436	56225	5079	8024	37614	41028	53945	61888	49176	3784	53695	13096	1193
Input variables[2]	2, 35, 36, 37, 38, 39, 40, 41, 42, 43, 44, 15, 32, 34, 22	1, 2, 3, 35, 36, 38, 40, 41, 43, 7, 26, 34, 22	2, 3, 35, 36, 38, 40, 41, 43, 7, 26, 34, 22	1, 3, 35, 36, 38, 40, 41, 43, 7, 26, 34, 22	1, 2, 35, 36, 38, 40, 41, 43, 7, 26, 34, 22	1, 2, 3, 36, 38, 40, 41, 43, 7, 26, 34, 22	1, 2, 3, 35, 38, 40, 41, 43, 7, 26, 34, 22	1, 2, 3, 35, 36, 40, 41, 43, 7, 26, 34, 22	1, 2, 3, 35, 36, 38, 41, 43, 7, 26, 34, 22	1, 2, 3, 35, 36, 38, 40, 43, 7, 26, 34, 22	1, 2, 3, 35, 36, 38, 40, 41, 7, 26, 34, 22	1, 2, 3, 35, 36, 38, 40, 41, 43, 26, 34, 22	1, 2, 3, 35, 36, 38, 40, 41, 43, 7, 26, 34	1, 2, 3, 35, 36, 38, 40, 41, 43, 7, 34, 22	1, 2, 3, 35, 36, 38, 40, 41, 43, 7, 26, 22	35, 36, 38, 40, 41, 43, 7, 26, 34, 22	1, 2, 3, 7, 26, 34, 22	1, 2, 3, 35, 36, 38, 40, 41, 43, 26, 34	1, 2, 3, 35, 36, 38, 40, 41, 43, 7, 22	1, 2, 3, 35, 36, 38, 41, 43	35, 40, 7, 26, 34,22
Verification																					
E10	-0,024	-0.021	-0.022	-0.024	-0.022	-0.027	-0.023	-0.028	-0.028	-0.023	-0.025	-0.027	-0.025	-0.024	-0.024	-0.029	-0.042	-0.027	-0.025	-0.045	-0.07
E50	-0,011	0.0002	0.0006	0.0029	-0.0005	-0.0005	0.0019	0.0013	0.0021	0.0011	0.0004	0.0009	-0.0001	0.0006	0.0007	0.0025	-0.0005	0.0044	-0.0013	0.0018	0.0036
E90	0,033	0.025	0.03	0.032	0.028	0.028	0.034	0.031	0.03	0.032	0.032	0.035	0.03	0.029	0.027	0.03	0.043	0.041	0.028	0.047	0.057
MAE	0,018	0.015	0.017	0.017	0.017	0.018	0.018	0.019	0.018	0.018	0.018	0.018	0.017	0.017	0.016	0.018	0.026	0.021	0.017	0.03	0.043
RMSE	0,026	0.020	0.022	0.023	0.022	0.023	0.024	0.025	0.023	0.024	0.024	0.025	0.021	0.022	0.021	0.024	0.034	0.027	0.022	0.040	0.055
NS	0,833	0.893	0.865	0.87	0.882	0.864	0.852	0.846	0.861	0.858	0.862	0.842	0.877	0.877	0.883	0.858	0.708	0.816	0.88	0.594	0.224

[1]J: number of cycles used in the best model validation result.

[2]Input variables: 1: elevation; 2: Slope; 3: TWI; 7: Season; 15: Global solar radiation; 18: Cumulative 7-day ETo ; 22: Cumulative 45-day ETo ; 24: Cumulative 6-h rainfall; 26: Cumulative 1-day rainfall; 32: Cumulative 15-day rainfall; 34: EWMA of rainfall in the hour before sampling; 35: Land use and cover; 36: Soil bulk density; 37: Macroporosity; 38: Microporosity; 39: Total Porosity; 40: Soil water tension; 41: Clay; 42: Silt; 43: Total Sand; 44: Very Coarse sand.

CAPÍTULO 3

Influence of Initial Soil Moisture and Precipitation on Runoff Generation in a Small Catchment

Guilherme Kruger Bartels [1], Nilza Maria dos Reis Castro [1], Gilberto Loguercio Collares [2]

[1] Instituto de Pesquisas Hidráulicas, Universidade Federal do Rio Grande do Sul (Institute of Hydraulic Research, Federal University of Rio Grande do Sul - IPH/UFRGS), Av. Bento Gonçalves, 9500, Porto Alegre - RS, Brazil.

[2]Centro de Desenvolvimento Tecnológico, Universidade Federal de Pelotas (Center for Technological Development, Federal University of Pelotas - CDTec/UFPel), Rua Gomes Carneiro 01, Pelotas - RS, Brazil.

Abstract

We investigated the relationships among soil moisture, rainfall, and runoff in a catchment in southern Brazil to evaluate the impact of antecedent soil moisture (Θ_i) on the runoff coefficient. We analyzed 104 rainfall-runoff events over four years of monitoring, and soil moisture data were obtained from a robust model of artificial neural networks. The results indicate a significant relationship between runoff depth and total precipitation (P). The antecedent soil moisture index (ASI) exhibited a significant Pearson correlation coefficient with runoff only when used in conjunction with P (ASI+P). The relationship between Θ_i and the runoff coefficient was significant but weak, with a large dispersion of the runoff coefficient for soil water content above field capacity. Although a threshold was not evident between Θi and the runoff coefficient, the highest runoff coefficients were recorded in events whose Θi was close to or greater than the field capacity.

Keywords: soil water content, rainfall events, antecedent soil moisture, runoff generation

3.1 Introduction

The hydrological response of a watershed to a single precipitation event is related to its interaction with various factors that control runoff (Castillo et al., 2003). Among these, the antecedent soil moisture, that is, the soil water content at the beginning of a precipitation event, is a crucial factor that, together with the hydraulic characteristics of the soil, influences the water storage capacity in the soil and, therefore, the runoff generation in the watershed (Uber et al., 2018). Under high initial soil moisture conditions, rainfall events of a certain depth and intensity can cause a solid reaction to runoff, whereas the same event occurring under conditions of low soil water content can drive runoff to small magnitudes (Meißl et al., 2020).

Several authors have highlighted the importance of soil water content in generating runoff in hydrographic basins of different scales, both in semi-arid and more humid regions (James and Roulet, 2009; Penna et al., 2011; Zhang et al. ., 2011; Nied et al., 2013; Uber et al., 2018; Schoener and Stone, 2019). Others have analyzed the response sensitivity of event-based hydrological models under different soil moisture conditions (Castillo et al., 2003; Tramblay et al., 2010; Hu et al., 2015; Grillakis et al., 2016; Morbidelli et al., 2016). For example, in a tropical dry forest watershed, Farrick and Branfireun (2014) observed that after reaching certain thresholds of soil water content and precipitation, the magnitude of the runoff was governed by the rainfall event characteristics rather than by previous soil moisture conditions. In a study of 100 watersheds in Australia, the increased the magnitude of precipitation events also reduced the effect of antecedent moisture on flood volume (Bennett et al., 2018).

Generally, there are two processes for generating runoff in a watershed: i) when the rainfall intensity exceeds the soil infiltration capacity, the runoff is dependent on the intensity of the rainfall and the characteristics of the surface layer of the soil; ii) when rainfall exceeds the water storage capacity in the soil, saturation overland flow occurs, and the runoff is dependent on precipitation depth (Scherrer et al., 2007).

Thus, threshold behavior can characterize the processes of flow formation in a watershed. Studies have shown that higher runoff coefficients occur only if a specific soil moisture condition is reached (Penna et al., 2011; Huza et al., 2014; Mcmillan et al., 2014; Meißl et al., 2014; Meißl et al. al., 2020). However, this threshold behavior may not be evident in some watersheds that present high dispersion of runoff coefficients, mainly under high soil moisture conditions, as reported by Uber et al. (2018). This could be due to the spatial and temporal dynamics of soil moisture (Huza et al., 2014).

In Brazil, recent efforts have been made to create hydrological databases on a continental scale (Chagas et al., 2020; Almagro et al., 2021). However, a soil moisture data time series was not available. Even in experimental watersheds, a recent review showed that soil moisture is poorly monitored in Brazil (Melo et al., 2020). Additionally, the soil moisture monitoring network of the National Center for Monitoring and Early Warning of Natural Disasters (CEMADEN) is restricted to the semiarid region of Brazil (Zeri et al., 2020). The scarcity of long-term observations of soil moisture measurement networks and their uneven distribution is not limited to Brazil (Sungmin and Orth, 2021). To circumvent this, some authors have used indirect information, such as the antecedent precipitation index, to characterize antecedent moisture conditions (Rodríguez-Blanco et al., 2012; Zhao et al., 2019; Bennedtt et al., 2018). However, the weak relationship between precipitation before the events and the initial soil moisture compromises the use of such information (Brocca et al., 2008; Hagen et al., 2020).

In this study, we investigated the relationship between soil moisture, rainfall, and runoff in a headwater catchment in southern Brazil to evaluate the possible impact of antecedent soil moisture on the runoff coefficient. We used surface and subsurface soil moisture data obtained from a robust model of artificial neural networks (ANNs) previously developed specifically for the study area of this research (Bartels et al., 2021). The developed model was trained and validated using soil moisture data collected in situ, making it possible to evaluate the uncertainties associated with soil moisture estimates. By analyzing 104 rainfall-runoff events from four years of monitoring in combination with antecedent soil moisture estimates, we intend to answer the following questions:

- Which precipitation characteristics are most relevant to the increase in the runoff?
- What are the combined effects of antecedent soil moisture conditions and total precipitation on runoff?
- What is the relationship between the soil moisture at the beginning of the event and the runoff coefficient? Is it possible to establish a clear threshold between the antecedent soil moisture and runoff coefficient?

3.2 Materials and methods

3.2.1 Study Site

This study was conducted in the Arroio do Ouro headwater, located south of the state of Rio Grande do Sul, Brazil (Figure 3.1). The Arroio do Ouro headwater is a third-order (Strahler scheme) catchment area of 2.16 km^2, with an altitude between 238.6 m and 329.9 m and a 10% average slope. The study region is located in the Pelotas Batholith, a plutonic complex including granite, gabbro, and diorite, within the geotectonic unit of the Dom Feliciano Belt, in the eastern portion of the Sul-Rio-Grandense Shield (Philipp et al., 2016). The classification soils of the Arroio do Ouro watershed are Acrisols and Regosols (FAO, 2014), characterized by being shallow with a predominantly sandy-loam texture (35–75% sand) (Bartels et al., 2016, 2021).

The land use in the catchment did not change during the analysis period. The main agricultural activity is soybean and corn cultivation, which accounts for 21.6% of the catchment area during summer. These crops are replaced by pastures such as ryegrass (*Lolium multiflorum*) in winter. Soil management in agricultural areas is characterized by conventional and minimal tillage. In addition to maintaining residues on the soil surface in some areas, no other conservation measures, such as terraces, have been implemented. However, the main land use is natural grassland (51.4%). Dairy cattle and meat production activities are the main economic activities of the farmers. The riparian areas represent important parts of the catchment (23.3%), indicating the conservation of the marginal regions of the channels, thus preventing the occurrence of erosion on the banks of the channels.

According to the Köppen climate classification, the region's climate is of the "Cfa" type, with well-distributed rainfall throughout the year (Alvares et al., 2013).

Information obtained from the meteorological station of the Instituto Nacional de Meteorologia (INMET) from 1971—2020 showed that the average annual precipitation in the region was 1.399 ± 297 mm with a reference evapotranspiration (ETo) of 1.080 ± 36 mm (Figure 3.1). The average monthly rainfall was well distributed throughout the year, with a minimum of 103 ± 69 mm (December) and a maximum of 147 ± 95 mm (February). In contrast, ETo presented a minimum monthly average of 36 ± 3 mm in June (winter) and a maximum monthly average of 150 ± 11 mm in December (summer).

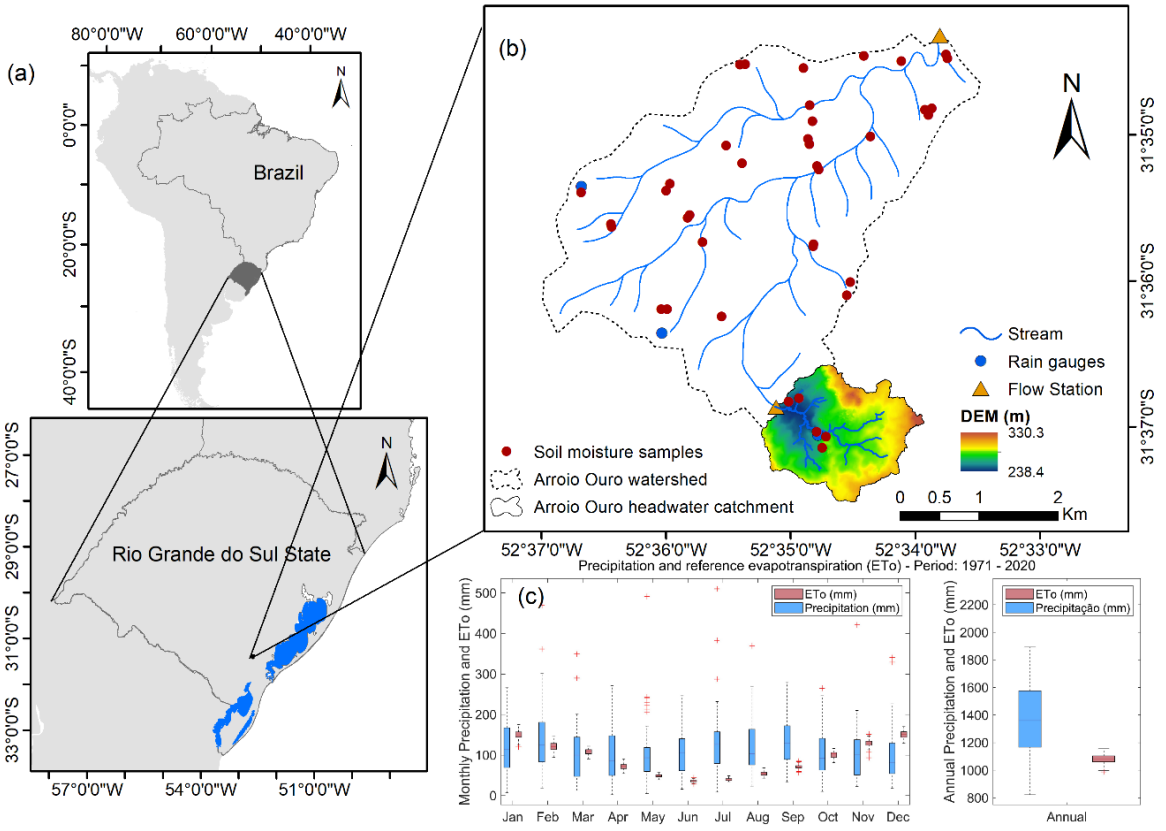

Figure 3.1 - (a) Study area in the State of Rio Grande do Sul, Brazil; (b) Arroio do Ouro watershed, Arroio do Ouro headwater catchment showing digital elevation model, streams (blue lines), soil moisture samples (red points), rain gauges (blue points) and flow station (yellow triangle); (c) Precipitation and reference evapotranspiration for period 1971 – 2020.

3.2.2 Soil Water Retention Curves

A total of 75 sample points in the catchment were sampled to determine the soil water retention curves (Bartels et al., 2016; Tronco, 2020). At each point, three undisturbed soil samples were collected in volumetric rings (0.076 m diameter; 344.1 cm^3) using an Uhland soil sampler in the surface layer (0—10 cm) and subsurface (10—20 cm). Soil water retention curves (SWRCs) were obtained by applying tensions of 1, 6, and 10 kPa in a tension table (Reinert and Reichert, 2006), 33 and 100 kPa in Richard's chambers (Klute, 1986). For low soil moisture content, which corresponds to tensions of 500, 1000, and 1500 kPa, a psychrometer Dewpoint Potential Meter WP4 (Decagon Devices, 2007) was used. For the 75 sampling points, SWRCs were fitted using the van Genuchten (1980) model.

3.2.3 Soil Moisture Time-Series

Soil moisture measurements were obtained from the study developed by Bartels et al. (2021), who investigated the use of ANN models to estimate soil moisture in the Arroio do Ouro watershed. The authors developed robust soil moisture estimation models for the surface (0-10 cm) and subsurface (10-20 cm) layers by collecting soil moisture data from 39 monitoring points. We took advantage of the database developed by the authors and constructed a soil moisture time series with ANN models for five monitoring points within the Arroio do Ouro catchment. The ANN models were used to develop the soil moisture series for the surface and subsurface layers based on the availability of the input data and statistical performance during the model verification step. The statistical indicators used in this step were based on the errors between the observed and simulated values, such as the mean absolute error (MAE) and quantiles of the error distribution (10% and 90%). The surface layer model used 11 network input variables and presented the following error distribution statistics in $cm^3\ cm^{-3}$: MAE = 0.031, E10 = -0.049, E90 = 0.044. In contrast, the subsurface layer model was fitted with 11 network input variables and presented the following errors in $cm^3\ cm^{-3}$: MAE = 0.024, E10 = -0.038, and E90 = 0.041. More information regarding the performance of the ANN models is provided in the Supporting Information (Table S3.1 and Figure S3.1). Both models presented satisfactory performances, with symmetrical distributions of errors (E10 versus E90)

and MAE values near zero during the verification stage. These results encouraged us to use these models to construct soil moisture time series.

The soil moisture time series was generated at 15 min intervals from August 2017 to September 2021 (Figure 3.2). We carefully removed all ANN model values extrapolated from the time series of soil moisture. That is, data outside the domain (extreme values) in the network training stage, both in terms of input and output variables (soil moisture), were removed (data gaps in Figure 3.2). We then used the soil moisture series from the five sites (Figure 3.1b) to obtain the average volumetric soil moisture and calculate the antecedent soil moisture index (ASI) for one hour before the start of an event:

$$ASI = \sum_{i=1}^{N}(\overline{\theta_i} \times d_i) \quad (1)$$

where *i* represents the soil layers, *N* is the number of soil layers, $\overline{\theta_i}$ is the average volumetric soil water content at the five monitored points in layer *i* ($cm^3\ cm^{-3}$), and *di* is the depth of layer *i* (10 cm). To determine the upper and lower limits of the average volumetric soil moisture and the ASI, the quantiles considered here were 5% and 95% error distributions between the observed and estimated values with soil moisture models.

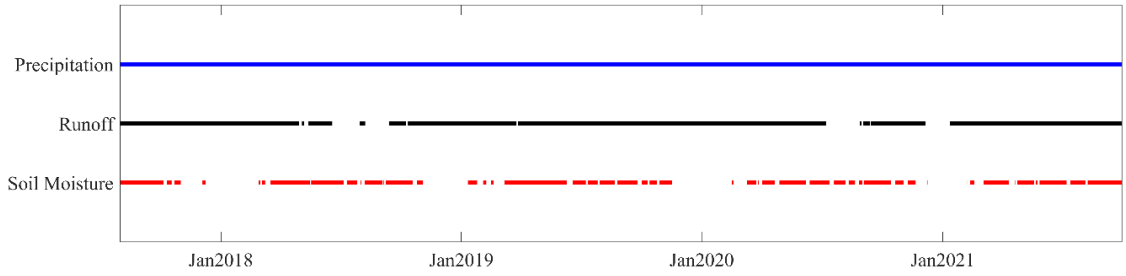

Figure 3.2 - Temporal coverage of the runoff, precipitation, and soil moisture time series.

3.2.4 Precipitation Data

Precipitation data from 8/2017 to 9/2021 were obtained from three rain gauges (Figure 3.1) with a temporal resolution of 15 min. We used the mean precipitation, calculated using the Thiessen polygon, to identify and characterize the rainfall events. We adopted the following criteria to identify rain events: (i) a rainfall event must have a total rainfall of at least 6 mm; (ii) precipitation readings below 0.2 mm in 15 min were excluded; (iii) rainfall events were separated if no rainfall was recorded for at least three hours. Within the considered time period, we identified 241 rainfall

events that met all conditions described. To differentiate rainfall events by their characteristics, events were grouped using Ward's hierarchical clustering (Ward, 1963) and Euclidean distance as dissimilarity measures (Everitt and Dunn, 1991). Cluster analysis was based on total rainfall (mm), rainfall duration (h), maximum 15 min intensity (mm/h), and mean intensity of the rainfall event (mm/h). To calculate the Euclidean distance, the characteristics of precipitation events must be weighted the same; thus, it was necessary to standardize the variables characterizing precipitation events (Urgilés et al., 2021).

3.2.5 Discharge and rainfall - runoff events

Discharge was measured continuously at the outlet catchment (Figure 3.1) using a Doppler acoustic meter (Sontek-IQ Plus) with a temporal resolution of 10 min. The equipment was installed on a channel bed to measure the flow depth and velocity. A vertical acoustic beam measures the flow depth or built-in pressure sensor when vertical acoustic beam data are not available. The flow velocity was measured with four 3.0 MHz acoustic beams angled upstream, downstream, and to the left and right banks, tracing the flow velocity profile along the column (Fulford and Kimball, 2015). All discharge data were acquired using a Doppler acoustic meter. Periods in which only stage data were available were discarded.

Baseflow must be eliminated to quantify the runoff coefficient of each rainfall event. To separate the base flow, we used the recursive digital filter (RDF) proposed by Lyne and Hollick (1979) because of its ease of application and good correlation with other physical methods such as electrical conductivity (Uber et al., 2018). According to the recommendation of Ladson et al. (2013), the value of the filter parameter α was centered at 0.98. Therefore, we used the approach proposed by Meißl et al. (2020) to analyze the uncertainty of the baseflow estimate. We systematically tested 49 values of the α-filter parameter, ranging from 0.969 to 0.993. The runoff of each event was obtained by subtracting the median value of the base flow, and the upper and lower limits were considered quantiles of 5% and 95% of the base flow. The master recession curve parameterization tool (MRCPtool; Carlotto and Chaffe, 2019) was used for baseflow separation. Rainfall-runoff events were identified at the start of the rainfall event and ended 12 h after the rainfall event

ended or until the start of the next rainfall event. The runoff coefficient of each event was defined as the ratio between the runoff depth and the total event precipitation. Finally, we analyzed 104 rainfall-runoff events because of the availability of rainfall, runoff, and soil moisture data.

3.3 Results

3.3.1 Characteristics of rainfall events

We identified 241 rainfall events over four years (8/2017 to 9/2021). The events were clustered into three types according to the characteristics specified below (Figure 3.3): (i) C1: events with low total precipitation, short duration, low mean intensity, and low maximum 15 min intensity (n = 190); (ii) C2: events with high total precipitation, long duration, low mean intensity, and mean maximum 15 min intensity (n = 27); and (iii) C3: events with intermediate total precipitation, short duration, and high mean and maximum 15 min intensities (n = 24). Most of the analyzed events (79% of the total) had short durations and low intensities (C1, Figure 3.4a). However, the precipitation from these events represented 54% of the total precipitation recorded across all events (Figure 3.4b). Although Cluster 2 rainfall events occurred in a smaller number (11% of the total), their fraction of the total precipitation was high (32%). This cluster of events was important in winter (June 21 to September 22), representing 45% of the total precipitation (Figure 3.4b). In contrast, events with short durations and high intensities (C3) occurred in smaller numbers (10% of the total) and were more important in the summer period (December 21 to March 21), where they represented 41% of the volume of precipitation (Figure 3.4b).

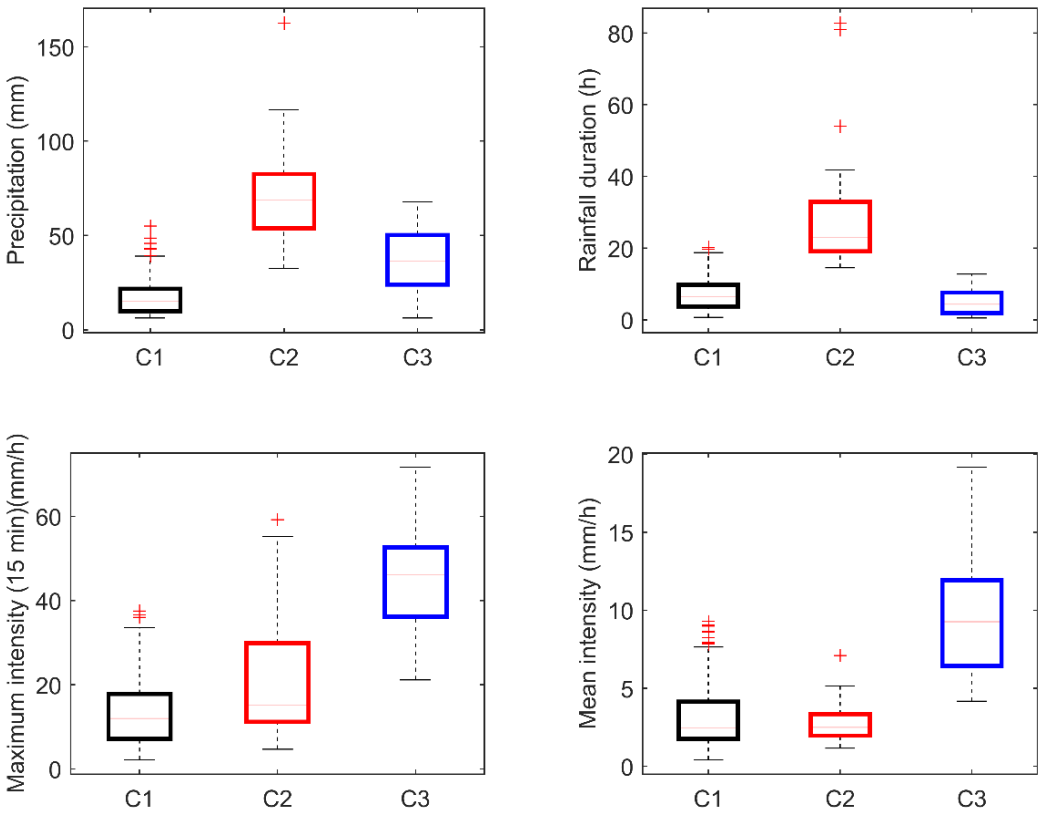

Figure 3.3 - Characteristics of the three clustered types of rainfall events (C1–C3) in terms of total precipitation (a), rainfall duration (b), maximum 15 min intensity (c), and mean intensity (d).

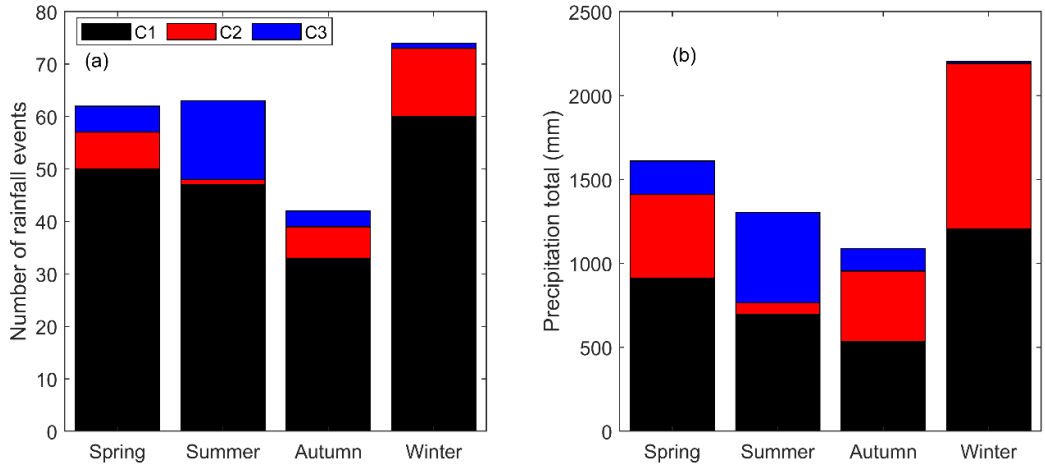

Figure 3.4 - Distribution of events grouped into three clusters according to season (a) number of precipitation events; (b) precipitation total.

3.3.2 Rainfall-runoff relationships

From the 2017 to 2021 dataset, we analyzed 104 rainfall-runoff events, given the mutual availability of precipitation, runoff, and soil moisture data. The total precipitation during these events ranged from 6.2 to 112.9 mm, with a mean of 24.9 mm. Rainfall duration ranged from 0.5 to 54 h with a mean duration of 9.9 h. The mean rainfall intensities ranged from 0.4 to 15.6 mm h^{-1}. The maximum 15 min intensities presented values between 2.4 and 60 mm h^{-1} with 95% of events < 34 mm h^{-1}. The surface runoff depth generated for each event presented values between 0.04 and 21.5 mm (Figure 3.5), and the Pearson correlation coefficient showed a statistically significant linear relationship with the total precipitation (r = 0.877; ρ < 0.05, Figure 3.5a), the same way that maximum 15 min intensity (r = 0.336; ρ < 0.05, Figure 3.5b), however, with a greater dispersion. In contrast, Pearson's coefficient showed a non-significant weak linear relationship between surface runoff depth and mean rainfall intensity (r = 0.04; ρ > 0.05, Figure 3.5c). The vertical gray bars in Figure 3.5 indicate the uncertainty associated with hydrograph separation, considering the different values of the α parameter of the recursive digital filter (considering the 5% and 95% confidence intervals). As can be seen, this uncertainty is associated with the magnitude of the surface runoff of each event.

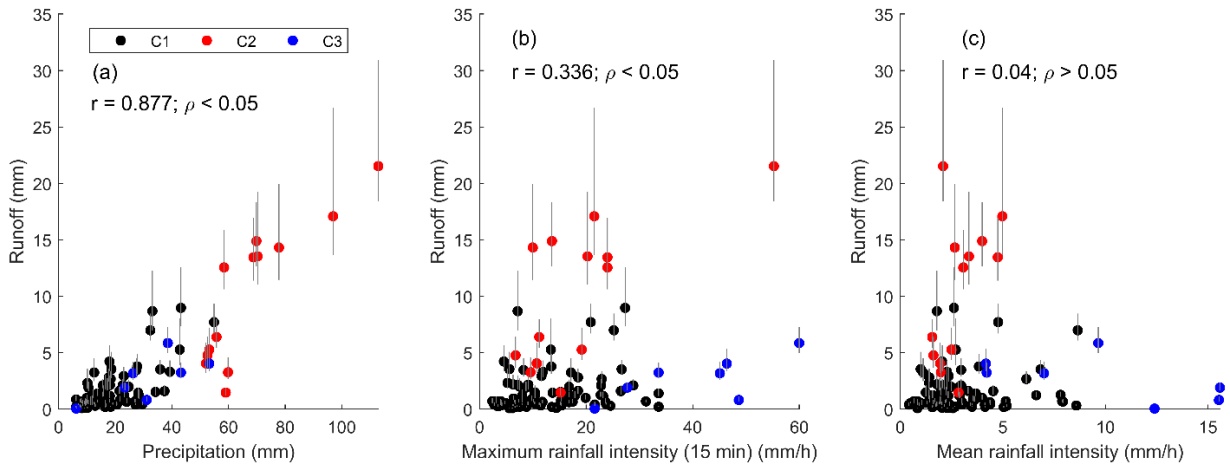

Figure 3.5 - Relationships surface runoff depth and (a) precipitation total (P), (b) maximum 15 min rainfall, (c) mean rainfall intensity.

3.3.3 Soil moisture's contribution to runoff generation

3.3.3.1 Antecedent Soil Moisture Index

The antecedent soil moisture index (ASI) for the two soil layers (0 – 20 cm) was calculated using Eq. (1) to characterize the soil surface water storage. The ASI presented values between 36.7 to 67.7 mm with a mean of 56.6 mm. The Pearson's coefficient results in a weak linear relationship between ASI and runoff depth (r = 0.216; $\rho < 0.05$, Figure 3.6a), indicating that ASI alone exerts little control over runoff. This changed when the ASI was added to the total precipitation (P) of each event (Figure 3.6b). The strong and significant linear relationship between ASI+P and surface runoff (r = 0.858; $\rho < 0.05$, Figure 3.6b) demonstrated that the use of ASI+P exerted greater control over surface runoff. The horizontal gray bars in Figure 3.6 indicate the uncertainty associated with the soil moisture values (considered in the ANN models) calculated from the distribution quantiles of the 5% and 95% errors. In this way, the distribution of errors presented for soil moisture associated with the ANN models was homogeneous for all precipitation events, contrary to what was observed with the uncertainty associated with the separation of the hydrographs (vertical gray bars).

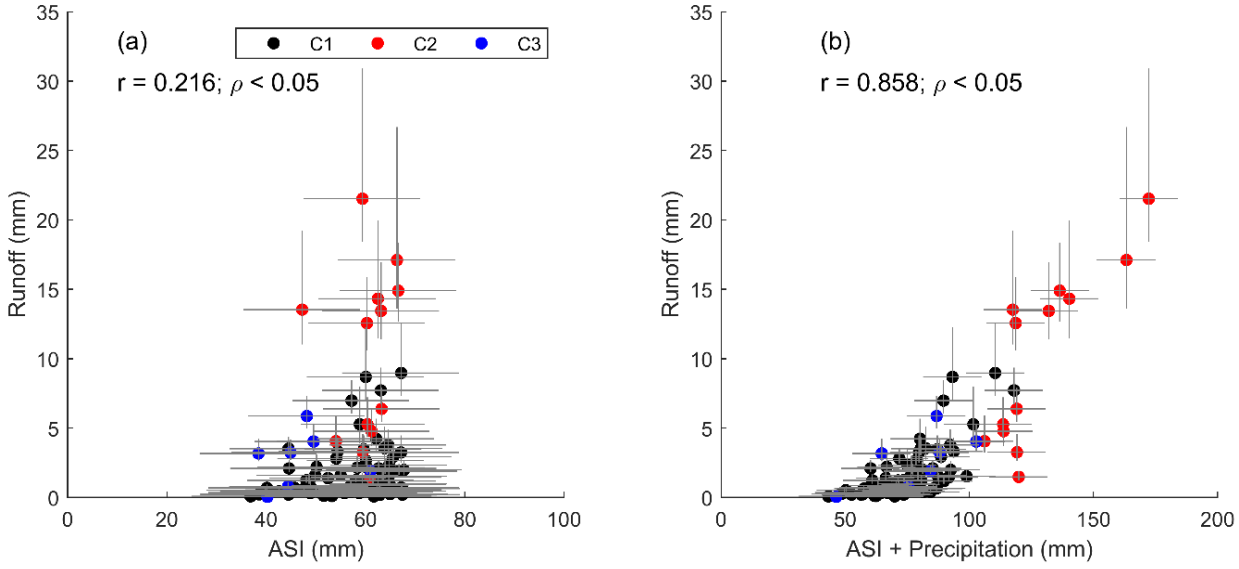

Figure 3.6 - Relationships between runoff and (a) antecedent soil moisture index (ASI), (b) ASI + Precipitation.

3.3.3.2 Runoff coefficients

The runoff coefficients calculated for the 104 analyzed events varied between 0.008 and 0.262, with mean values of 0.09. Antecedent soil moisture to the events varied between 0.18 and 0.34 cm^3 cm^{-3} with a mean of 0.28 cm^3 cm^{-3}, considering the two analyzed layers (0–20 cm). Pearson's coefficient showed a significant linear relationship between antecedent soil moisture and runoff coefficient ($r = 0.357$; $\rho < 0.05$, Figure 3.7). However, this relationship was weak given the high variability of the runoff coefficient, especially when the antecedent soil moisture was close to or higher than the mean (Figure 3.7). Only 15% of the events had runoff coefficients greater than 0.17. Eight events were in cluster C1 and seven were in cluster C2. Even so, events grouped into clusters C1 and C2 had very different runoff coefficients, with values close to zero (Figure 3.7).

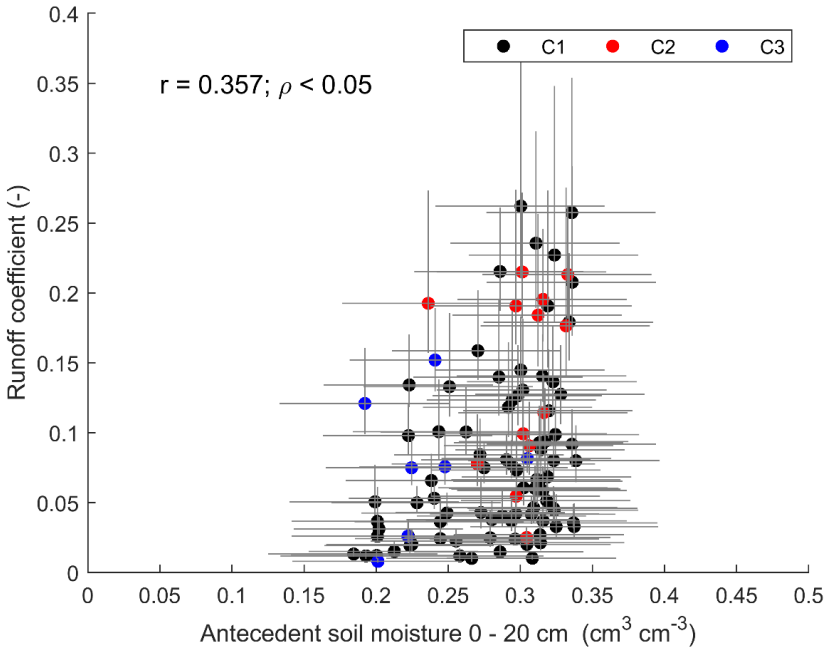

Figure 3.7 - Relationships between antecedent soil moisture and runoff coefficient.

3.4 Discussion

3.4.1 Effects of rainfall characteristics on runoff

The dependence of runoff on rainfall characteristics is consistent with that observed in other studies conducted on hillslopes and watersheds (Wei et al., 2020; Zhang et al., 2021; Wang et al., 2022). The strong relationship between total precipitation and runoff depth (Figure 3.5a) indicates that when soil water storage deficits are satisfied, the runoff response depends on the characteristics of the rainfall event, as demonstrated in other watersheds (Penna et al., 2011; Farrick and Branfireun, 2014). The highest observed runoff depths were observed in the events with the highest total precipitation and longest duration, which usually occurs in winter and spring. However, the mean rainfall intensity did not show a significant relationship with runoff, corroborating the findings of previous studies (Farrick and Branfireun, 2014; Uber et al., 2018; Zhang et al., 2021). The events analyzed in the Arroio do Ouro catchment may characterize the importance of the initial soil moisture conditions. Virtually all of the most intense events (cluster C3) had below-average initial soil moisture conditions (Figure 3.7). Owing to the low water content in the soil, it is unlikely that the soil reached saturation, starting with saturated flow for these events. Despite the high maximum 15 min intensity, it is unlikely that these events exceeded the infiltration capacity of the soil surface layers (Bartels et al., 2016).

3.4.2 Antecedent soil moisture threshold for runoff reaction

There was no evidence of an antecedent soil moisture threshold with the runoff coefficient for the events analyzed in the Arroio do Ouro catchment area. Some studies indicate limited soil moisture, above which significant increases in the runoff coefficient occur. For example, Penna et al. (2011) analyzed the influence of soil moisture on surface runoff generation processes in an alpine watershed and identified a threshold value for soil moisture (approximately 45 vol%), above which runoff increased significantly. In an alpine watershed, Meißl et al. (2020) found an explicit threshold behavior where runoff coefficients above 0.23 only occurred when the mean soil moisture exceeded 43.5 vol%. A study by Huza et al. (2014) in a watershed in southern France showed a lower initial soil moisture threshold (22 vol%). In other studies, however, the antecedent soil moisture threshold to generate runoff coefficient increases was not clear, as also shown in our results (Figure 3.7). When evaluating the influence of initial soil moisture in a southern France catchment,

Uber et al. (2018) found a threshold of 34 vol% of the initial soil moisture to generate a high runoff coefficient. However, the authors reported that only three events below this threshold were considered; thus, more measurements are needed to corroborate this result.

The high dispersion of the runoff coefficient, found mainly under conditions of higher initial soil moisture, indicates a very complex relationship that is dependent on other poorly understood factors and processes (Uber et al., 2018). Thus, the weak relationship between the antecedent soil moisture and the runoff coefficient may be associated with the limitations of the precipitation measurement owing to either the hydrograph separation method or the fact that the antecedent soil moisture is only one among many different factors that influence flow (Meißl et al., 2020). Furthermore, the sensitivity of the runoff coefficient to the antecedent soil moisture may be related to the dominant runoff process. In experimental plots in Switzerland, Scherrer et al. (2007) observed that sites with dominant surface flows are slightly affected by the antecedent moisture condition, as the response is rapid in both dry and humid conditions. In contrast, the plots with dominant subsurface flow were very sensitive to antecedent soil moisture.

Other studies have reported the effects of soil moisture nearing field capacity on soil water movement. In tank experiments, Song and Wang (2019) noted that soil moisture near field capacity was a threshold between rainfall and runoff events that generated lower and higher runoff coefficients. Similarly, Ruggenthaler et al. (2015) found that field capacity is a threshold for surface runoff estimates on experimental slopes in Austria. Meyles et al. (2006) observed that soil moisture above field capacity generated an exponential increase in discharge in a headwater catchment in southeast Dartmoor (UK). In the Arroio do Ouro catchment, the high variability of the runoff coefficient may be associated with soil moisture close to the field capacity. Analysis of the soil water retention curves obtained at 75 sampling sites in the catchment (Figure 3.8a) showed that the median field capacity was ~0.29 cm^3 cm^{-3} for both layers (Figure 3.8b), considering the field capacity at a matric potential of -10 kPa (Timm et al., 2020) adjusted to the van Genuchten (1980) model. This value is similar to that of the mean soil moisture before the events (0.28 cm^3 cm^{-3}); the events that recorded the highest runoff coefficients presented antecedent soil moisture very

close to or higher than the field capacity (Figure 3.7), considering the median of the soil water retention curves.

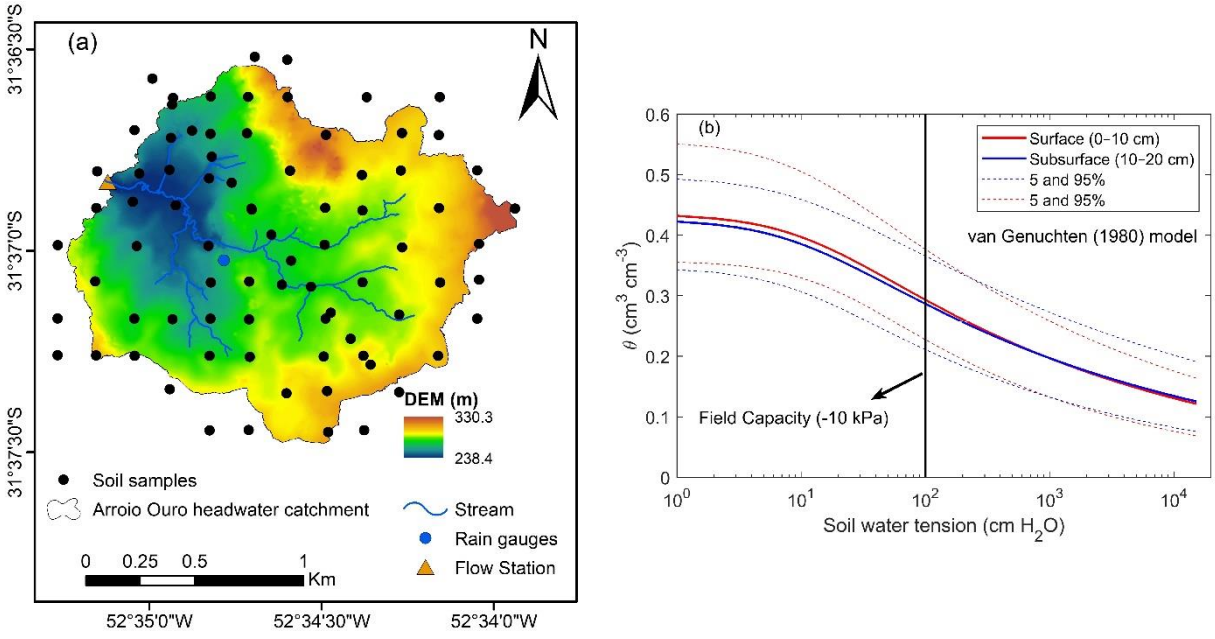

Figure 3.8 - (a) Arroio do Ouro catchment showing digital elevation model, streams (blue lines), soil water retention curve samples (black dots), rain gauges (blue dots) and flow station (yellow triangle); (b) Soil water retention curve for layer 0–10 cm (red line) and 10–20 cm (blue lines).

Under soil moisture conditions close to or greater than field capacity, the water content available for drainage and flow is limited mainly by rainfall rather than by soil water storage conditions (Farrick and Branfireun, 2014). This is more evident in the relationship between runoff depth and ASI + precipitation (Figure 3.6b). Events with ASI+P values below field capacity (approximately 58 mm) resulted in runoff below 5 mm. On the other hand, events in which the ASI+P depth was higher than the total porosity may have reached soil saturation in at least 50% of the soil water retention curves (approximately 86 mm), generating runoff of the order of 0.6 to 21.5 mm. If we look more closely, events with a runoff depth greater than 9 mm were those whose ASI+P exceeded the total porosity (approximately 104 mm), considering the 95% confidence interval. In other words, the highest runoff levels were only observed when the entire catchment reached soil saturation. Soils under saturation conditions led to a more significant amount of rapid surface flow and water-filled pores favoring the rapid start of subsurface flow (Meißl et al., 2020).

3.5 Study Limitations and Research Recommendations

As described in Section 3.2.3, we used ANN models to generate the soil moisture time series. Both models (surface and subsurface layers) had satisfactory performances with very symmetrical errors and MAE values close to zero (Figure S3.1). However, it was necessary to remove a series of soil moisture data to extrapolate the ANN models. The ANN models that were built can only represent the entire data domain (extreme values), for both input and output variables, in the form of soil moisture (Bartels et al., 2021). Thus, of all rainfall events (241), many had to be removed from the analysis, resulting in only 104 rainfall-runoff events being analyzed, given the mutual availability of precipitation, discharge, and antecedent soil moisture data. Additionally, continuous analysis of soil moisture throughout rainfall-runoff events was not possible because many events, especially those with high precipitation, had periods with input values outside the domain of the data used in the ANN training.

We recommend that future research compiles soil moisture data that is mainly collected under moisture conditions close to soil saturation. From rainfall–runoff events, it is possible to obtain more precise information on the mechanisms by which runoff is generated in the Arroio do Ouro catchment. Additionally, we considered installing piezometers to examine the connectivity between runoff and groundwater (Pavlin et al., 2021), using tracers to separate hydrographs (de Barros et al., 2021), and piecewise regression analysis (PRA) to examine the behavior of different controls on runoff coefficients (Zhang et al., 2021).

3.6 Conclusions

This study aimed to evaluate the influence of initial soil moisture on the hydrological response in a southern Brazil catchment. For this, we used robust ANN models to generate a soil moisture time series and analyzed 104 rainfall-runoff events with available data for precipitation, discharge, and antecedent soil moisture. The results revealed a linear and statistically significant relationship between the runoff depth generated and the total precipitation for each event. However, a weak and non-significant relationship was found between the mean rainfall intensity and

runoff depth. On the other hand, the antecedent soil moisture index showed a solid and significant Pearson correlation coefficient with runoff depth only when used in conjunction with the event's total precipitation (ASI +P).

There was a significant relationship between antecedent soil moisture and the runoff coefficient. However, this is a weak relationship with a large dispersion of the runoff coefficient, especially when the antecedent soil moisture is above field capacity. It is unclear whether there is a threshold between the antecedent soil moisture and runoff coefficient for the events analyzed in the catchment. However, our results indicated that the highest runoff coefficients were recorded in events whose initial soil moisture was very close to or greater than the field capacity. Unfortunately, continuous soil moisture analysis throughout rainfall-runoff events is not available because of limitations in ANN model development, which made it difficult to analyze the mechanisms by which runoff is generated in the Arroio do Ouro catchment.

Acknowledgements

We would like to thank NEPE-HidroSedi at the Federal University of Pelotas (UFPel) for providing laboratory analyses and field surveys and the Agricultural Meteorology Laboratory of the Brazilian Corporation of Agricultural Research (EMBRAPA) for providing the meteorological data used in this study. We would also like to thank the National Council for Scientific and Technological Development (CNPq) for financing the Ph.D. fellowship [grant number 141235/2017-9] for the first author and research productivity fellowships for the second author. The funders had no role in the study design, collection, analysis, interpretation of data, writing of the report, or the decision to submit the article for publication.

References

Almagro A, Oliveira PTS, Meira Neto AA, Roy T, Troch P. 2021. CABra: A novel large-sample dataset for Brazilian catchments. *Hydrology and Earth System Sciences* **25** (6): 3105–3135 DOI: 10.5194/hess-25-3105-2021

Alvares, C.A., Stape, J.L., Sentelhas, P.C., de Moraes Gonçalves, J.L., and Sparovek. G., 2013. Köppen's climate classification map for Brazil. *Meteorologische Zeitschrift,* 22 (6), 711–728. DOI: 10.1127/0941-2948/2013/0507

de Barros, C.A.P., Govers, G., Minella, J.P.G., and Ramon, R, 2021. How water flow components affect sediment dynamics modeling in a Brazilian catchment. *Journal of Hydrology,* 597 (February). DOI: 10.1016/j.jhydrol.2021.126111

Bartels, G.K., Castro, N.M., Dos, R., Pedrollo, O., and Collares, G.L., 2021. Soil moisture estimation in two layers for a small watershed with neural network models: Assessment of the main factors that affect the results. *CATENA,* 207 (July),105631. DOI: 10.1016/j.catena.2021.105631

Bartels, G.K., Terra, V.S.S., Cassalho, F., Lima, L.S., Reinert, D.J., and Collares, G.L., 2016. Spatial variability of soil physical and hydraulic properties in the southern Brazil small watershed. *African Journal of Agricultural,* 11 (49): 5036–5042. DOI: 10.5897/AJAR2016.11812

Bennett, B., Leonard, M., Deng, Y., and Westra, S. 2018. An empirical investigation into the effect of antecedent precipitation on flood volume. *Journal of Hydrology,* 567 (September), 435–445. DOI: 10.1016/j.jhydrol.2018.10.025

Brocca, L., Melone, F., and Moramarco, T., 2008. On the estimation of antecedent wetness conditions in rainfall–runoff modelling. *Hydrological Processes,* 22 (5), 629–642. DOI: 10.1002/hyp.6629

Carlotto, T. and Chaffe, P.L.B., 2019. Master Recession Curve Parameterization Tool (MRCPtool): Different approaches to recession curve analysis. *Computers & Geosciences,* 132 (February), 1–8. DOI: 10.1016/j.cageo.2019.06.016

Castillo, V., Gómez´Plaza, A., and Martínez-Mena, M., 2003. The role of antecedent soil water content in the runoff response of semiarid catchments: a simulation approach. *Journal of Hydrology,* 284 (1–4), 114–130. DOI: 10.1016/S0022-1694(03)00264-6

Chagas, V.B.P, Chaffe, P.L.B., Addor, N., Fan, F.M., Fleischmann, A.S., Paiva, R.C.D., and Siqueira, V.A., 2020. CAMELS-BR: Hydrometeorological time series and landscape attributes for 897 catchments in Brazil. *Earth System Science Data,* 12 (3), 2075–2096. DOI: 10.5194/essd-12-2075-2020

Decagon Devices Inc., 2007. WP4 Dewpoint PotentiaMeter operator's manual.

Everitt, B.S., and Dunn, G., 1991. *Applied multivariate data analysis*. London: Edward Arnold.

Farrick, K.K. and Branfireun, B.A., 2014. Soil water storage, rainfall and runoff relationships in a tropical dry forest catchment. *Water Resources Research,* 50 (12), 9236–9250. DOI: 10.1002/2014WR016045

Food and Agriculture Organization of the United Nations. 2014. *World reference base for soil resources 2014: International soil classification system for naming soils and creating legends for soil maps*. FAO: Rome.

Fulford, J.M. and Kimball, S., 2015. *Hydraulic Laboratory Testing of SonTek-IQ Plus*. U.S. Geological Survey. DOI: http://dx.doi.org/10.3133/ofr20151139

Grillakis, M.G., Koutroulis, A.G., Komma, J., Tsanis, I.K., Wagner, W., and Blöschl, G., 2016. Initial soil moisture effects on flash flood generation – A comparison between basins of contrasting hydro-climatic conditions. *Journal of Hydrology*, 541, 206–217. DOI: 10.1016/j.jhydrol.2016.03.007

Hagen, K., Berger, A., Gartner, K., Geitner, C., Kofler, T., Kogelbauer, I., Kohl, B., Markart, G., Meißl, G., and Niedertscheider, K., 2020. Event-based dynamics of the soil water content at Alpine sites (Tyrol, Austria). *CATENA,* 194 (November 2019). 104682 DOI: 10.1016/j.catena.2020.104682

Hu, W., She, D., Shao, M., Chun, K.P., and Si, B., 2015. Effects of initial soil water content and saturated hydraulic conductivity variability on small watershed runoff simulation using LISEM. *Hydrological Sciences Journal,* 60 (6), 1137–1154. DOI: 10.1080/02626667.2014.903332

Huza, J., Teuling, A.J., Braud, I., Grazioli, J., Melsen, L.A., Nord, G., Raupach, T.H., and Uijlenhoet, R., 2014. Precipitation, soil moisture and runoff variability in a small river catchment (Arde`che, France) during HyMeX Special Observation Period 1. *Journal of Hydrology,* 516. 330–342. DOI: 10.1016/j.jhydrol.2014.01.041

James, A.L. and Roulet, N.T., 2009. Antecedent moisture conditions and catchment morphology as controls on spatial patterns of runoff generation in small forest catchments. *Journal of Hydrology,* 377 (3–4),: 351–366. DOI: 10.1016/j.jhydrol.2009.08.039

Klute, A., 1986. Water retention: Laboratory methods. Methods Soil Anal. Part 1 Phys. Mineral. Methods 9, 635–662. https://doi.org/10.2136/sssabookser5.1.2ed.c26

Ladson, A.R., Brown, R., Neal, B., and Nathan, R., 2013. A standard approach to baseflow separation using the Lyne and Hollick filter. *Australian Journal of Water Resources,* 17 (1), 25–34. DOI: 10.7158/W12-028.2013.17.1.CITATIONS

Lyne, V. and Hollick, M., 1979. Stochastic time-variable rainfall-runoff modeling. In *Australian National Conference Publication 79*. Perth: Institution of Engineers Australia, 89–92.

McMillan, H., Gueguen, M., Grimon, E., Woods, R., Clark, M., and Rupp, D.E., 2014. Spatial variability of hydrological processes and model structure diagnostics in a 50 km^2 catchment. *Hydrological Processes,* 28 (18), 4896–4913. DOI: 10.1002/hyp.9988

Meißl, G., Zieher, T., and Geitner, C., 2020. Runoff response to rainfall events considering initial soil moisture – Analysis of 9-year records in a small Alpine catchment (Brixenbach valley, Tyrol, Austria). *Journal of Hydrology: Regional Studies,* 30 (March), 100711. DOI: 10.1016/j.ejrh.2020.100711

Melo, D.C.D., Anache, J.A.A., Almeida, C. das N., Coutinho, J.V., Ramos Filho, G.M., Rosalem, L.M.P., Pelinson, N.S., Ferreira, G.L.R.A., Schwamback, D., Calixto,

K.G., et al., 2020. The big picture of field hydrology studies in Brazil. *Hydrological Sciences Journal,* 65 (8), 1262–1280. DOI: 10.1080/02626667.2020.1747618

Meyles, E.W., Williams, A.G., Ternan, J.L., Anderson, J.M., and Dowd, J.F., 2006. The influence of grazing on vegetation, soil properties and stream discharge in a small Dartmoor catchment, southwest England, UK. *Earth Surface Processes and Landforms,* 31 (5), 622–631. DOI: 10.1002/esp.1352

Morbidelli, R., Saltalippi, C., Flammini, A., Corradini, C., Brocca, L., Govindaraju, R.S., 2016. An investigation of the effects of spatial heterogeneity of initial soil moisture content on surface runoff simulation at a small watershed scale. *Journal of Hydrology,* 539, 589–598. DOI: 10.1016/j.jhydrol.2016.05.067

Nied, M., Hundecha, Y., and Merz, B., 2013. Flood-initiating catchment conditions: a spatio-temporal analysis of large-scale soil moisture patterns in the Elbe River basin. *Hydrology and Earth System Sciences,* 17 (4), 1401–1414. DOI: 10.5194/hess-17-1401-2013

Pavlin, L., Széles, B., Strauss, P., Blaschke, A.P., and Blöschl, G., 2021. Event and seasonal hydrologic connectivity patterns in an agricultural headwater catchment. *Hydrology and Earth System Sciences,* 25 (4), 2327–2352. DOI: 10.5194/hess-25-2327-2021

Penna, D., Tromp-van Meerveld, H.J., Gobbi, A., Borga, M., and Dalla Fontana, G., 2011. The influence of soil moisture on threshold runoff generation processes in an alpine headwater catchment. *Hydrology and Earth System Sciences,* 15 (3), 689–702. DOI: 10.5194/hess-15-689-2011

Philipp, R.P., Bom, F.M., Pimentel, M.M., Junges, S.L., and Zvirtes, G., 2016. SHRIMP U-Pb age and high temperature conditions of the collisional metamorphism in the Varzea do Capivarita Complex: Implications for the origin of Pelotas Batholith, Dom Feliciano Belt, southern Brazil. *Journal of South American Earth Sciences,* 66, 196–207. DOI: 10.1016/j.jsames.2015.11.008

Reinert, D.J., Reichert, J.M., 2006. Coluna de areia para medir a retenção de água no solo: protótipos e teste. Ciência Rural 36, 1931–1935. https://doi.org/10.1590/s0103-84782006000600044

Rodríguez-Blanco, M.L., Taboada-Castro, M.M., and Taboada-Castro, M.T., 2012. Réponse pluie-débit et coefficients de ruissellement événementiels dans une region humide (nordouest de l'Espagne). *Hydrological Sciences Journal,* 57 (3), 445–459. DOI: 10.1080/02626667.2012.666351

Ruggenthaler, R., Schöberl, F., Markart, G., Klebinder, K., Hammerle, A., and Leitinger, G., 2015. Quantification of soil moisture effects on runoff formation at the hillslope scale. *Journal of Irrigation and Drainage Engineering,* 141 (9), 05015001. DOI: 10.1061/(asce)ir.1943-4774.0000880

Scherrer, S., Naef, F., Fach, A.O., and Cordery, I. 2007. Formation of runoff at the hillslope scale during intense precipitation. *Hydrology and Earth System Sciences,* 11 (2), 907–922. DOI: 10.5194/hess-11-907-2007

Schoener, G., Stone, and M.C., 2019. Impact of antecedent soil moisture on runoff from a semiarid catchment. *Journal of Hydrology,* 569 (October 2018), 627–636. DOI: 10.1016/j.jhydrol.2018.12.025

Song, S. and Wang, W., 2019. Impacts of antecedent soil moisture on the rainfall-runoff transformation process based on high-resolution observations in soil tank experiments. *Water (Switzerland),* 11 (2), 15–20. DOI: 10.3390/w11020296

Sungmin, O. and Orth, R. 2021. Global soil moisture data derived through machine learning trained with in-situ measurements. *Scientific Data,* 8 (1). 1–14. DOI: 10.1038/s41597-021-00964-1

Timm, L.C., Pires, L.F., Centeno, L.N., Bitencourt, D.G.B., Parfitt, J.M.B., and de Campos, A.D.S., 2020. Assessment of land levelling effects on lowland soil quality indicators and water retention evaluated by multivariate and geostatistical analyses. *Land Degradation and Development,* 31 (8), 959–974. DOI: 10.1002/ldr.3529

Tramblay, Y., Bouvier, C., Martin, C., Didon-Lescot, J-F., Todorovik, D., and Domergue, J-M., 2010. Assessment of initial soil moisture conditions for event-based rainfall–runoff modelling. *Journal of Hydrology,* 387 (3–4), 176–187. DOI: 10.1016/j.jhydrol.2010.04.006

Tronco, R.G., 2020. Funções de pedotransferência para a estimativa da retenção de água na bacia hidrográfica do Arroio do Ouro – RS, Brasil. Eng. Constr. Archit. Manag. Federal University of Pelotas.

Uber, M., Vandervaere, J-P., Zin, I., Braud, I., Heistermann, M., Legoût, C., Molinié, G., and Nord, G., 2018. How does initial soil moisture influence the hydrological response? A case study from southern France. *Hydrology and Earth System Sciences,* 22 (12), 6127–6146. DOI: 10.5194/hess-22-6127-2018

Urgilés, G., Célleri, R., Trachte, K., Bendix, J., and Orellana-Alvear, J., 2021. Clustering of rainfall types using micro rain radar and laser disdrometer observations in the tropical Andes. *Remote Sensing,* 13 (5), 991. DOI: 10.3390/rs13050991

van Genuchten, M.T., 1980. A closed-form equation for predicting the hydraulic conductivity of unsaturated soils1. *Soil Science Society of America Journal,* 44 (5), 892. DOI: 10.2136/sssaj1980.03615995004400050002x

Wang, S., Yan, Y., Fu, Z., and Chen, H., 2022. Rainfall-runoff characteristics and their threshold behaviors on a karst hillslope in a peak-cluster depression region. *Journal of Hydrology,* 605 (July 2021), 127370. DOI: 10.1016/j.jhydrol.2021.127370

Ward, J.H., 1963. Hierarchical Grouping to Optimize an Objective Function. *Journal of the American Statistical Association,* 58 (301), 236–244. DOI: 10.1080/01621459.1963.10500845

Wei, L., Qiu, Z., Zhou, G., Kinouchi, T., and Liu, Y., 2020. Stormflow threshold behaviour in a subtropical mountainous headwater catchment during forest recovery period. *Hydrological Processes,* 34 (8), 1728–1740. DOI: 10.1002/hyp.13658

Zeri, M., Costa, J.M., Urbano, D., Cuartas, L.A., Ivo, A., Marengo, J., and dos Santos Alvalá, R.C., 2020. *A soil moisture dataset over the Brazilian semiarid region*. Mendeley Data, V2. DOI: 10.17632/xrk5rfcpvg.2

Zhang, G., Cui, P., Gualtieri, C., Zhang, J., Ahmed Bazai, N., Zhang, Z., Wang, J., Tang, J., Chen, R., and Lei, M., 2021. Stormflow generation in a humid forest

watershed controlled by antecedent wetness and rainfall amounts. *Journal of Hydrology,* 603 (PC), 127107. DOI: 10.1016/j.jhydrol.2021.127107

Zhang, Y., Wei, H., and Nearing, MA., 2011. Effects of antecedent soil moisture on runoff modeling in small semiarid watersheds of southeastern Arizona. *Hydrology and Earth System Sciences,* 15 (10), 3171–3179. DOI: 10.5194/hess-15-3171-2011

Appendix A. Supplementary data

Table S3.1 - Statistical verification performance of the selected models for surface (0-10 cm), and subsurface layer (10-20 cm).

Model	surface	Subsurface
Input variables[1]	1, 2, 36, 38, 39, 41, 43, 24, 31, 18, 22	1, 2, 36, 38, 39, 41, 43, 26, 31, 18, 22
Verification		
E10	-0.049	-0.038
E50	-0.01	-0.0013
E90	0.044	0.041
MAE	0.031	0.024
NS	0.763	0.848

[1]Input variables: 1: elevation; 2: Slope; 18: Cumulative 7-day ETo; 22: Cumulative 45-day ETo ; 24: Cumulative 6-h rainfall; 31: Cumulative 10-day rainfall; 36: Soil bulk density; 38: Microporosity; 39: Total Porosity; 41: Clay; 43: Total Sand.
Details about the input variables can be found in Bartels et al. (2021).

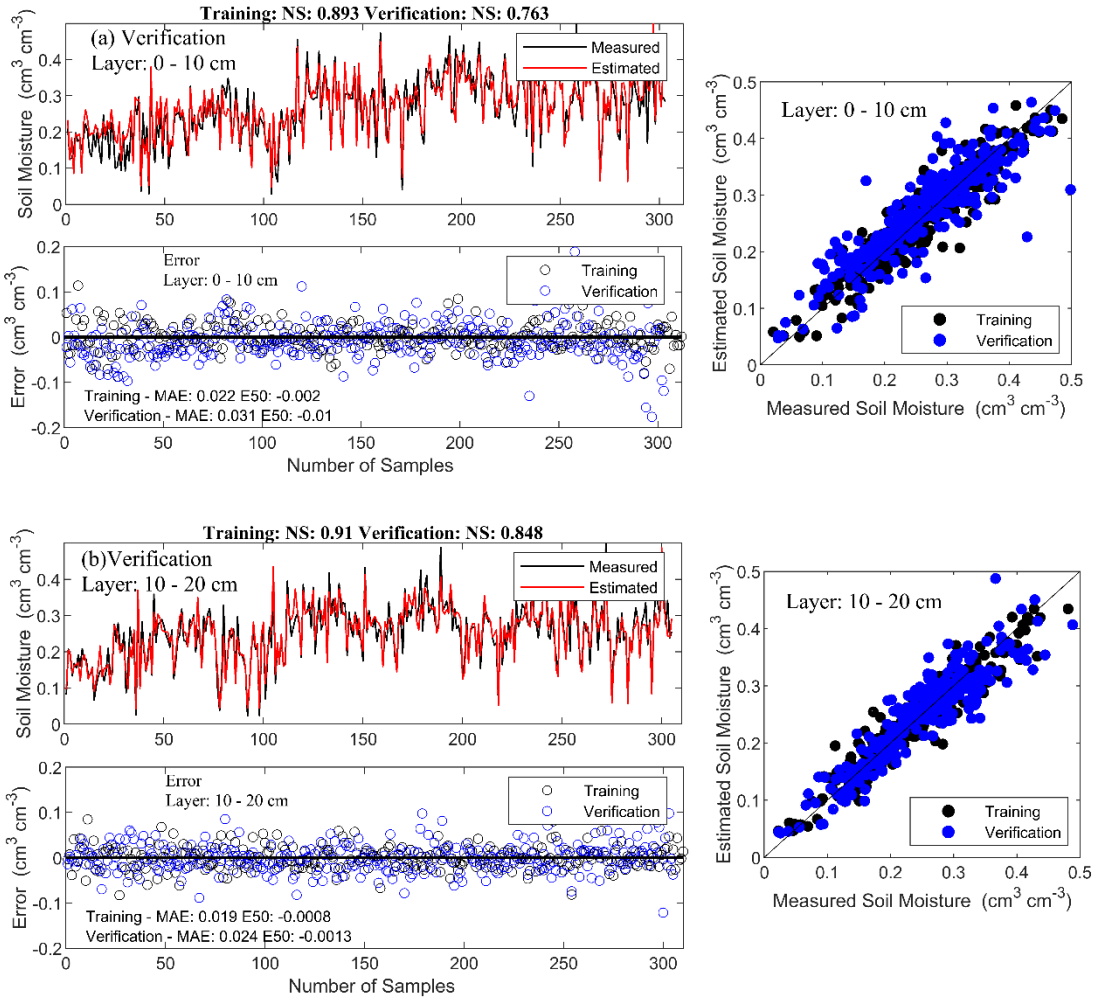

Figure S3.1 - Model performance during the verification process. (a) surface layer; (b) subsurface layer. Soil moisture measurements and estimates in relation to the ideal adjusted values (1:1 line) for training (black dots) and verification (blue dots) for both models. Error: difference between the measurements and estimates for training (black dots) and verification (blue dots) for both models.

References - Supplementary data

Bartels, G.K., Castro, N.M. dos R., Pedrollo, O., Collares, G.L., 2021. Soil moisture estimation in two layers for a small watershed with neural network models: Assessment of the main factors that affect the results. CATENA 207, 105631. https://doi.org/10.1016/j.catena.2021.105631

CAPÍTULO 4

Runoff generation and the relevance of initial soil moisture: consequences of hydrographs simulated with the OpenLISEM in a small catchment

Guilherme Kruger Bartels [a], Nilza Maria dos Reis Castro [a], Gilberto Loguercio Collares [b]

[a] Instituto de Pesquisas Hidráulicas, Universidade Federal do Rio Grande do Sul (Institute of Hydraulic Research, Federal University of Rio Grande do Sul -IPH/UFRGS), Av. Bento Gonçalves, 9500, Porto Alegre - RS, Brazil.

[b] Centro de Desenvolvimento Tecnológico, Universidade Federal de Pelotas (Center for Technological Development, Federal University of Pelotas - CDTec/UFPel), Rua Gomes Carneiro 01, Pelotas - RS, Brazil.

Abstract

Several hydrological processes are associated with the initial soil moisture condition (Θ_i) and rainfall event characteristics. Runoff generation can be sensitive to the soil moisture conditions preceding a precipitation event owing to the rapid response in a small watershed. In event-based hydrological models, Θ_i must be considered an input parameter. However, its dynamic behavior limits the possibility of regular and continuous monitoring. In this study, we investigated the use of an Θ_i estimation approach using an artificial neural network (ANN) model to calibrate and validate hydrographs simulated with open source Limburg Soil Erosion Model (OpenLISEM) in a small catchment in southern Brazil. We used 11 rainfall-runoff events for the OpenLISEM calibration and four events during validation. The satisfactory results obtained during the calibration (Nash-Sutcliffe coefficients of 0.53 to 0.90) indicated adequately represented the simulated hydrograph shapes. The robust and innovative approach to estimating Θ_i from ANN models proved promising based on the solid results obtained during the OpenLISEM validation stage. The uncertainties associated with the values of Θ_i caused pronounced changes in the estimates of

peak runoff and peak time, but to a lesser extent. Overall, even when uncertainties in the estimation of Θ_i in complex events are considered, the shape of the hydrographs could be represented.

Keywords: soil moisture, hydrological modeling, uncertainty analysis, artificial neural networks

4.1 Introduction

Runoff generation in watersheds results from precipitation events, soil hydraulic characteristics, and the condition of soil moisture (Zehe and Sivapalan, 2009). The flow response of a small watershed through a rainfall event is fast and sensitive to antecedent soil moisture conditions. As soil moisture can vary significantly, even on a sub-daily time scale, the water content in the soil can be used as a determinant in the production of runoff during rainfall or a flash flood (Grillakis et al., 2016). In addition to controlling overland flow, higher soil moisture promotes connections between the preferential flow paths (Sidle et al., 2001). As the saturated area increases, the number of active preferential flow paths also increases, generating a greater subsurface flow on the hillslope (Sidle et al., 2000). Thus, the preferential paths become more connected with the wetter soil, requiring a smaller volume of water (precipitation) to activate the preferential subsurface flow (Guo et al., 2014).

Thus, regardless of the dominant flow generation process in a watershed, the initial soil moisture condition (Θ_i) is essential for event-based hydrological modelling. Unlike continuous simulations, the antecedent moisture condition must be measured and entered into event-based modeling or calibrated based on the observed hydrograph (Hossain et al., 2019). Among the methodologies used to determine soil moisture information for implementation in event-based models, we highlight the measurements carried out in the soil, in situ data from remote sensing, and indices such as the antecedent precipitation index (Sunwoo and Choi, 2017; Tramblay et al., 2010; Vargas et al., 2021). However, due to the dynamic behavior of soil moisture (Gao et al., 2013; Huang et al., 2016; Suo et al., 2018; Zhu et al., 2014), which is affected by climate, soil, relief, and cover, both at the surface and in deeper layers (Bartels et al., 2021b), representing soil water content using only antecedent precipitation information in the form of indices may not be a promising strategy (Brocca et al., 2008; Hagen et al., 2020).

Among the event-based models, the open source Limburg Soil Erosion Model (OpenLISEM) was designed to simulate the generation of runoff and erosion (De Roo, 1996; De Roo et al., 1996a, 1996b; Jetten, 2018). Among the processes that are incorporated in OpenLISEM, the interception of rainfall, surface water storage, infiltration, surface runoff, and flow in the drainage network are highlighted (Bout and Jetten, 2018). The model continues with constant improvements and the possibility of

selecting different flow approximation methods (Bout and Jetten, 2018). Acceptable calibration of simulated hydrographs with OpenLISEM has been extensively reported in Brazil (de Barros et al., 2021a; dos Santos et al., 2021; Rodrigues et al., 2014) and other countries (Grum et al., 2017; Lefrancq et al., 2017; Stolte et al., 2003); however, information on validation is more limited (de Barros et al., 2014; Ebling et al., 2021; Vargas et al., 2021). The complexity of runoff generation processes in a watershed and the spatial and temporal variability of control factors, such as Θ_i, compromise the validation of event-based physical models (de Barros et al., 2014).

Initial soil moisture plays an important role in generating runoff in a watershed. Furthermore, the OpenLISEM is highly sensitive to the soil water content (Sheikh et al., 2010). Thus, in this study, we investigated a robust Θ_i estimation approach that can be used for the calibration and validation of hydrographs simulated with OpenLISEM in a small watershed in southern Brazil. We used soil moisture data obtained from a model of artificial neural networks (ANNs) developed specifically for this research area (Bartels et al., 2021b). Further, we determined the effects of uncertainties associated with the estimation of Θ_i in the simulated hydrographs during the model calibration step. A database related to the hydraulic characteristics of the soil of high quality and a more detailed digital elevation model (DEM) (resolution of 5 m) were implemented in the simulations as simplifications of the basin geometry can affect the volume runoff and peak flow (Hessel, 2005; Tan et al., 2015; Zhang et al., 2009).

4.2 Materials and methods

4.2.1 Study Site

This study was conducted in the Arroio do Ouro catchment, which is located in the south of the state of Rio Grande do Sul, Brazil (Figure 4.1). This catchment has an area of 2.16 km^2, an altitude between 238.6 m and 329.9 m, and a mean slope of 10%. The predominant relief is smooth, and undulating, and its soils are classified as Acrisols and Regosols (FAO, 2014), and characterized as shallow with a dominant sandy-loam texture (35–75% sand) (Bartels et al., 2021b, 2016). The land uses in the catchment include native pasture, native forest, and agricultural cultivation, with 51.4, 23.3, and 21.6%, respectively. Other land uses correspond to 3.7%.

The region's climate is subtropical with hot summers, according to the Köppen climate classification “Cfa,” with well-distributed rainfall throughout the year (Alvares et al., 2013). The average annual precipitation in the region is 1,399 ± 297 mm and the evapotranspiration reference (ETo) is 1,080 ± 36 mm based on information obtained from the meteorological station of the Instituto Nacional de Meteorologia (INMET), located near the study site (approximately 27 km) from 1971-2020.

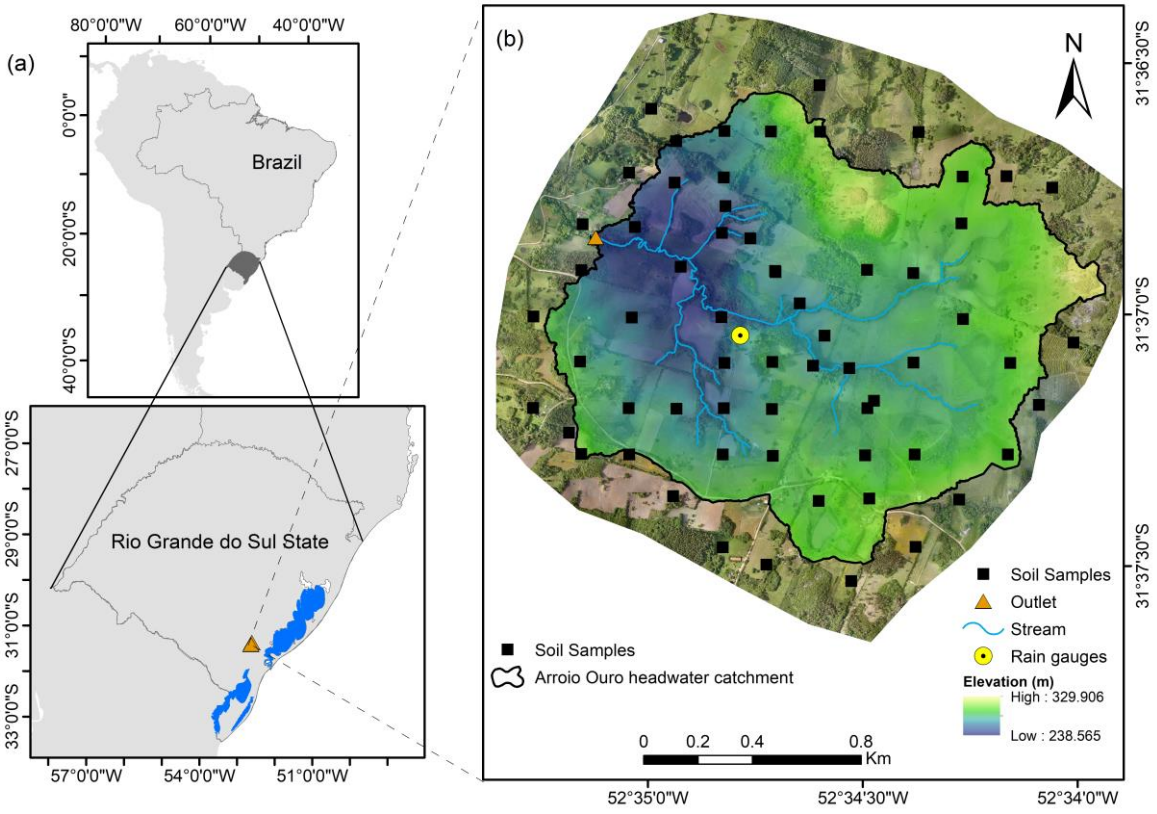

Figure 4.1 - (a) Location of the study area in the State of Rio Grande do Sul, Brazil; (b) Arroio do Ouro catchment showing a digital elevation model, streams (blue lines), soil samples (black dots), rain gauge (yellow dot) and flow station (yellow triangle).

4.2.2 Hydrological monitoring in the Arroio do Ouro Catchment

The discharge was measured continuously at the catchment outlet (Figure 4.1) using a Doppler Sontek-IQ Plus acoustic meter, and data were collected at 10-min intervals. The equipment was installed on a channel bed, and the flow depth and flow

velocity were measured. This acoustic meter uses a pressure transducer or a vertical acoustic beam to measure the flow depth in the monitoring section. The flow velocity profile was measured using four 3.0 MHz acoustic beams angled upstream, downstream, and to the left and right channel banks (Fulford and Kimball, 2015). Rainfall data were obtained from a rain gauge installed in the central region of the catchment (Figure 4.1). In periods when this rain gauge was non-operational, a hyetograph from another rain gauge was used. Owing to the proximity between the rain gauges (approximately 1.7 km) and the homogeneous characteristics of the relief, the registered precipitation in both areas is homogeneous.

The hydrograph was separated into two components for each analyzed event: surface runoff and baseflow. For the analyses performed using OpenLISEM, the baseflow was disregarded. A recursive digital filter (RDF) was used to separate the baseflow proposed by Lyne and Hollick (1979). This methodology is easy to apply and is correlated with other physical methods, such as electrical conductivity (Uber et al., 2018). For this study, $\alpha = 0.98$, where α is the filter adjustment parameter. This value was used based on tests of 49 values of the α filter parameter carried out for 104 rainfall-runoff events (8/2017 to 9/2021) in the Arroio do ouro catchment (Bartels et al., submitted). For the analysis of hydrological modeling using OpenLISEM, we used 15 rainfall-runoff events, 11 events for model calibration and four events in the validation stage. These events were chosen based on the magnitude of peak flows observed during the four years of monitoring. One event has a peak discharge lower than the median (E1), and two other events (E2 and E3) have a peak discharge of less than 75% of the observed for the 104 events. The other events have a greater magnitude, five (E5, E6, E7, E8, and E13) with peak discharge lower than 90%, and the others (E4, E9, E10, E11, E12, E14, and E15) are events whose peak discharge is exceeded in only 10% of the 104 events that occurred in the period. All selected events had available precipitation, flow, and Θ_i data. The characteristics of these rain events and antecedent soil moisture are presented in Table 4.1.

Table 4.1 - Characteristics of rainfall-runoff events and Θ_i used for the calibration and validation of OpenLISEM.

Events	Date	Q_{peak} ($m^3\ s^{-1}$)	Q_{runoff} (mm)	Total Rainfall (mm)	Rainfall duration (min)	Mean Rainfall intensity (mm h^{-1})	Máximum 15 min intensity (mm h^{-1})	Θ_i ($cm^3\ cm^{-3}$)
Calibration								
E1	08/08/2017	0.156	0.61	16.2	120	8.1	20.0	0.316
E2	27/09/2017	0.373	1.27	15.0	150	6.0	19.2	0.291
E3	01/10/2017	0.527	2.69	18.6	180	6.2	29.6	0.301
E4	18/10/2017	2.449	11.80	46.8	285	9.9	20.8	0.315
E5	27/10/2017	0.638	1.92	22.4	105	12.8	25.6	0.303
E6	24/03/2018	1.220	4.05	56.8	765	4.5	46.4	0.242
E7	01/04/2018	0.811	3.51	43.4	330	7.9	28.8	0.218
E8	15/01/2019	0.754	3.15	26.6	235	6.8	44.0	0.184
E9	18/01/2019	1.238	13.46	72.0	1485	2.9	20.0	0.2227
E10	08/09/2019	1.466	7.71	53.2	690	4.6	31.2	0.315
E11	03/10/2019	3.090	12.55	60.8	1155	3.2	32.0	0.298
Validation								
E12	29/10/2019	1.723	6.95	32.4	240	8.1	22.4	0.281
E13	26/03/2021	1.226	5.86	38.6	210	11.0	40.0	0.232
E14	13/09/2021	1.599	11.45	55.8	675	5.0	12.0	0.335
E15	20/09/2021	2.342	8.67	48.8	1110	2.6	22.0	0.332

Θ_i, initial soil moisture mean (0 – 20 cm); Q_{peak}, runoff peak; Q_{runoff}, total runoff.

4.2.3 Measurement and estimation of the input parameters in OpenLISEM

The OpenLISEM was designed to simulate the runoff in individual rainfall events, incorporated into a GIS environment, with model algorithms applied to each grid cell of the study site (Merritt et al., 2003). Thus, the information in the model was obtained from maps in PCRaster (Karssenberg et al., 2010), which contained properties related to soil, relief, vegetation, and surface, in addition to tabulated information, such as rainfall intensity. The main processes incorporated in OpenLISEM include interception, surface storage in microdepressions, infiltration, surface flow, and channel flow (Jetten, 2018). An overview of the input values used in OpenLISEM is presented in Table 4.2. The measurement process and estimates are presented below. In OpenLISEM, the following infiltration submodels can be used: Smith and Parlange (1978) and SWATRE (Belmans et al., 1983), which use a solution of the Richards equation, and the Green-Ampt model (Green and Ampt, 1911) for one or two layers of soil. This study used the Green-Ampt model, which assumes a wetting front that moves downwards in the soil layers due to rainfall infiltration (Green and Ampt, 1911). Owing to the characteristics of shallow soils in the catchment, only one layer of soil with a depth of 0.50 m was considered; deeper

layers were considered impermeable. Therefore, the Green–Ampt model with one layer was used for the infiltration simulation. The simulations with OpenLISEM (version 6.62) were performed with a spatial resolution of 5 m and a temporal resolution of 20 s.

4.2.3.1 Digital elevation model (DEM)

As more detailed characteristics of the relief in the study area are needed, a DEM was prepared using different sources of information. Topographic and geodetic surveys were carried out using total station and global navigation satellite system (GNSS) receivers in real-time kinematic (RTK) mode, in addition to information from unmanned aerial vehicles (UAVs). The use of photogrammetry techniques to process images obtained with UAVs can yield information from the terrain surface with high spatial resolution. However, in areas with dense vegetation (e.g., forests), mapping using conventional topography is necessary to obtain the altitude of the terrain and not the height above the vegetation. A total of 20,480 points were surveyed, representing a density of approximately 95 points per hectare. With these points, a DEM was generated with maps of the drainage network and flow direction in a grid with 5 m pixel resolution. A portion of the collected points (1,000 points) was not used in the DEM interpolation process and was only used for the validation of the final product. The low mean absolute error obtained (MAE = 0.35 m) indicated that the DEM was accurate, representing the quality and fidelity of the relief characteristics in the catchment (Figure S4.1 in Supplementary Material). Higher quality than would be obtained with terrain elevation data from the Shuttle Radar Topography Mission (SRTM), which overall has a vertical accuracy of 16 m absolute error with 90% confidence (Mukul et al., 2017).

Table 4.2 - Input parameters used in the simulation with OpenLISEM.

	Parameters	Range	Unit	Determination	Source
Vegetation	Leaf area index	0.0–6.1	$m^2\ m^{-2}$	Literature	(Campoe, 2008; Heiffig et al., 2006; Pillar et al., 2009; Sachet et al., 2015; Zuluaga, 2014)
	Fraction with vegetation	0.3–1.0	–	Literature	(Heiffig et al., 2006; Moro, 2011)
	Height of vegetation	0.0–6.0	m	Field/Literature	This study and Moro (2011)
Surface	Random soil roughness	0.7-3.3	cm	Field observation	This study
	Manning's *n* coefficient	0.03–0.16	–	Literature	(Jetten, 2018)
Soil	Ksat	63 - 418	$mm\ h^{-1}$	Field/Laboratory	(Bartels et al., 2016; Tronco, 2020)
	Total porosity	0.31 – 0.54	$cm^3\ cm^{-3}$	Field/Laboratory	(Bartels et al., 2016; Tronco, 2020)
	Matric potential	3.6 – 15296	cm	Field/Laboratory	(Bartels et al., 2016; Tronco, 2020)
	Initial soil moisture	0.19 - 0.32	$cm^3\ cm^{-3}$	Model ANN	(Bartels et al., 2021)
Basic map	Digital elevation model	238 - 330	m	Field observation	This study
	Drainage network	–	–	Field observation	This study
	Roads	–	–	Field observation	This study
	Land use	–	–	Field observation	This study
Channel	Flow direction	–	–	Field observation	This study
	Width	2.2	m	Field observation	This study
	Shape	0	–	Literature	(Jetten, 2018)
	Manning's *n* coefficient	0.08-0.20	–	Hydraulic modeling	(Loguercio, 2018)

4.2.3.2 Soil physical parameters

The database used to provide the soil attributes was obtained from Bartels et al. (2016) and Tronco (2020). Both studies used the same methodologies for the collection process and laboratory analysis. A total of 65 points were sampled to determine the total porosity and soil water retention curve (SWRC). The saturated soil hydraulic conductivity (Ksat) was characterized by sampling 12 of the 65 points. Three undisturbed soil samples were collected at each point in volumetric rings (0.076 m diameter; 344.1 cm^3) using a Uhland soil sampler in the 0-10 cm and 10-20 cm soil layers. Ksat was determined in the laboratory using a constant head permeameter (Klute and Dirksen, 1986).

The total porosity was obtained with 100% of the pores filled with water. SWRC was obtained by applying tensions of 1, 6, and 10 kPa in a tension table (Reinert and Reichert, 2006), and 33 and 100 kPa in Richard's chambers (Klute, 1986). For low soil moisture content (tensions of 500, 1000, and 1500 kPa), a psychrometer (Dewpoint Potential Meter WP4) (Decagon Devices Inc., 2007) was employed. Further, for the 65 sampling points, SWRC was fitted using the van Genuchten (1980) model. The adjustment of the SWRC proved to be adequate given the low error between the observed volumetric moisture values and those adjusted with the van Genuchten model (Figure S4.2 in Supplementary Material). Many researchers used the equation by Rawls et al. (1983) to determine the matric potential from soil characteristics (dos Santos et al., 2021; Grum et al., 2017). However, as this equation only uses the total porosity and the fractions of clay and sand of soil, the matric potential remains constant for all events. In this study, the initial soil moisture (described below) was related to the respective matric potential obtained at each sampled point. This method considers the spatial and temporal variabilities of the matric potential at the wetting front. The inverse distance weighting (IDW) method (Bonham-Carter, 1994) was also used to spatialize the soil physical parameters.

4.2.3.3 Estimation of initial soil moisture (Θ_i)

Soil moisture estimation was performed using the ANNs models proposed by Bartels et al. (submitted). The robust models were developed for the 0-10 cm and 10-20 cm layers at 39 sampling points. According to the researchers, the models performed satisfactorily with the symmetrical distribution of errors and a mean absolute error (MAE) close to zero. Therefore, we used the ANNs models developed by Bartels et al. (submitted) to estimate the initial soil moisture for the 65 points of SWRCs. The mean Θ_i between 0-10 and 10-20 cm layers was used on the one-layer Green-Ampt model.

4.2.3.4 Other OpenLISEM calibration parameters

Vegetation-related parameters, such as leaf area index, fraction of soil covered with vegetation, and vegetation height, were obtained from the literature (Table 4.2). The height of the native forest was estimated using a digital surface model obtained using the UAV. The random soil roughness (RR), which is used in OpenLISEM to estimate the fraction of water stored on the soil surface (micro-depressions), was obtained using a 1 m-long profilometer, with readings performed every 5 cm, in 31 locations distributed in the catchment. These sites were chosen based on the different characteristics of the relief and also to cover the different uses and land cover. The RR data were grouped according to the land use and cover type. To simulate runoff, we used an approach in which the kinematic flow and the Manning equation for flow velocity were implemented using an established flow direction network (Bout and Jetten, 2018). The Manning's n parameter for the slope (Manning's n slope) was initially calculated using the relationship between the RR and the fraction of soil with vegetation cover (Jetten, 2018). For the channel, Manning's n coefficient (Manning's n channel) was initially determined using hydraulic modeling (de Ávila, 2018).

4.2.4 Calibration and validation processes

The calibration process in OpenLISEM is performed manually by adjusting several parameters independently for each rainfall-runoff event. Several authors have described Ksat and Θ_i as the most influential parameters for hydrological

simulations among the calibrated parameters (de Barros et al., 2021; dos Santos et al., 2021; Grum et al., 2017), requiring a calibration process due to the high sensitivity of the model to these parameters or the low representativeness of field samples in characterizing the complexity of a watershed. However, we considered Θ_i obtained with the ANN models to represent the soil water content before the rainfall event. Thus, we did not calibrate Θ_i and the respective matric potentials obtained with the SWRCs. Accordingly, three parameters were adjusted for each of the 11 calibrated events: Ksat, Manning's n slope, and Manning's n channel. In OpenLISEM, this calibration process is performed by a multiplicative factor, which proportionally increases or decreases the original value for each grid cell. The best fit of each parameter was determined by trial and error, with efforts to minimize the differences between the observed and simulated values based on the following hydrograph characteristics: runoff peak (Q_{peak}), time until peak (Q_{time}), runoff volume (Q_{runoff}), and shape of the hydrographs. We used the approach proposed by Vargas et al. (2021) in the validation stage. The mean values obtained for the calibrated parameters were used to validate the simulated hydrographs based on four other rainfall-runoff events.

4.2.5 Analysis of the Θ_i uncertainty in the simulated hydrographs

We analyzed the uncertainty of the Θ_i estimate for 11 calibrated events. Briefly, we considered the distribution of errors associated with the ANN models for the generation of the Θ_i series. The quantiles of 5% and 95% of error distribution (E5 and E95, respectively) between the observed and estimated values with soil moisture models were considered to determine the upper and lower limits of Θ_i. Accordingly, the mean Θ_i in each simulated event increased ($\Theta_i + E_{95}$) and decreased ($\Theta_i + E_5$), and the respective values of the matric potential were adjusted to the new values of soil moisture.

4.2.6 Evaluation of performance

As a statistical indicator to analyze the quality of the simulations with OpenLISEM, we used the Nash-Sutcliffe (NS) efficiency coefficient (Nash and Sutcliffe, 1970) and the percentage of bias (Pbias). NS indicates the similarity between the simulated values and the observed data and is used to assess the

general shape of the simulated hydrograph. According to recommendations by Moriasi et al. (2007), NS values greater than 0.75 are considered very good, 0.65 < NS ≤ 0.75, good; 0.50 < NS ≤ 0.65, satisfactory; and less than 0.50, unsatisfactory. Pbias represents the mean tendency of the simulated data to be higher or lower than the observed value. Positive values indicate an overestimation bias and negative values indicate an underestimation bias. Thus, Pbias was calculated for Q_{peak}, Q_{time}, and Q_{runoff}. A Pbias < ±10 was considered very good, ±10 < Pbias < ±15, good; ±15 < Pbias< ±25, satisfactory; and Pbias > ±25, unsatisfactory (Moriasi et al., 2007).

4.3 Results and discussion

4.3.1 Calibration of OpenLISEM with Θ_i obtained using the ANN models

The calibration process in the OpenLISEM was performed manually for each simulated event. A multiplication factor was applied for Ksat, Manning's n slope, and Manning's n channels. The trial-and-error calibration process is typically adopted in OpenLISEM to adequately represent the shape of the hydrographs, Q_{peak}, Q_{time}, and Q_{runoff} at the catchment outlet. For the 11 calibrated events, the value of Manning's n slope was multiplied by a factor from 0.9 to 1.6. The multiplicative factor adopted for Manning's n channel ranged from 0.9 to 1.30 (Table 4.3). As expected, the most significant change in the values initially adopted occurred with Ksat, with multiplicative factor values between 0.01 and 0.06 (Table 4.3). The reduction in Ksat values during calibration was consistent with that observed by other researchers (de Barros et al., 2021b; de Barros et al., 2021a; Hessel et al., 2006). Grum et al. (2017) also observed significant reductions in calibrated Ksat values compared to field measurements for two small catchments in northern Ethiopia. The researchers emphasized the difficulty of representing Ksat on a watershed scale from the sample points. By evaluating the impact of two DEM sources (interpolated 5-m resolution SRTM and field topographic survey with GNSS/RTK) in the southern Brazil catchment, de Barros et al. (2021b) also found significant reductions in the Ksat value for both DEM sources. Although no significant gains in the simulation of hydrological variables were found using the DEM obtained with the field survey,, the researchers argued that the better representation of relief and landscape reduced the need to modify the original values during OpenLISEM calibration. For the simulations

Table 4.3 - Calibration parameters and efficiency analysis of calibration OpenLISEM.

Events	Date	Ksat (% of measured)	Manning's n slope (% of estimated)	Manning's n channel (% of estimated)	Qpeak ($m^3 s^{-1}$)		Qrunoff (mm)		Pbias (%)			NS (-)
					Obs	Sim	Obs	Obs	Q_{peak}	Q_{time}	Q_{runoff}	
E1	08/08/2017	4.0	130	100	0.156	0.169	0.61	0.53	8.47	6.67	-13.03	0.65
E2	27/09/2017	3.0	110	130	0.373	0.406	1.27	1.07	8.75	0.00	-15.20	0.83
E3	01/10/2017	3.0	160	110	0.527	0.589	2.69	1.65	11.75	9.09	-38.76	0.53
E4	18/10/2017	5.0	90	90	2.449	2.220	11.80	9.06	-9.35	0.00	-23.23	0.79
E5	27/10/2017	5.0	125	90	0.638	0.673	1.92	1.56	5.41	14.60	-18.75	0.78
E6	24/03/2018	6.0	140	115	1.220	1.262	4.05	2.88	3.43	0.00	-28.93	0.85
E7	01/04/2018	4.0	125	110	0.811	0.848	3.51	1.94	4.59	0.00	-44.58	0.61
E8	15/01/2019	1.0	140	130	0.754	0.770	3.15	1.98	2.23	0.00	-37.01	0.73
E9	18/01/2019	2.0	120	110	1.238	1.202	13.46	7.79	-2.95	-7.98	-42.13	0.55
E10	08/09/2019	5.0	120	120	1.466	1.349	7.71	6.59	-7.95	-2.13	-14.50	0.90
E11	03/10/2019	6.0	110	100	3.090	2.900	12.55	8.06	-6.14	1.94	-35.77	0.85

Ksat, saturated soil hydraulic conductivity; Manning's n slope, Manning's n coefficient for slope; Manning's n channel, Manning's n coefficient for channel;Obs, observed data; Sim, simulated data; Q_{peak}, runoff peak; Q_{time}, time until peak; Q_{runoff}, total runoff; NS, Nash and Sutcliffe coefficient of efficiency; Pbias, percentage bias.

with OpenLISEM in the Arroio do Ouro catchment, we used a DEM with a resolution of 5 m, which represented the characteristics of the relief with quality and fidelity.

In addition to the high sensitivity to Ksat values, both Manning coefficients (Manning's n slope and Manning's n channel) were important for adequately representing hydrographs in the catchment outlet. According to Bout and Jetten (2018), mean flood depth and velocity were mainly affected by input parameters, such as the Manning coefficient. However, using single fixed values for the Manning coefficients during the event period can serve as a limitation. As observed by Ferguson et al. (2017), Manning's n tends to decrease with increasing discharge in mixed-bed channels. A similar behavior of reduced flow resistance with increasing discharge was identified in the Arroio do Ouro-mixed bedrock alluvial channel (Bartels et al., 2021a).

In general, the calibration of the parameters resulted in a good fit of the OpenLISEM simulations to the observed hydrographs for the 11 analyzed events (Table 4.3 and Figure 4.2). The Nash-Sutcliffe coefficient presented a 'very good' and 'good' performance for most events (eight events) according to the classification by Moriasi et al. (2007), indicating good simulation of the shape of the hydrographs. The other three events (E3, E7 and E9) showed ‘satisfactory' performances. However, many researchers reported difficulty in adequately simulating the shape of hydrographs using OpenLISEM (de Barros et al., 2021a; de Barros et al., 2021b; Grum et al., 2017).

Based on the Pbias calculated for Q_{peak} and Q_{time}, all events had very good performance according to Moriasi et al. (2007), except Q_{time} for event E5, and Q_{peak} for event E3. The worst performance was observed when runoff volume (Q_{runoff}) was estimated. In every event, OpenLISEM underestimated the Q_{runoff}. This result was obtained by other researchers (de Barros et al., 2021b; Lefrancq et al., 2017), and can be explained by the omission of subsurface flow in the simulations (Lefrancq et al., 2017).

For six events, the underestimation was greater than 28%, indicating unsatisfactory performance. For the events E3, E7 and E8, the falling limb of the simulated hydrograph was found to decrease rapidly, limiting the improvement in the

accuracy of the simulated runoff volume. According to Hessel et al. (2006), this finding may indicate underestimation of Manning's n values. During our simulations, an increase in Manning's n was not found to improve the results, causing a decrease in the discharge peaks. Further, the effect of the initial soil moisture in the OpenLISEM simulations may also lead to this result. The lowest values of Θ_i were recorded in four of these six events (E6, E7, E8, and E9), indicating that LISEM has difficulty adequately simulating the runoff volume under drier soil conditions. By evaluating the effects of different stages of vegetation recovery in a forest watershed, Van Eck et al. (2016) also observed that OpenLISEM performed worse in estimating runoff when the soil was drier.

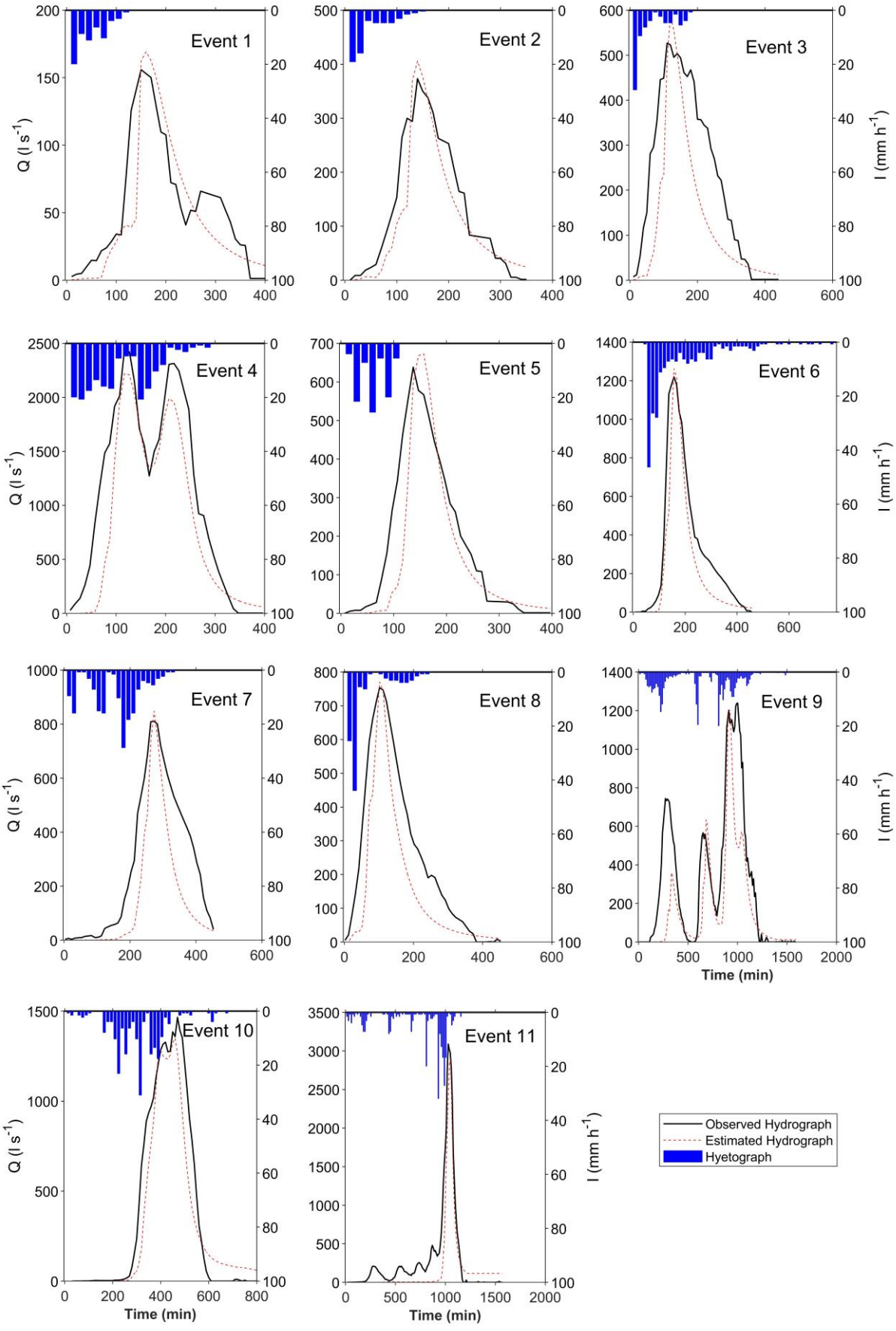
Event 1
Event 2
Event 3
Event 4
Event 5
Event 6
Event 7
Event 8
Event 9
Event 10
Event 11
Q (l s-1)
I (mm h-1)
Time (min)
Observed Hydrograph
Estimated Hydrograph
Hyetograph

Figure 4.2 - The observed and simulated hydrographs during the calibration of OpenLISEM for the 11 selected rainfall-runoff events and the observed hyetograph.

OpenLISEM consistently simulated events with more complex hydrographs comprising two or more flow peaks, which occurred for events E4 and E9. However, the model could not simulate small peaks, which occur both after a larger runoff peak (E1) and before a large runoff peak (E11). The difficulties faced by the model in adequately simulating smaller peaks in more complex events are consistent with those observed by other researchers (de Barros et al., 2021a; Grum et al., 2017). For event E11, the low intensity at the beginning of rainfall may have led to a more significant initial soil storage, limiting the adequate simulation of runoff. Besides the lower intensity of rain that generated the second peak of flow, event E1 was the smallest event among the simulated events. The difficulty of simulating small events has already been observed in the literature (Hessel et al., 2006).

4.3.2 Effect of Θ_i uncertainties on the runoff simulated by OpenLISEM

As previously mentioned, to analyze the uncertainty of Θ_i estimation, we considered quantiles of 5% and 95% of the error distribution. The ANN model had a satisfactory performance with a symmetrical distribution of errors, considering the 0 – 20 cm layer: E5 = -0.059 $cm^3\ cm^{-3}$, E95 = 0.058 $cm^3\ cm^{-3}$ (Bartels et al., submitted). As observed in other studies (dos Santos et al., 2021; Hu et al., 2015; Sheikh et al., 2010), the simulated hydrographs were strongly affected by the conditions of previous soil moisture for the calibrated events in the Arroio do Ouro catchment (Figure 4.3).

As expected, the increase and decrease in the mean Θ_i values caused increases and decreases in Q_{peak}, respectively, but with different magnitudes. Although the increase in Θ_i caused a Pbias (considering the simulated hydrograph) between 56.1 and 452.9% in the runoff peak, the decrease in Θ_i represented a decrease between 52.2 and 95.9% in Q_{peak} (Table 4.4). In a small catchment in southern Brazil, dos Santos et al. (2021) observed that reductions in Θ_i caused less pronounced changes in Q_{peak} than increases in Θ_i. The event that presented the smallest overestimation of Q_{peak} (Pbias = 56.1%) was a complex event formed by a hydrograph of three peaks (E9). The highest observed flow was found to occur at the end of the event. The increase in Θ_i caused a more pronounced increase in Q_{peak} at

the first peak of the event than that simulated with the mean Θ_i (Figure 4.3). This finding indicates that Θ_i is particularly important for simulations at the beginning of the events. The time until the peak was markedly less affected by the increase and decrease in Θ_i. For six events, the increase in Θ_i did not cause a pronounced reduction in Q_{time} (Pbias < |10|%). However, in six events, the decrease in Θ_i caused an increase in the time until peak flow occurred (Pbias > 25%).

Even with the increase or decrease in Θ_i, the simulations with OpenLISEM were found to maintain the characteristics of the shape of the hydrographs, such as those that had more than one peak flow (E4 and E9, Figure 4.3), ultimately characterizing the proper calibration of the input parameters. By simulating the effect of systematic increases and decreases in Θ_i, dos Santos et al. (2021) found that OpenLISEM presented difficulties in properly representing hydrographs during the formation of a rainfall event by two or more peaks separated by a period of lower precipitation intensity.

Table 4.4 - Efficiency analysis of OpenLISEM based on the uncertainties in the estimation of Θ_i.

Events	Date	Pbias (%)*			
		Q_{peak} ($\Theta_i + E_5$)	Q_{peak} ($\Theta_i + E_{95}$)	Q_{time} ($\Theta_i + E_5$)	Q_{time} ($\Theta_i + E_{95}$)
1	08/08/2017	-87.9	317.3	56.3	-18.8
2	27/09/2017	-95.9	171.7	107.1	-14.3
3	01/10/2017	-92.5	125.3	66.7	-16.7
4	18/10/2017	-57.8	105.7	85.5	76.9
5	27/10/2017	-83.5	152.5	12.7	-12.7
6	24/03/2018	-95.4	241.0	51.0	-6.4
7	01/04/2018	-94.2	270.2	11.0	-7.3
8	15/01/2019	-91.0	452.9	58.8	-9.8
9	18/01/2019	-92.7	56.1	4.3	-1.1
10	08/09/2019	-52.6	313.2	2.2	-2.2
11	03/10/2019	-52.2	191.6	0.0	-1.0

Q_{peak}: runoff peak; Q_{time}: time until peak; Pbias: percentage bias; Θ_i: mean initial soil moisture; E_5: error in the estimation of soil moisture (quantile 5%), E_{95}: error in the estimation of soil moisture (quantile 95%). * Considering the simulated hydrographs with Θ_i means.

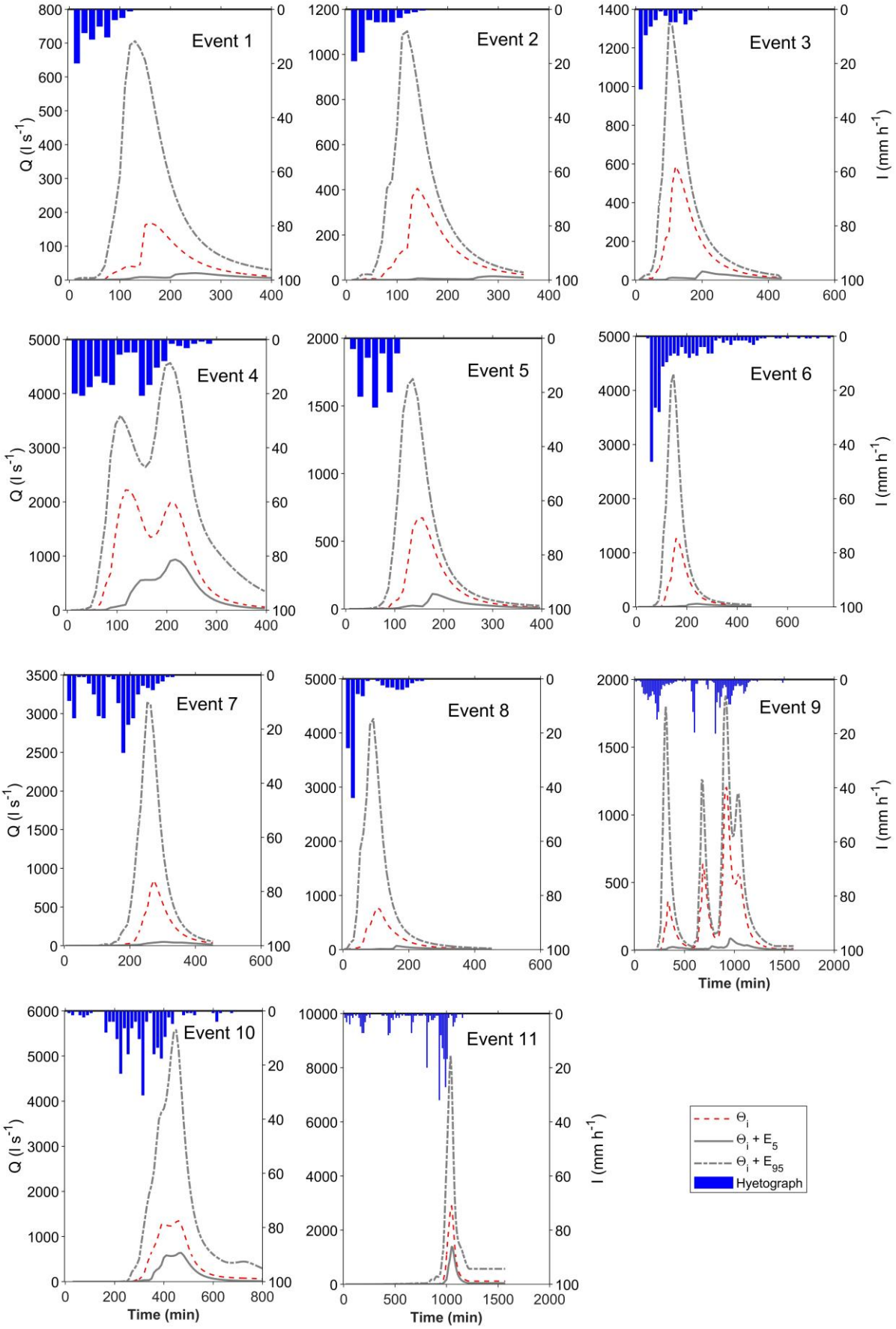
Event 1
Event 2
Event 3
Event 4
Event 5
Event 6
Event 7
Event 8
Event 9
Event 10
Event 11
Q (l s-1)
I (mm h-1)
Time (min)
Θi
Θi + E5
Θi + E95
Hyetograph

Figure 4.3 - The simulated hydrographs with Θ_i and the respective hydrograph based on the uncertainties of E_5 (Θ_i + E_5) and E_{95} (Θ_i + E_{95}), and the observed hyetograph.

4.3.3 Validation of OpenLISEM

The good performance obtained during the event calibration stage and the adequate representation of the hydrographs, even considering the uncertainties associated with Θ_i, encouraged us to carry out the validation stage with the four events that had not been analyzed. We used the mean of the calibrated parameters for the 11 events (Ksat, Manning's n slope, and Manning's n channel) in sets with the Θ_i series obtained using the ANN models and the adjustments for the respective matric potentials. The validated events presented satisfactory performance for the Nash-Sutcliffe coefficient, according to the classification by Moriasi et al. (2007), which indicates that OpenLISEM adequately simulated the shape of the hydrographs (Figure 4.4 and Table 4.5). However, the adequate representation of the runoff volume, with an underestimation for three events (Pbias > |10|%), remains the main difficulty of the model. Event E14 presented the most considerable underestimation of the runoff peak (Pbias = -25%). Of the events used in the validation, this event had a long duration and a hyetograph that remained more constant throughout the rainfall event. On one hand, this is a simulated hydrograph without pronounced peak flow. However, the flow remained higher for a longer period. The simulation proved adequate even for a more complex event with two peaks (E13). Given the reported difficulties in simulating smaller events using OpenLISEM, events with a greater magnitude were used for validation. However, the total precipitation, maximum 15 min intensity, Q_{peak}, or Q_{runoff} of the events used in the calibration were not extrapolated. As for Θ_i, only the E14 and E15 events had slightly higher values than those observed in the events used in the calibration (Θ_i of 0.33 for both), which may have caused the overestimation of Q_{peak} in E15.

Table 4.5 - Efficiency analysis of validation using OpenLISEM.

Events	Date	Q_{peak} (m^3 s^{-1})		Q_{runoff} (mm)		Pbias (%)			NS
		Obs	Sim	Obs	Sim	Q_{peak}	Q_{time}	Q_{runoff}	(-)
12	29/10/2019	1.723	1.816	6.952	3.61	5.41	0.00	-48.06	0.51
13	26/03/2021	1.226	1.459	5.863	5.33	19.03	0.00	-9.11	0.67
14	13/09/2021	1.599	1.199	11.452	10.03	-25.03	-16.51	-12.39	0.75
15	20/09/2021	2.342	3.245	8.666	7.49	38.52	0.00	-13.56	0.61

Obs, observed data; Sim, simulated data; Q_{peak}: runoff peak; Q_{time}: time until peak; Q_{runoff}: total runoff; NS: Nash and Sutcliffe coefficient of efficiency; Pbias: percentage bias.

Despite the importance of validation in hydrological modeling, this step has been employed in a limited number of studies that developed simulations with event-based models, especially OpenLISEM (de Barros et al., 2014; Ebling et al., 2021; Vargas et al., 2021). For example, in a small catchment in southern Brazil, de Barros et al. (2014) achieved satisfactory results in representing the flow processes for four validated events. The researchers pointed out that the high spatial discretization of the parameters related to the soil and surface contributed to this result. In the simulations performed, a better representation of the relief characteristics obtained with a DEM and the high-quality set of available soil data helped in the calibration process and consequently, in the adequate validation of the events. A crucial point of our research is the approach for estimating Θ_i from a robust ANN model developed specifically for the Arroio do Ouro catchment. The results obtained during validation ensured that Θ_i estimates were adequate for the simulated events. Such finding indicates that the adopted procedure is a good alternative for obtaining a highly complex input parameter in OpenLISEM. In other studies, a simplified approach was used to estimate Θ_i based on antecedent precipitation alone (de Barros et al., 2021a; Vargas et al., 2021). However, in the Arroio do Ouro catchment, rainfall is less important in estimating the soil water content about other characteristics, such as soil properties, especially in the subsurface (Bartels et al., 2021b). Thus, the use of only antecedent precipitation as an indicator of antecedent soil moisture conditions is not recommended for the Arroio do Ouro catchment.

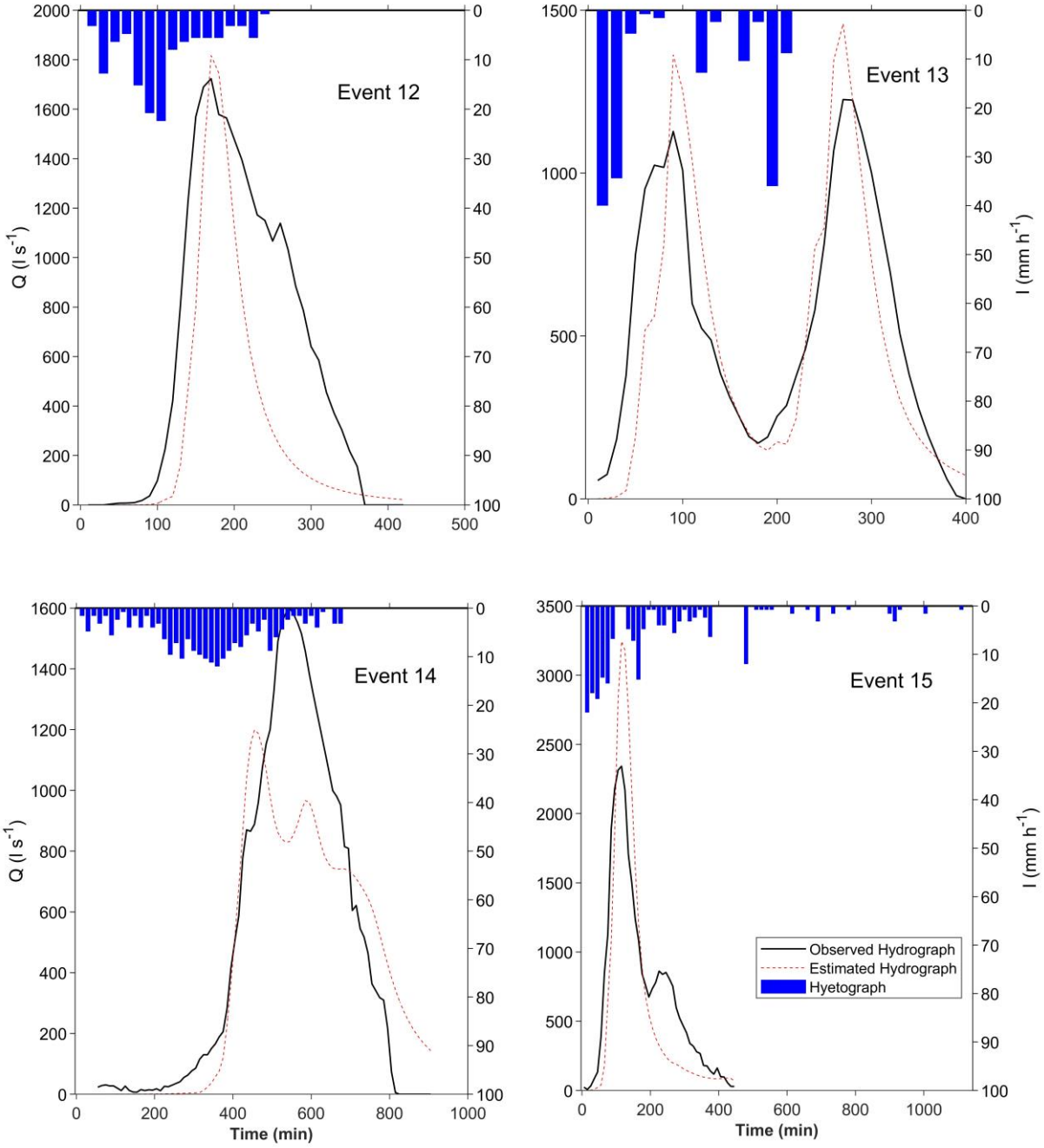

Figure 4.4 - The observed and simulated hydrographs during the validation of OpenLISEM for the four selected rainfall-runoff events and the observed hyetograph.

4.4 Conclusions

In this study, we proposed the use of Θ_i obtained from ANN models as an input parameter for the OpenLISEM. Soil moisture models were developed specifically for the Arroio do Ouro catchment, and the effects of their uncertainties on runoff generation were analyzed. The good results obtained during the calibration of the OpenLISEM revealed that the input parameters (Ksat, Manning's n slope, and Manning's n channel) were adjusted correctly, thereby representing the runoff generation processes in the catchment. The use of a DEM that suitably represented the relief characteristics of the catchment combined with a high-quality database related to soil characteristics favored the event calibration process. The robust and innovative approach to estimate Θ_i from ANN models proved promising based on the satisfactory results obtained during OpenLISEM validation. The uncertainties associated with Θ_i estimates caused more pronounced changes in Q_{peak} and to a lesser extent, Q_{time}. However, the shape of the hydrographs in more complex events can be represented, even when considering these uncertainties.

Acknowledgements

We thank NEPE-HidroSedi at the Federal University of Pelotas (UFPel) for providing the facilities used for the laboratory analyses and field surveys. We thank the National Council for Scientific and Technological Development (CNPq) for financing the PhD fellowship [grant number 141235/2017-9] for the first author and the research productivity fellowships for the second author. The funders had no role in the study design, collection, analysis, and interpretation of data, in the writing of the report, or in the decision to submit the article for publication.

References

Alvares, C.A., Stape, J.L., Sentelhas, P.C., de Moraes Gonçalves, J.L., Sparovek, G., 2013. Köppen's climate classification map for Brazil. Meteorol. Zeitschrift 22, 711–728. https://doi.org/10.1127/0941-2948/2013/0507

Bartels, G.K., Castro, N.M. dos R., Collares, G.L., Fan, F.M., 2021a. Performance of bedload transport equations in a mixed bedrock–alluvial channel environment. Catena 199, 105108. https://doi.org/10.1016/j.catena.2020.105108

Bartels, G.K., Castro, N.M. dos R., Pedrollo, O., Collares, G.L., 2021b. Soil moisture estimation in two layers for a small watershed with neural network models: Assessment of the main factors that affect the results. CATENA 207, 105631. https://doi.org/10.1016/j.catena.2021.105631

Bartels, G.K., Castro, N.M.D.R., Collares, G.L., n.d. Influence of Initial Soil Moisture and Precipitation on Runoff Generation in a Small Catchment. Hydrol. Sci. J.

Bartels, G.K., Terra, V.S.S., Cassalho, F., Lima, L.S., Reinert, D.J., Collares, G.L., 2016. Spatial variability of soil physical and hydraulic properties in the southern Brazil small watershed. African J. Agric. 11, 5036–5042. https://doi.org/10.5897/AJAR2016.11812

Belmans, C., Wesseling, J.G., Feddes, R.A., 1983. Simulation model of the water balance of a cropped soil: SWATRE. J. Hydrol. 63, 271–286. https://doi.org/10.1016/0022-1694(83)90045-8

Bonham-Carter, G.F., 1994. Geographic information systems for geoscientists: modelling with GIS. Pergamon Press, Tarrytown, New York,.

Bout, B., Jetten, V.G., 2018. The validity of flow approximations when simulating catchment-integrated flash floods. J. Hydrol. 556, 674–688. https://doi.org/10.1016/j.jhydrol.2017.11.033

Brocca, L., Melone, F., Moramarco, T., 2008. On the estimation of antecedent wetness conditions in rainfall–runoff modelling. Hydrol. Process. 22, 629–642. https://doi.org/10.1002/hyp.6629

Campoe, O., 2008. Efeito de práticas silviculturais sobre a produtividade primária líquida de madeira, o índice de área foliar e a eficiência do uso da luz em plantios de restauração da Mata Atlântica. USP.

de Ávila, P.L., 2018. Modelagem hidráulica unidimensional aplicada no estudo de coeficientes de rugosidade. Federal University of Pelotas.

de Barros, Cláudia Alessandra Peixoto, Govers, G., Minella, J.P.G., Ramon, R., 2021a. How water flow components affect sediment dynamics modeling in a Brazilian catchment. J. Hydrol. 597. https://doi.org/10.1016/j.jhydrol.2021.126111

de Barros, C.A.P., Minella, J.P.G., Dalbianco, L., Ramon, R., 2014. Description of hydrological and erosion processes determined by applying the LISEM model in a rural catchment in southern Brazil. J. Soils Sediments 14, 1298–1310. https://doi.org/10.1007/s11368-014-0903-7

de Barros, C. A.P., Minella, J.P.G., Schlesner, A.A., Ramon, R., Copetti, A.C., 2021b. Impact of data sources to DEM construction and application to runoff and

sediment yield modelling using LISEM model. J. Earth Syst. Sci. 130. https://doi.org/10.1007/s12040-020-01547-1

DE ROO, A.P.J., 1996. The LISEM project: an introduction. Hydrol. Process. 10, 1021–1025. https://doi.org/10.1002/(SICI)1099-1085(199608)10:8<1021::AID-HYP407>3.0.CO;2-I

DE ROO, A.P.J., OFFERMANS, R.J.E., CREMERS, N.H.D.T., 1996a. LISEM: a single-event, physically based hydrological and soil erosion model for drainage basins. Ii: sensitivity analysis, validation and application. Hydrol. Process. 10, 1119–1126. https://doi.org/10.1002/(SICI)1099-1085(199608)10:8<1119::AID-HYP416>3.0.CO;2-V

DE ROO, A.P.J., WESSELING, C.G., RITSEMA, C.J., 1996b. LISEM: a single-event physically based hydrological and soil erosion model for drainage basins. I: theory, input and output. Hydrol. Process. 10, 1107–1117. https://doi.org/10.1002/(SICI)1099-1085(199608)10:8<1107::AID-HYP415>3.0.CO;2-4

Decagon Devices Inc., 2007. WP4 Dewpoint PotentiaMeter operator's manual.

dos Santos, R.C.V., Vargas, M.M., Timm, L.C., Beskow, S., Siqueira, T.M., Mello, C.R., Soares, M.F., de Moura, M.M., Reichardt, K., 2021. Examining the implications of spatial variability of saturated soil hydraulic conductivity on direct surface runoff hydrographs. Catena 207. https://doi.org/10.1016/j.catena.2021.105693

Ebling, É.D., Reichert, J.M., Zuluaga Peláez, J.J., Rodrigues, M.F., Valente, M.L., Lopes Cavalcante, R.B., Reggiani, P., Srinivasan, R., 2021. Event-based hydrology and sedimentation in paired watersheds under commercial eucalyptus and grasslands in the Brazilian Pampa biome. Int. Soil Water Conserv. Res. 9, 180–194. https://doi.org/10.1016/j.iswcr.2020.10.008

Ferguson, R.I., Sharma, B.P., Hardy, R.J., Hodge, R.A., Warburton, J., 2017. Flow resistance and hydraulic geometry in contrasting reaches of a bedrock channel. Water Resour. Res. 53, 2278–2293. https://doi.org/10.1002/2016WR020233

Food and Agriculture Organization of the United Nations, 2014. World reference base for soil resources 2014: International soil classification system for naming soils and creating legends for soil maps. FAO, Rome.

Fulford, J.M., Kimball, S., 2015. Hydraulic Laboratory Testing of SonTek-IQ Plus. U.S. Geological Survey. https://doi.org/http://dx.doi.org/10.3133/ofr20151139

Gao, X., Wu, P., Zhao, X., Wang, J., Shi, Y., Zhang, B., 2013. Estimation of spatial soil moisture averages in a large gully of the Loess Plateau of China through statistical and modeling solutions. J. Hydrol. 486, 466–478. https://doi.org/10.1016/j.jhydrol.2013.02.026

Green, W.H., Ampt, G.A., 1911. STUDIES ON SOIL PHYSICS . Studies on Soil Physics. J. Agric. Sci. 4, 1.

Grillakis, M.G., Koutroulis, A.G., Komma, J., Tsanis, I.K., Wagner, W., Blöschl, G., 2016. Initial soil moisture effects on flash flood generation – A comparison between basins of contrasting hydro-climatic conditions. J. Hydrol. 541, 206–217. https://doi.org/10.1016/j.jhydrol.2016.03.007

Grum, B., Woldearegay, K., Hessel, R., Baartman, J.E.M., Abdulkadir, M., Yazew, E., Kessler, A., Ritsema, C.J., Geissen, V., 2017. Assessing the effect of water harvesting techniques on event-based hydrological responses and sediment yield at a catchment scale in northern Ethiopia using the Limburg Soil Erosion Model (LISEM). Catena 159, 20–34. https://doi.org/10.1016/j.catena.2017.07.018

Guo, L., Chen, J., Lin, H., 2014. Subsurface lateral preferential flow network revealed by time-lapse ground-penetrating radar in a hillslope. Water Resour. Res. 50, 9127–9147. https://doi.org/10.1002/2013WR014603

Hagen, K., Berger, A., Gartner, K., Geitner, C., Kofler, T., Kogelbauer, I., Kohl, B., Markart, G., Meißl, G., Niedertscheider, K., 2020. Event-based dynamics of the soil water content at Alpine sites (Tyrol, Austria). CATENA 194, 104682. https://doi.org/10.1016/j.catena.2020.104682

Heiffig, L.S., Câmara, G.M.D.S., Marques, L.A., Pedroso, D.B., Piedade, S.M.D.S., 2006. Fechamento E Índice De Área Foliar Da Cultura Da Soja. Bragantia, Campinas 65, 285–295.

Hessel, R., 2005. Effects of grid cell size and time step length on simulation results of the Limburg soil erosion model (LISEM). Hydrol. Process. 19, 3037–3049. https://doi.org/10.1002/hyp.5815

Hessel, R., van den Bosch, R., Vigiak, O., 2006. Evaluation of the LISEM soil erosion model in two catchments in the East African Highlands. Earth Surf. Process. Landforms 31, 469–486. https://doi.org/10.1002/esp.1280

Hossain, S., Hewa, G.A., Wella-Hewage, S., 2019. A Comparison of Continuous and Event-Based Rainfall–Runoff (RR) Modelling Using EPA-SWMM. Water 11, 611. https://doi.org/10.3390/w11030611

Hu, W., She, D., Shao, M., Chun, K.P., Si, B., 2015. Effets de la variabilité de la teneur en eau initiale du sol et de la conductivité hydraulique à saturation sur la simulation du ruissellement en petit bassin versant en utilisant LISEM. Hydrol. Sci. J. 60, 1137–1154. https://doi.org/10.1080/02626667.2014.903332

Huang, X., Shi, Z.H., Zhu, H.D., Zhang, H.Y., Ai, L., Yin, W., 2016. Soil moisture dynamics within soil profiles and associated environmental controls. Catena 136, 189–196. https://doi.org/10.1016/j.catena.2015.01.014

Jetten, V., 2018. OpenLISEM: Documentation & User Manual. Utrecht University, Utrech.

Karssenberg, D., Schmitz, O., Salamon, P., de Jong, K., Bierkens, M.F.P., 2010. A software framework for construction of process-based stochastic spatio-temporal models and data assimilation. Environ. Model. Softw. 25, 489–502. https://doi.org/10.1016/j.envsoft.2009.10.004

Klute, A., 1986. Water retention: Laboratory methods. Methods Soil Anal. Part 1 Phys. Mineral. Methods 9, 635–662. https://doi.org/10.2136/sssabookser5.1.2ed.c26

Klute, A., Dirksen, C., 1986. Hydraulic conductivity and diffusivity: Laboratory methods, in: Klute, A. (Ed.), Methods of Soil Analysis, Part 1: Physical and Mineralogical Methods. Madison, pp. 687–734. https://doi.org/10.2136/sssabookser5.1.2ed.c28

Lefrancq, M., Van Dijk, P., Jetten, V., Schwob, M., Payraudeau, S., 2017. Improving runoff prediction using agronomical information in a cropped, loess covered catchment. Hydrol. Process. 31, 1408–1423. https://doi.org/10.1002/hyp.11115

Lyne, V., Hollick, M., 1979. Stochastic Time-Variable Rainfall-Runoff Modeling, in: Australian National Conference Publication 79. Institution of Engineers Australia., Perth, pp. 89–92.

Merritt, W.S., Letcher, R.A., Jakeman, A.J., 2003. A review of erosion and sediment transport models. Environ. Model. Softw. 18, 761–799. https://doi.org/10.1016/S1364-8152(03)00078-1

Moriasi, D.N., Arnold, J.G., Liew, M.W. Van, Bingner, R.L., Harmel, R.D., Veith, T.L., 2007. Model evaluation guidelines for systematic quantification of accuracy in watershed simulations. Am. Soc. Agric. Biol. Eng. 50, 885–900.

Moro, M., 2011. Evaluation of the LISEM model for the simulation of hydrosedimentologic processes in a small rural cathment on the basalt slopes of Rio Grande do Sul, Brazil. Federal University of Rio Grande do Sul.

Mukul, Manas, Srivastava, V., Jade, S., Mukul, Malay, 2017. Uncertainties in the Shuttle Radar Topography Mission (SRTM) Heights: Insights from the Indian Himalaya and Peninsula. Sci. Rep. 7, 1–10. https://doi.org/10.1038/srep41672

Nash, J.E., Sutcliffe, J. V, 1970. River Flow Forecasting Through Conceptual Models Part I- A Discussion of Principles. J. Hydrol. 10, 282–290. https://doi.org/10.1016/0022-1694(70)90255-6

Pillar, V.. D., Muller, S.D., Castilhos, Z.. S., Jacques, A.V.A., 2009. Campos Sulinos: conservação e uso sustentável da biodiversidade, Ministério do Meio Ambiente – MMA. Brasilia.

Rawls, W.J., Brakensick, D.L., Soni, B., 1983. Agricultural management effects on soil water processes. Part I: soil water retention and Green and Ampt infiltration parameters. Trans. - Am. Soc. Agric. Eng. 26, 1747–1751. https://doi.org/10.13031/2013.33837

Reinert, D.J., Reichert, J.M., 2006. Coluna de areia para medir a retenção de água no solo: protótipos e teste. Ciência Rural 36, 1931–1935. https://doi.org/10.1590/s0103-84782006000600044

Rodrigues, M.F., Reichert, J.M., Minella, J.P.G., Dalbianco, L., Ludwig, R.L., Ramon, R., Rodrigues, L.A., Borges Júnior, N., 2014. Hydrosedimentology of nested subtropical watersheds with native and eucalyptus forests. J. Soils Sediments 14, 1311–1324. https://doi.org/10.1007/s11368-014-0885-5

Sachet, M.R., Penso, G.A., Pertille, R.H., Guerrezi, M.T., Citadin, I., 2015. Estimativa da área foliar de pessegueiro por método não-destrutivo. Ciência Rural 45, 2161–2163. https://doi.org/10.1590/0103-8478cr20140185

Sheikh, V., van Loon, E., Hessel, R., Jetten, V., 2010. Sensitivity of LISEM predicted catchment discharge to initial soil moisture content of soil profile. J. Hydrol. 393, 174–185. https://doi.org/10.1016/j.jhydrol.2010.08.016

Sidle, Fujieda, M., Shimizu, T., Tsuboyama, Y., Noguchi, S., Hosoda, I., 2000. Stormflow generation in steep forested headwaters: A linked hydrogeomorphic paradigm. Hydrol. Process. 14, 369–385.

Sidle, R.C., Noguchi, S., Tsuboyama, Y., Laursen, K., 2001. A conceptual model of preferential flow systems in forested hillslopes: evidence of self-organization. Hydrol. Process. 15, 1675–1692. https://doi.org/10.1002/hyp.233

Smith, R.E., Parlange, J.-Y., 1978. A parameter-efficient hydrologic infiltration model. Water Resour. Res. 14, 533–538. https://doi.org/10.1029/WR014i003p00533

Stolte, J., Liu, B., Ritsema, C.J., Van Den Elsen, H.G.M., Hessel, R., 2003. Modelling water flow and sediment processes in a small gully system on the Loess Plateau in China. Catena 54, 117–130. https://doi.org/10.1016/S0341-8162(03)00060-2

Sunwoo, W., Choi, M., 2017. Robust Initial Wetness Condition Framework of an Event-Based Rainfall–Runoff Model Using Remotely Sensed Soil Moisture. Water 9, 77. https://doi.org/10.3390/w9020077

Suo, L., Huang, M., Zhang, Y., Duan, L., Shan, Y., 2018. Soil moisture dynamics and dominant controls at different spatial scales over semiarid and semi-humid areas. J. Hydrol. 562, 635–647. https://doi.org/10.1016/j.jhydrol.2018.05.036

Tan, M.L., Ficklin, D.L., Dixon, B., Ibrahim, A.L., Yusop, Z., Chaplot, V., 2015. Impacts of DEM resolution, source, and resampling technique on SWAT-simulated streamflow. Appl. Geogr. 63, 357–368. https://doi.org/10.1016/j.apgeog.2015.07.014

Tramblay, Y., Bouvier, C., Martin, C., Didon-Lescot, J.F., Todorovik, D., Domergue, J.M., 2010. Assessment of initial soil moisture conditions for event-based rainfall-runoff modelling. J. Hydrol. 387, 176–187. https://doi.org/10.1016/j.jhydrol.2010.04.006

Tronco, R.G., 2020. Pedotransfer functions for estimating water retention in the watershed of Arroio do Ouro - RS, Brazil. Eng. Constr. Archit. Manag. Federal University of Pelotas.

Uber, M., Vandervaere, J.-P., Zin, I., Braud, I., Heistermann, M., Legoût, C., Molinié, G., Nord, G., 2018. How does initial soil moisture influence the hydrological response? A case study from southern France. Hydrol. Earth Syst. Sci. 22, 6127–6146. https://doi.org/10.5194/hess-22-6127-2018

Van Eck, C.M., Nunes, J.P., Vieira, D.C.S., Keesstra, S., Keizer, J.J., 2016. Physically-Based Modelling of the Post-Fire Runoff Response of a Forest Catchment in Central Portugal: Using Field versus Remote Sensing Based Estimates of Vegetation Recovery. L. Degrad. Dev. 27, 1535–1544. https://doi.org/10.1002/ldr.2507

van Genuchten, M.T., 1980. A Closed-form Equation for Predicting the Hydraulic Conductivity of Unsaturated Soils1. Soil Sci. Soc. Am. J. 44, 892. https://doi.org/10.2136/sssaj1980.03615995004400050002x

Vargas, M.M., Beskow, S., de Mello, C.R., de Moura, M.M., Nunes, M.C.M., Faria, L.C., Aquino, L.S., 2021. Capability of LISEM to estimate flood hydrographs in a watershed with predominance of long-duration rainfall events. Nat. Hazards 109, 593–614. https://doi.org/10.1007/s11069-021-04850-2

Zehe, E., Sivapalan, M., 2009. Threshold behaviour in hydrological systems as (human) geo-ecosystems: Manifestations, controls, implications. Hydrol. Earth Syst. Sci. 13, 1273–1297. https://doi.org/10.5194/hess-13-1273-2009

Zhang, J.X., Wu, J.Q., Chang, K., Elliot, W.J., Dun, S., 2009. Effects of DEM Source and Resolution on WEPP Hydrologic and Erosion Simulation: A Case Study of Two Forest Watersheds in Northern Idaho. Trans. ASABE 52, 447–457. https://doi.org/10.13031/2013.26838

Zhu, H.D., Shi, Z.H., Fang, N.F., Wu, G.L., Guo, Z.L., Zhang, Y., 2014. Soil moisture response to environmental factors following precipitation events in a small catchment. Catena 120, 73–80. https://doi.org/10.1016/j.catena.2014.04.003

Zuluaga, J.J.Zp., 2014. Hidrologia comparativa em bacias hidrograficas com eucalipto e campo. Dr. Thesis. Federal University of Santa Maria.

Appendix A. Supplementary data

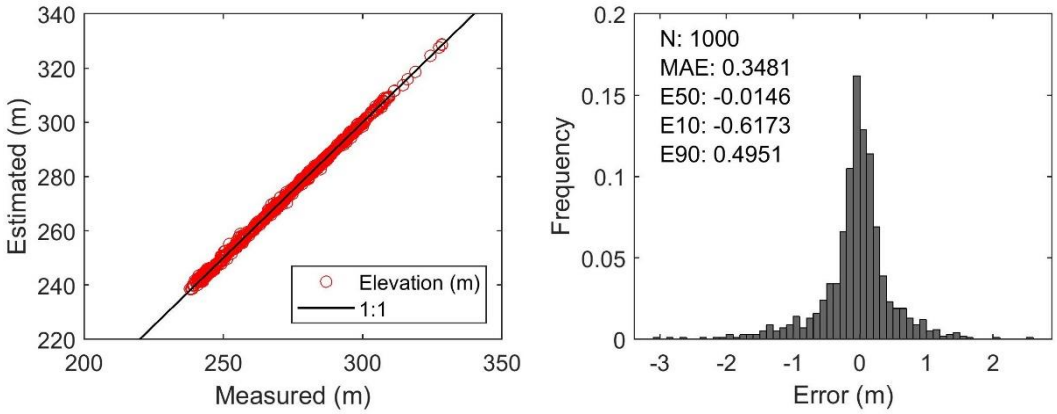

Figure S4.1 - Quality assessment of the DEM developed for the Arroio do Ouro headwater catchment. Elevation measurements and estimates in relation to the ideal adjusted values (1:1 line). Error: difference between the measurements and estimates.

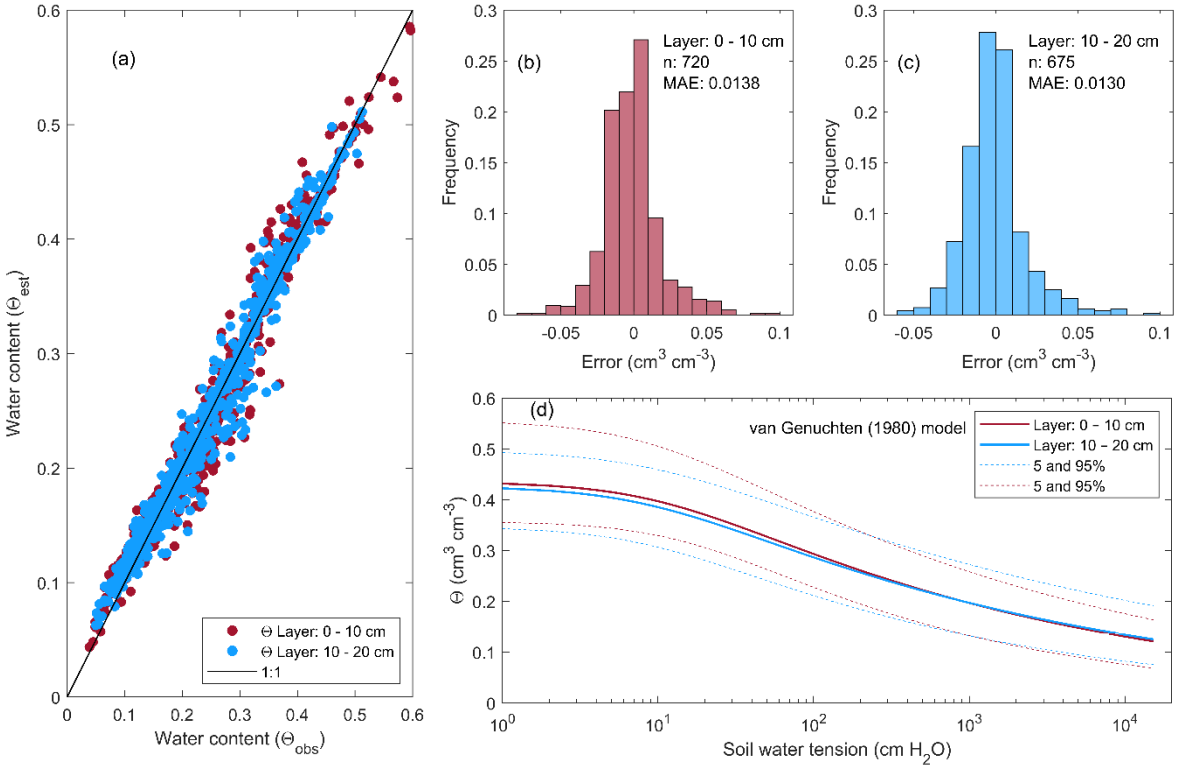

Figure S4.2 - Evaluation of the quality of soil water retention curves (SWRC) adjusted for van Genuchten (1980) model, (a) Measured (Θobs) and estimated (Θest) soil water content measurements. Error: difference between measured and estimated values for (b) layer: 0 - 10 cm, (c) layer: 10 - 20 cm. (b) Median SWRC for layer 0 - 10 cm (red lines) and 10 - 20 cm (blue lines).

CAPÍTULO 5

5.1 Conclusões

Neste estudo buscou-se avaliar os principais fatores que contribuem para a dinâmica da umidade do solo bem como a influência da umidade antecedente na geração de escoamento. Para isso, esta pesquisa desenvolveu-se na pequena bacia hidrográfica do Arroio do Ouro, localizada no sul do Brasil. De modo a contornar a indisponibilidade de medidas de umidade do solo, realizaram-se campanhas de amostragem da umidade do solo. A seguir, desenvolveu-se um modelo de redes neurais artificiais para a estimativa consistente da umidade do solo e foi realizada a análise dos principais fatores que afetam os resultados destes. Estes modelos foram desenvolvidos usando quatro categorias de dados de entrada (propriedades do solo, topografia, variáveis climáticas, e as variáveis relacionadas à precipitação).

Os modelos de redes neurais artificiais apresentaram um excelente desempenho na estimativa da umidade do solo, tanto para a camada superficial, quanto para a camada subsuperficial. Estes resultados foram alcançados utilizando todas às quatro categorias de variáveis, mostrando que todas afetam a dinâmica da umidade do solo. No entanto, a relevância que cada categoria de variáveis possui difere da camada superficial para a subsuperficial. Para a camada superficial o clima seguido das propriedades do solo foram as categorias de variáveis mais importantes. Na camada subsuperficial ocorre o inverso, com mais importância para as variáveis relacionadas ao solo, seguidas do clima. De uma forma geral, as condições climáticas determinaram as mudanças na umidade do solo para a camada superficial, enquanto na camada mais profunda, a dinâmica da umidade do solo está mais relacionada com as propriedades do solo, que controlam a infiltração e retardam os efeitos da chuva e clima.

Quanto aos aspectos relacionados à geração de escoamento na bacia hidrográfica do Arroio do Ouro, apesar de observada uma relação entre a umidade antecedente do solo e o coeficiente de escoamento, esta é uma relação fraca com grande dispersão do coeficiente de escoamento, quando a umidade antecedente do solo está acima da capacidade de campo. Desta forma, não está clara a existência de um limiar entre a umidade antecedente do solo e o coeficiente de escoamento.

Porém, os mais altos coeficientes de escoamento ocorreram em condições de umidade do solo superior à capacidade de campo. A precipitação total foi a característica do evento de chuva de maior importância para a lâmina de escoamento, já a intensidade média da precipitação, não apresentou relação.

A utilização da umidade antecedente como parâmetro de entrada nas simulações com o OpenLISEM mostrou-se promissora, visto os resultados sólidos encontrados durante a etapa de validação do modelo. Mesmo considerando as incertezas associadas às estimativas da umidade do solo antecedente, foi possível representar a forma de hidrogramas complexos. Estas incertezas ocasionaram mudanças mais pronunciadas nas estimativas das vazões de pico e em menor magnitude para o tempo até atingir a vazão de pico.

Os modelos de redes neurais artificiais desenvolvidos neste estudo para a estimativa da umidade do solo, possuem a limitação da capacidade de representar apenas o domínio dos dados utilizados durante a etapa de treinamento e verificação. Esta é uma limitação geral do desenvolvimento de modelos empíricos. Assim, muitos dados de umidade do solo extrapolados, foram removidos da análise. Desta forma, não foi possível realizar uma análise contínua da umidade do solo no decorrer dos eventos de chuva-vazão. Assim, para obter informações mais claras sobre os processos de geração de escoamento, é oportuno a compilação de mais informações de umidade do solo, principalmente durante a ocorrência dos eventos de chuva-vazão.

CAPÍTULO 6

6.1 Apêndice A

6.1.1 Características do solo e de uso e cobertura na bacia hidrográfica do Arroio do Ouro

A bacia hidrográfica do Arroio do Ouro é uma sub-bacia do Arroio Pelotas, sendo localizada entre os municípios de Pelotas e Morro Redondo, e seu escoamento converge para a bacia hidrográfica Mirim-São Gonçalo que possui uma área de aproximadamente 62.250 Km^2 (Fernandes et al., 2021). Na bacia hidrográfica do Arroio do Ouro estão presentes pequenas propriedades familiares, tendo como principais atividades econômicas desenvolvidas o cultivo de espécies como milho, soja e tabaco, além de atividades de pecuária leiteira e de corte (Bartels, 2015).

O local de estudo está inserido na região geomorfológica do Escudo Uruguaio-Sul-Rio-Grandense, mais precisamente localizada nas regiões fisiográficas da serra do sudeste e encosta do sudeste, sendo uma região se caracteriza por apresentar predomínio de Argissolos, Neossolos, Planossolos e Cambissolos (Streck et al., 2008). Na região da bacia, Cunha et al. (1996) determinou as classes de solo através de um acervo técnico da Agência da Lagoa Mirim (ALM). Os solos foram classificados em podzólicos bruno-acinzentados, podzólicos Vermelho-Amarelo, regossolos e litossolos. As classes de solo foram reorganizadas de acordo com o Sistema Brasileiro de Classificação dos Solos de 2006, apresentando para a bacia solos das classes de Argissolos e Neossolos. Como Cunha et al. (1996) não fornece de forma isolada a localização das classes de solo e sim associações por unidade, aqui não é apresentado um mapa com a classificação dos solos. As classes de solo estão muitas vezes associadas ao relevo do local, enquanto que o relevo fortemente ondulado e montanhoso caracterizam a ocorrência de solos muito rasos, nas regiões com relevo plano ou suave ondulado o desenvolvimento de solos mais profundos é maior (Cunha et al. 1996). Na bacia hidrográfica do Arroio do Ouro o relevo ondulado é predominante, com 54% da área, seguido pelo suave ondulado e forte ondulado com 24,6 e 16,8%, respectivamente (Tabela 6.1 e Figura 6.1).

Tabela 6.1 – Distribuição das classes de declividade na bacia hidrográfica do Arroio do Ouro.

Declividade (%)	Relevo	Área (%)
0 – 3	Plano	4,5
3 - 8	Suave Ondulado	24,6
8 - 20	Ondulado	54,0
20 - 45	Forte Ondulado	16,8
45 - 75	Montanhoso	0,2
> 75	Forte Montanhoso	0,0

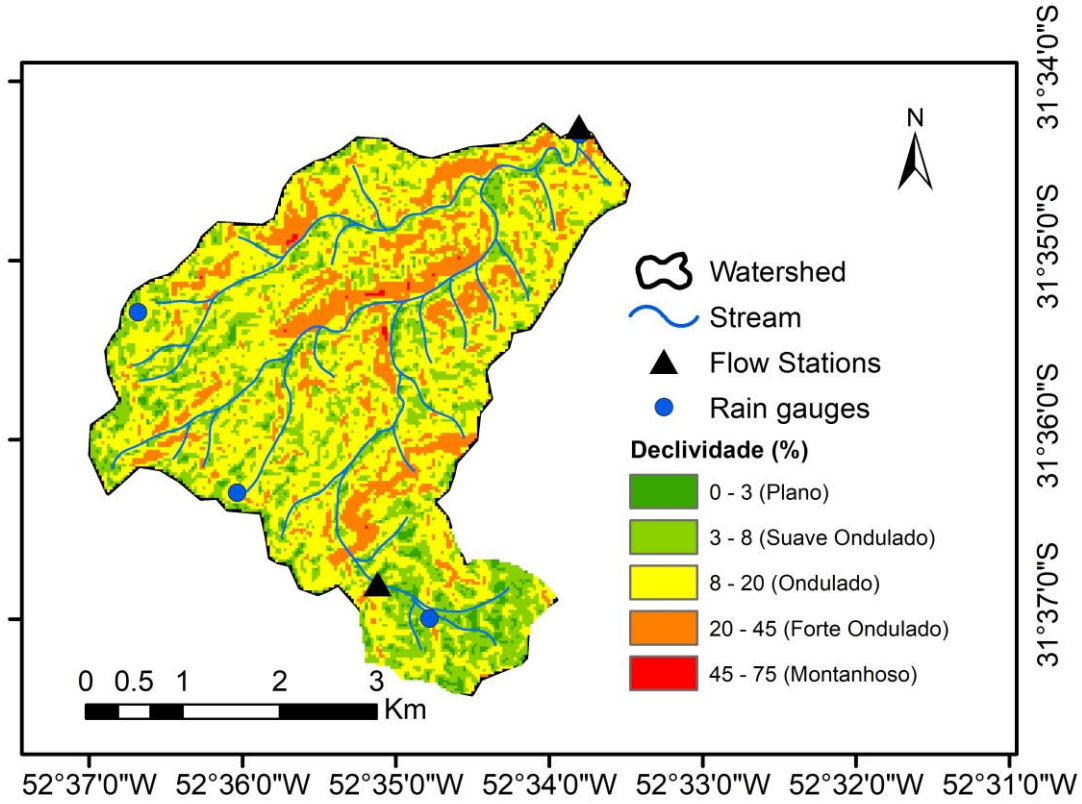

Figura 6.1 – Mapa de declividade da bacia hidrográfica do Arroio do Ouro.

Os usos do solo foram classificados utilizando imagens de satélite obtidas para o ano de 2021. Na Tabela 6.2 e Figura 6.2, estão apresentados os usos do solo e observa-se como principal uso o campo nativo, seguido das áreas com floresta nativa, ocupado 38,8 e 33,7% da área, respectivamente. As áreas com cultivo anual (19,5%) são destinadas, no verão, principalmente para a cultura da soja (*Glycine max*) e em menor escala do milho (*Zea mays*) e, no inverno, com pastagens anuais. As áreas com reflorestamento são destinadas para extração de madeira, sendo

utilizadas principalmente em carvoarias e indústrias da região. Já as áreas utilizadas com fruticultura são em quase sua totalidade, cultivadas com pêssego (*Prunus persica*), tendo como principal destino as agroindústrias da região. As principais modificações de uso do solo que ocorreram nos últimos anos (de 2014 para 2021), na bacia hidrográfica do Arroio do Ouro, considerando o levantamento realizado por Bartels (2015), foram o aumento de 5,5% das áreas com cultivo anual, e por consequência uma redução de 4,6% das áreas de campo nativo e 0,8% das áreas de reflorestamento.

Tabela 6.2 – Distribuição dos usos e coberturas do solo na bacia hidrográfica do Arroio do Ouro para o ano de 2021.

Uso do solo	Área (km^2)	Área (%)
Campo	6.67	38.8
Mata nativa	5.79	33.7
Cultivo anual	3.34	19.5
Reflorestamento	0.58	3.4
Fruticultura	0.54	3.2
Estradas	0.13	0.8
Água	0.06	0.4
Construções	0.05	0.3

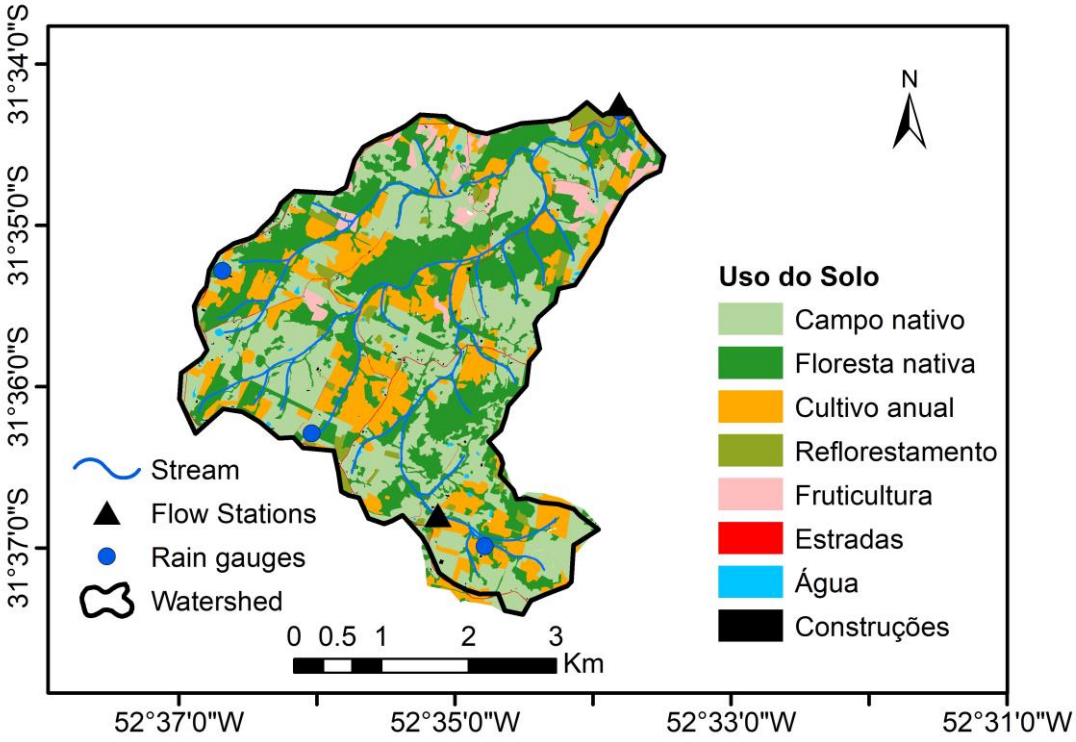

Figura 6.2 – Uso do solo na bacia hidrográfica do Arroio do Ouro para o ano de 2021.

Referências

Bartels, G. K., 2015. Monitoramento hidrossedimentológico numa bacia hidrográfica do Escudo Sul-Rio-Grandense. Dissertação de Mestrado. Universidade Federal de Pelotas.

Cunha, N.G., Silveira, R.J.C., Severo, C.R.S., 1996. Estudo dos solos do município de Morro Redondo. Pelotas, EMBRAPA-CPATC, Ed. UFPel, 28 p

Fernandes, F. D. M., Collares, G. L., Corteletti, R. (2021). A água como elemento de integração transfronteiriça: o caso da Bacia Hidrográfica Mirim-São Gonçalo. Estudos Avançados, *35*, 59-77.

Streck, E. V.; Kämpf, N.; Dalmolin, R. S. D.; Klamt, E.; Nascimento, P. C. do; Schneider, P.; Giasson, E.; Pinto, L. F. S., 2008. Solos do Rio Grande do Sul. 2.ed. Porto Alegre: EMATER/RS-ASCAR, 222 p.